2009

FABRICATION AND CHARACTERIZATION OF BIOACTIVE, COMPOSITE ELECTROSPUN BONE TISSUE ENGINEERING SCAFFOLDS INTENDED FOR CLEFT PALATE REPAIR

Parthasarathy Madurantakam
Virginia Commonwealth University

School of Engineering
Virginia Commonwealth University

This is to certify that the dissertation prepared by Parthasarathy Annapillai Madurantakam entitled FABRICATION AND CHARACTERIZATION OF BIOACTIVE, COMPOSITE ELECTROSPUN BONE TISSUE ENGINEERING SCAFFOLDS INTENDED FOR CLEFT PALATE REPAIR has been approved by his committee as satisfactory completion of the dissertation requirement for the degree of Doctor of Philosophy in Biomedical Engineering

Gary L. Bowlin, Ph.D., Department of Biomedical Engineering

David G. Simpson, Ph.D., Department of Anatomy and Neurobiology

Matthew J. Beckman, Ph.D., Department of Orthopedics

Peter C. Moon, Ph.D., School of Dentistry

Bhavna Shroff, DDS, MDentSc, MPA, Department of Orthodontics

Thomas W. Haas, Ph.D., Department of Biomedical Engineering

Hu Yang, Ph.D., Department of Biomedical Engineering

Gerald E. Miller, Ph.D., Chair, Department of Biomedical Engineering

Russell D. Jamison, Ph.D., Dean of School of Engineering

Rosalyn Hobson, Ph.D., Dean of School of Engineering

Douglas F. Boudinot, Dean of the Graduate School

November 24, 2009

FABRICATION AND CHARACTERIZATION OF BIOACTIVE, COMPOSITE ELECTROSPUN BONE TISSUE ENGINEERING SCAFFOLDS INTENDED FOR CLEFT PALATE REPAIR

A dissertation submitted in partial fulfillment of the requirements for the degree of Doctor of Philosophy in Biomedical Engineering at Virginia Commonwealth University.

by

PARTHASARATHY ANNAPILLAI MADURANTAKAM
Bachelor of Dental Surgery, Tamilnadu Government Dental College and Hospital, India, (1998)
Master of Dental Surgery, Tamilnadu Government Dental College and Hospital, India, (2003)

Director: GARY L. BOWLIN
PROFESSOR, BIOMEDICAL ENGINEERING

Virginia Commonwealth University
Richmond, Virginia
December, 2009

ACKNOWLEDGEMENT

First and foremost, this dissertation is a tribute to any parent who believes that education is the best legacy they can leave to the generation next. I have been lucky to have such supportive parents, who in spite of facing greatest financial hardship, never compromised on their commitment to providing quality education. I would like to remind them that I am still their kid and whatever I may achieve in my life would not have been possible without their numerous sacrifices. I would like to thank my brothers who influenced my way of thinking and backing me whenever I needed them. It would be inadequate to describe the support and unconditional love of my wife, Lathika who for some reason believes in my ability more than my own self. We wish and hope to impart all these values to our son, Shravan.

A special mention goes to Dr. Bowlin who have played multiple roles in my life for the past 5 years. From being a faculty who created a spark in tissue engineering, he blossomed into a mentor who could see what is best for me and guided me in the right direction. I will be forever indebted to diverse opportunities he gave me including teaching graduate classes, participating in the National Inventors Competition and complete freedom to explore my numerous ideas. His trust in me is something I will be proud of.

A big thanks to Dr. Moon, a fatherly figure who has been a personal friend for the past couple of years. His methodical approach to problems I run into kept me busy and more importantly made me think. I pray for his good health and continued presence in the university guiding many more students.

Dr. Matthew Beckman will hold a special place in my heart for his personality and cheerfulness. I learnt from him the art of asking right questions, importance of experimental design and interpreting data in the correct context. He literally held my hand and walked me through the rigorous processes of cell culture and writing grants.

Dr. Simpson is someone who has helped me through the years whenever I get stuck and meet a dead end with my project. A brilliant out-of-the-box thinker, he has always bailed me out by showing a way out that set the ball rolling again. I am sure any graduate student will pray for such intervention but I am one of the lucky few to get him as my advisor.

Dr. Shroff has been my role model even before I came to US. She bowled me over in out first meeting with her down-to-earth personality and enthusiasm for research. In spite of being an eminent orthodontist, her passion for basic science research convinced me to believe that these interests are not exclusive and can co-exist. Her clinical insight about cleft palate repair has been invaluable.

I would also like to thank Drs. Yang and Haas for their constant inputs and guidance throughout these years and keeping me on my toes especially during the committee meetings.

Table of Contents

List of Figures

Page

Abstract

FABRICATION AND CHARACTERIZATION OF BIOACTIVE, COMPOSITE ELECTROSPUN BONE TISSUE ENGINEERING SCAFFOLDS INTENDED FOR CLEFT PALATE REPAIR

By Parthasarathy Annapillai Madurantakam, Ph.D

A Dissertation submitted in partial fulfillment of the requirements for the degree of Doctor of Philosophy in Biomedical Engineering at Virginia Commonwealth University.

Virginia Commonwealth University, 2009

Major Director: Gary L Bowlin, PhD
Professor, Biomedical Engineering

Tissue Engineering is a scientific discipline that aims to regenerate tissues and organs that are diseased, lost or congenitally absent. It encompasses the use of suitable synthetic equivalents of native extracellular matrix that may or may not be supplemented with cells or relevant growth factors. Such scaffolds are designed to reside at the site of implantation for a variable period of time during which they induce the regeneration of native tissue. During this time, they also provide a template for new cells to attach, infiltrate, differentiate into appropriate phenotype and eventually restore function of the

concerned tissue. Among the factors that affect the outcome are the composition of scaffold, methods of fabrication, bulk properties of the scaffold and topography and architecture at the cellular level.

Bone is unique in the body in that it is one of the few tissues capable of complete regeneration even in adults, as seen during fracture healing. However, certain conditions (non-union of fractures, congenital and acquired bone deficiencies) exist in which the regenerative capacities of bone are exceeded and appropriate intervention becomes necessary. Current treatment options include autologous bone grafts harvested from iliac crest or de-cellularized allografts or synthetic substitutes made from metals, ceramics and polymers. However these options have serious limitations: while autografts are limited in supply, necessitate second surgery and show inadequate vascularization, allografts can transmit viral infections. Metals, ceramics and polymers are in essence structural replacements without performing any biological function. Other problems associated with these synthetic materials include adverse immune reactions, corrosion, stress-shielding and secondary fractures due to inadequate osseo-integration. Bone tissue engineering is a specialized field of research that provides an alternative strategy to repair bone defects by exploiting the advances in engineering and better understanding of bone biology.

Scaffold-based tissue engineering approach is a promising field that involves implantation of a biomaterial that is specifically matched in terms of biological and material properties to the tissue it replaces. This study explores the feasibility of using electrospinning as a potential fabrication strategy for bone tissue engineering applications, more specifically intended for cleft palate repair. This model represents a congenital

deformity that affects both hard and soft tissues and presents unique challenges and opportunities. Among the challenges are: the need for the implant allow growth of the most complex areas of the facial skeleton, integrate and grow with the patient through adolescence, the ability of the implant to not interfere with vital functions including breathing and feeding. Further the implant should provide a flexible matrix that can effectively support erupting teeth. In spite of these extreme demands, maxilla is a non load-bearing membranous bone, a favorable consideration from materials engineering perspective.

The present study is organized into three independent sections. The first section investigates developing strategies intended to improve the material properties of electrospun bone scaffold. Bone is composed of a high volume fraction (50%) of inorganic hydroxyapatite nanocrystals that is closely associated with collagen. The dispersal of brittle mineral is critical in not only strengthening the bone in compression but also contributes to the osteoconductivity of the matrix. Since loading of mineral in a bone scaffold is a serious limitation, we attempted to achieve improved loading of bone mineral by dual mineralization approach. We first incorporated nanocrystalline hydroxyapatite (nHA) directly into the scaffold by adding it to the electrospinning polymer solution. The second step involves inducing biomimetic mineralization of electrospun scaffolds by incubating them in simulated body fluid (SBF) for 2 weeks. The hypothesis was that the nanocrystalline hydroxyapatite seeded during electrospinning would act as sites for nucleation and further crystal growth when incubated in solution supersaturated with respect to calcium and phosphate ions. We tested this approach in two synthetic,

biocompatible polymers-polydioxanone and poly (lactide: glycolide) and four formulations of SBF with differential loading of nHA (0-50% by wt. of polymer). A modified Alizarin Red S (ARS) staining that specifically binds to calcium was developed that allowed us to quantify the mineral content of 3D scaffold with great accuracy. Results indicated a unique combination of factors: PDO scaffolds containing 50% nHA incubated in 1x revised-SBF incubated under static conditions gave maximum mineralization over a period of two weeks. We then sought to exploit these findings to engineer a stiffer scaffold by stacking multiple layers together and cold welding them under high pressure. Electrospun scaffolds (1, 2 or 4 layered stacks) were either compressed before or after mineralizing treatment with SBF. After two weeks, scaffolds were analyzed for total mineral content and stiffness by uniaxial tensile testing. Results indicated while compression of multiple layers significantly increases the stiffness of scaffolds, it also had lower levels of mineralization partly due to increased density of fibers and loss of surface area due to fiber welding. However this can be offset to a reasonable degree by increasing the number of stacks and hence this strategy can be successfully adopted to improve the mechanical properties of electrospun scaffolds.

The second section introduces a novel infrared imaging technique to quantify and characterize the biological activity of biomaterials, based on cell adhesion. Cells attach to the surface by the formation of focal contacts where multiple proteins including vinculin and talin assemble to signal critical processes like cell survival, migration, proliferation and differentiation. After allowing MG-63 osteoblasts to adhere to 2D biomaterial surface coated with extracellular matrix proteins (collagen, gelatin, fibronectin) cells were fixed

and probed with antibodies for vinculin and talin. Secondary antibodies, tagged with infrared-sensitive fluorescent dyes, were used to quantify the molecules of interest. In addition, the kinetics of focal contact formation in these different substrates was followed. Successful quantification of focal contacts were made and further research revealed phosphorylation of vinculin at pY-822 as one potential mechanism for recruitment of vinculin to focal contacts. Hence it could represent a subset of vinculin and might serve as a specific molecular marker for focal contacts. As an extension, we evaluated the possibility of using such an assay to quantify 3D electrospun tissue engineering scaffolds. We fabricated scaffolds of graded biological activity by electrospinning blends of polydioxanone and collagen in different ratios. Vinculin and talin expressed by MG-63 cultured on these scaffolds for 24 hours were quantified in a similar manner. Results indicate that while talin does not show a significant difference in expression among different scaffolds, vinculin showed a positive correlation with increasing biological activity of scaffolds. In conclusion, we have identified vinculin as a reliable marker of focal contacts in 3D scaffolds while phosphovinculin (pY-822) was more specific to focal contacts in coated 2D substrates. In both instances, infrared imaging proved to be reliable in study of focal contacts.

The third section aims to make the bone scaffolds osteoinductive- a property of a material to induce new bone formation even when implanted in subcutaneous and intramuscular heterotopic sites. Bone morphogenetic proteins (BMP) are potent cytokines that can induce migration, proliferation and differentiation of stem cells along osteoblastic lineage. The therapeutic efficacy of BMPs in the treatment of severe bone defects has been

identified and is currently FDA approved for specific orthopedic applications. BMPs are clinically administered in a buffer form that not only makes the treatment expensive but less effective. Suitable delivery systems for BMP delivery have been an intense area of investigation. We rationalized electrospinning as a strategy to incorporate BMP within the scaffold and that would enable controlled release when implanted. One of the drawbacks of using electrospinning to deliver bioactive molecules is the potential denaturing effect and eventual loss of activity of BMPs. The final section of this dissertation tries to develop sensitive and relevant assays that could answer intriguing questions about solvent-protein interaction. We chose to use the BMP-2/7 heterodimer as the osteoinductive molecule of choice because of its superior potency compared to homodimer counterparts. We characterized the detection and quantification of BMP-2/7 using a slot blot technique. Further, we used a novel cell line (C2C12 BRA) to test the retention of activity of BMP-2/7 that has been exposed to organic solvents. Results indicate significant loss of activity when BMPs are exposed to organic solvents but complete recovery was possible by diluting the solvent with an aqueous buffer.

Chapter 1: CLEFT PALATE - A CLINICAL NEED

1.1. INTRODUCTION

The face is one of the most complex parts of the human body from an anatomical and functional perspective. The maxilla with the palate plays a significant role in performing diverse functions like mastication, deglutition, respiration and speech. Given such complex functional anatomy, even a slight aberration during gestation can jeopardize the balance of normal craniofacial growth and development, as seen in craniofacial syndromes. The most common of all craniofacial anomalies, and the second most common of all birth defects, are clefts of the lip with or without cleft palate and cleft palate alone. These anomalies occur at a rate of 1 out of 600 live births in Whites and 1 out of 850 live births in African Americans, costing $176 million annually in direct medical costs alone [1].

Cleft palate arises from the failure of fusion of lateral palatal shelves with each other and to the primary palate leading to alveolar and palatal bony deficiency. A bony deficit at this structurally important area leads to collapse of the maxillary arch, distortion of dento-alveolar segments and derangement of occlusion. It also opens up a permanent communication between the mouth and nose leading to other associated complications. Treatment of cleft palate is multi-disciplinary and involves specialized procedures from birth to early adulthood in an established sequence. Definitive correction of palatal bone deficit is carried out at 7-9 years of age and is called Secondary Alveolar Bone Grafting (SABG). The reasons for bone grafting include: provide bony support to the teeth in line with and adjacent to the cleft, establish maxillary arch continuity, enhancement of naso-labial contour and facial esthetics. Bone grafting also increases the chances of spontaneous eruption of canines and ensures optimal bone support [2].

1. 2. CURRENT TREATMENT OPTIONS IN CLEFT PALATE REPAIR

The most preferred source of donor bone for secondary alveolar bone grafting is the *autologous cancellous bone* from the iliac crest [3, 4]. In addition to being non-immunogenic, autologous grafts are osteoconductive, osteoinductive and osteogenic and hence are considered 'gold' standard for bone grafts [4]. However, the use of autologous bone graft is associated with significant donor site morbidity including chronic pain [5], infection, neurovascular injuries, iliac wing fractures, change in gait, deep hematoma formation and scarring [6. 7]. Unpredictable resorption [8] and lack of mechanical strength precludes their use as structural grafts. *Allografts* can be harvested from live donors

(femoral heads during primary hip arthroplasty) or cadavers, processed and stored. They are devoid of cells, primarily osteoconductive, exhibit slow vascularization, incomplete incorporation and are susceptible to fatigue fracture [9, 10]. Allografts also carry the risk of infection transfer and unfavorable immune reactions [9, 11]. These disadvantages associated with sourcing natural bone tissue from humans highlight the need to develop synthetic substitutes.

1. 3. BONE TISSUE ENGINEERING

Research to develop synthetic alternatives to bone has been along two divergent directions- *biomaterials* approach resulting in a variety of ceramics, polymers, metals and *molecular biology* approach involving the use of biological molecules and gene therapy [12]. The limitations of either strategy to be successful in isolation call for an integrated approach in the development of synthetic bone substitutes. *Bone tissue engineering* is an emerging multi-disciplinary field in which synthetic or natural compounds are manipulated to produce biologically based replacement tissues and organs [13]. It involves implantation of three dimensional (3D) biodegradable matrices (scaffolds) that mimics the native extracellular matrix (ECM) to guide tissue regeneration. These matrices can also be used to deliver cells of interest to specific sites in high numbers to further accelerate healing. A variety of synthetic and natural polymers that support cell infiltration and subsequent replacement have been used as bone tissue constructs [14].

Chapter 2: NANOFIBROUS SCAFFOLDS AND TISSUE ENGINEERING

Preface: The following chapter is compiled from two review articles published in

Nanomedicine, February 2009, Vol. 4, No. 2, pages 193-206

and

Polymer International, 2007, Vol. 56, pages 1349-1360.

2. 1. ABSTRACT

Native extracellular matrix (ECM) provides structural support to the multi-cellular organism on a macroscopic scale and establishes a unique microenvironment (niche) to tissue and organ-specific cell types. Both these functions are critical for optimal function of the organism. These natural ECM comprised predominantly of fibrillar proteins, collagen and elastin, are synthesized as monomers but undergo hierarchical organization into well defined nano-scaled structural units. The interaction between the cells and ECM is dynamic, reciprocal and is essential for tissue development, maintenance of function, repair and regeneration processes. Tissue engineering scaffolds are synthetic, biomimetic ECM analogues that have shown great promise in regenerative medicine. Ongoing efforts in mimicking the native ECM in terms of composition and dimension have resulted in three strategies that permit generation of scaffolds in nanometer dimensions. While excellent reviews regarding the applications of these strategies in tissue engineering are available, a comprehensive review of the science behind these fabrication techniques do not exist. This review intends to fill this critical gap in the existing knowledge in the fast expanding field of nanofibrous scaffolds. A thorough understanding of the fabrication processes would enable us better exploit available technologies to produce superior tissue engineering scaffolds.

2. 2. INTRODUCTION

Multicellular organisms are characterized by complex 3D organizational network of cells and their supporting matrices to form tissues and organs. In exception to the circulatory cells, all other cell types are anchorage dependent for survival [15-17] and are associated with its own unique microenvironment composed of extracellular matrix (ECM) and interstitial fluid [18]. Cells are classified not only based on their function but also according to their relation to the ECM. For example, epithelial cells are characterized by minimal ECM, the basement membrane, while cells of connective tissue like bone, cartilage, blood vessel and dermis is characterized by an abundance of ECM. In this circumstance, the ECM is composed of specific elements that are structurally organized to allow for a specific function. The dominant component of the ECM is structural proteins-collagen, elastin and reticular fibers. These structural proteins exhibit multiple levels of organization. At the most fundamental level, they are synthesized as peptide monomers that are then covalently crosslinked to form polymers. These polymers self assemble to form fibrils and bundles of fibrils organize to form fibers. Further organization of fibers into fascicles gives the ECM its unique form to optimally perform its function [19]. One underlying theme in natural ECM is the organization of these proteins in the form of fibers even at the ultra-structural level. This is in contrast to the globular structure of functional proteins like enzymes and transport proteins. The ECM also binds to the dormant, inactive forms of growth factors, activating and releasing them upon need thus acting as their local reservoir. The organization of the natural ECM in the form of nanofibers not only provides

steady anchorage to cells by binding to integrins but also activates intra-cellular signaling pathways that ultimately affects almost all aspects of cell behavior [20]. The fibrous architecture of native ECM also plays a very important role in mechanotransduction; it deforms visco-elastically to external and internal stresses to keep the cells constantly informed of the mechanical stresses [21-23]. The cells may respond to this change in stress in a variety of ways including resorption of old ECM and laying down new matrix thus redefining and remodeling its own niche. This dynamic reciprocity is pivotal to evolution of multicellular organisms and its relevance cannot be overemphasized in normal processes of growth, development and regeneration [24-27] and even in disease states [28]. Given such physiological relevance, it comes as no surprise that a lot of effort have been invested in mimicking the dimensions and composition of native ECM. The interdisciplinary fields of tissue engineering and regenerative medicine have successfully identified three fabrication strategies to generate nanofibrous scaffolds: self assembly, phase separation and electrospinning. The application of these techniques in generating nanofibrous scaffolds for a variety of applications have been extensively and exhaustively reviewed in the literature [29-33]. This review attempts to demystify the science behind these techniques with the idea that a better understanding of the process will result in better control over the outcomes thus taking a step closer towards the goal of fabricating ideal scaffolds.

It is the conscious effort on the part of authors to look beyond the arbitrary boundaries separating the scientific disciplines into the more fundamental and universal binding laws of science. Even though each of the three strategies discussed below-self

assembly, phase separation and electrospinning might seem discrete and mutually independent from each other from academic standpoint, the governing principles of thermodynamics and equilibrium underlie these processes overlap. Infact, the phase separation is a special case of self assembly that occurs under specific conditions.

2. 3. STRATEGIES FOR NANOFIBROUS SCAFFOLD FABRICATION

2. 3.1. Self Assembly

Self assembly is a bottoms-up fabrication strategy that permits generation of defined 3D macroscopic structures from essentially uni-dimensional molecules. It involves autonomous organization of components into structurally well defined aggregates and is driven towards the system's thermodynamic minima resulting in stable and robust structures [34]. These structures, stabilized by multiple, weak, non-covalent interactions, can continue to expand to form ordered aggregates (irrespective of size scale) as long as the formation of product is favorable and stable in a given set of conditions.

Self assembly offers certain advantages that are unique. Since the molecules concerned interact at an atomic level driven by physical or chemical affinity, the sensitivity and specificity of the entire process is increased. In addition, since the non-specific interactions are energetically unfavorable, the system is robust and devoid of errors. In addition, the atomic level interactions between components are retained throughout the expansion process, thus providing a viable approach to retain nano-scale properties even in bulk materials [35].

Examples of molecular self assembly occur widely in biology and include formation of lipid bi-layers, protein folding and DNA helices. Infact, molecular self assembly is the most fundamental process of life and is the central phenomenon by which all biological macromolecules assemble in a living cell. One of the best examples of self assembly in biological systems directly relevant to tissue engineering is collagen.

Collagen refers to a diverse group of related proteins that share certain common traits but also exhibit wide differences to fulfill functional demands of specific connective tissue [36]. As a family, these proteins are made up of three polypeptide chains (α chains) that have Gly-X-Y repeat sequences in the primary sequence, where X is mostly proline and Y is mostly hydroxyproline. Current research indicates that at least 28 distinct types of collagen trimers are assembled from as much as 43 distinct α chains [37]. Since type I collagen is the most common type of fibrillar collagen and best understood, it will be used as a model molecule in this review. Self assembly of collagen can be studied at two levels: intracellular assembly of α chains into triple helical procollagen and extracellular assembly of procollagen into fibrils [36,38].

Formation of procollagen: Collagen, like many other proteins, is translated, modified and assembled in the rough endoplasmic reticulum. Type I collagen is a heterotrimer made of $\alpha 1_1$ (1), $\alpha 1_2$ (1) and α2 (1) chains. Each α chain consists of a central collagenous domain and terminal non-collagenous (NC) domains. Irrespective of the type of α chain, the central collagenous domain, made of Gly-X-Y repeats, spontaneously folds into a left-handed helix because of steric repulsion between proline residues in X position and hydroxyproline residues in Y position. Selection of correct stoichimetry of α chains is

important during assembly of trimeric procollagen molecule. Recent studies have shown that this information resides in the chain recognition region, a variable sequence of 15 residues in C-terminal NC domain [38]. Once the appropriate α chains are identified the polypeptides folds in a zipper-like fashion in the N terminal direction to form procollagen molecule that exhibits a right-handed superhelical structure. This tertiary folding is energetically favored because of lack of steric hindrances when the right-handed α helices wind around the central axis formed by glycine residues [39].

Extracellular assembly into fibrils: The terminal NC domain of secreted procollagen molecule is made up of a telopeptide and a propeptide sequence. Cleavage of C-terminal propeptides by extracellular proteinases renders procollagen insoluble and triggers the second phase of collagen self assembly: fibril formation. The insoluble tropocollagen spontaneously aggregates with other tropocollagen monomers in a D-staggered arrangement that results in axial growth of the fibril. Lateral and circumferential association of multiple fibrils results in increase in fiber diameter. Variable kinetics of N-terminal proteinases in various types of collagen has been observed. The resulting persistence of the N-propeptide on the surface has been implicated to sterically hinder fibril incorporation to the center thus playing a role in limiting fibril growth and fiber diameter [38].

Molecular self assembly, as an engineering strategy, refers to a biomimetic, bottoms-up approach in biomaterial fabrication in which pure molecules interact with one another in an aqueous environment to generate insoluble nanofibrous scaffolds stabilized by non-covalent interactions. In one experiment, Yokoi et al. demonstrated spontaneous

reassembly of synthetic peptides into nanofibers after all non-covalent interactions were disrupted by sonication of the scaffold [40].Currently, self assembly in tissue engineering is based on peptide-amphiphile (PA) or synthetic ionic peptide approaches.

Hartgerink et al. in a seminal paper [41] successfully engineered a synthetic bone mimetic nanofibrous scaffold that is based on peptide-amphiphile (PA) (**Figure 1**). The genius of this work lies in exploiting the basic tenets of biochemistry for applications in tissue engineering. This PA consisted of an acyl tail that confers hydrophobicity, four consecutive cysteine groups that would permit reversible crosslinking under appropriate oxidation state, a flexible linker consisting of a series of glycine residues, a phosphorylated serine residue to attract calcium ions and a cell recognition Arginine-Glycine-Aspartate (RGD) motif. When a large number of synthetic PAs are allowed to interact in an aqueous medium, the hydrophobic interaction drives the formation of fibrous network with the acyl tails forming the core of the nanofiber. Adjusting the pH resulted in a stable cross-linked

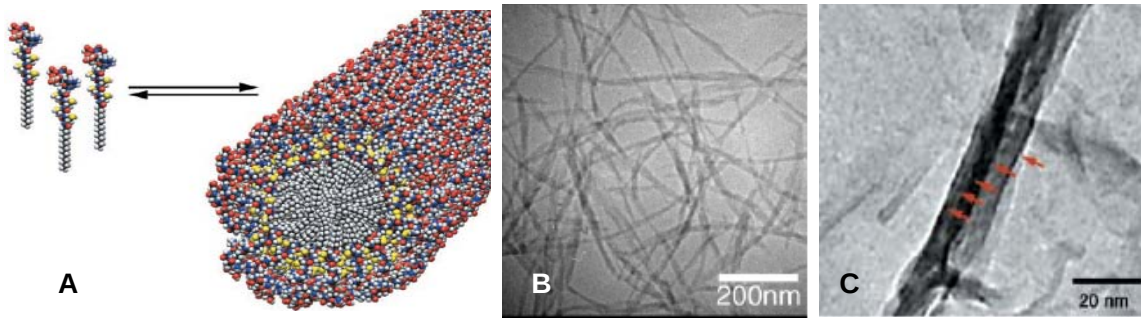

Figure 1: Peptide-Amphiphile strategy for generation of mineralized nanofibers. **A**. Schematic of the process of self assembled (PA). Hydrophobic aggregation of acyl chains in an aqueous environment drives the assembly nanofibers with the polar groups facing the outside. **B**. Cryo-TEM image showing a network of fibers with mean diameter of 7.1 nm in hydrated, native state. **C**. A 30 minute exposure of PA fibers to calcium and phosphate reveal dense mineral deposition on the fibers. Electron diffraction and energy dispersion X-ray spectroscopy (EDS) confirmed the mineral to be hydroxyapatite. (Jeffrey D. Hartgerink, et al. Science 294, 1684, 2001. Reprinted with permission from AAAS)

fibrous network and exposure to calcium resulted in formation of hydroxyapatite crystals along the long axis of the fiber-an orientation that is similar to that of native collagen fiber. Reversible assembly can be accomplished by change in pH or these thiol groups can be permanently oxidized with iodine to lend stability to the nanofibrous structure through a process called covalent capture.

In an interesting application of PAs, Silva et al. [42] mixed neural progenitor cell suspensions with aqueous solutions of PAs containing the epitope of laminin. The formation of 3D nanofibrillar network initiated upon mixing and the cells became encapsulated within the fibrils. The authors not only demonstrated cell survival during this process but also potency of laminin epitope on these progenitor cells in inducing neurite formation. The progenitor cells differentiated into neurons very early (1 day) exhibiting greater surface area than controls. More significant was the finding that astrocyte differentiation is inhibited while neuronal phenotype is enhanced in cells grown in PA network. This is exactly the opposite of controls where the astrocyte differentiation was a dominant effect. These findings are important because inhibition of astrocyte proliferation and prevention of glial scar is critical in neuronal regeneration following injury.

Zhang et al. exploited the inherent charge present in amino-acids to generate self-assembled peptide nanofibers [43-45]. He identified chemical complimentarity and structural compatibility to be key requirements in assembly of nanofibers and demonstrated self assembly of repetitive ionic self-complimentary peptide sequences (including Arginine-Alanine-Asparatate, RAD) into a stable hydrogel composed of

nanofibers. Furthermore, these peptides can be readily tailored with functional sequences of collagen, laminin, fibronectin and osteopontin to enhance cell response [46] (**Figure 2**).

This approach is in contrast to peptide-amphiphile strategy adopted by Hartgerink et al. where a combination of peptide and fatty acyl chain was used to drive self assembly. One of attractive features of either of these two approaches is the use of pure biological molecules as the building block of higher order structures and hence the concerns of biocompatibility, toxicity and immune response are irrelevant [47]. Infact, there is

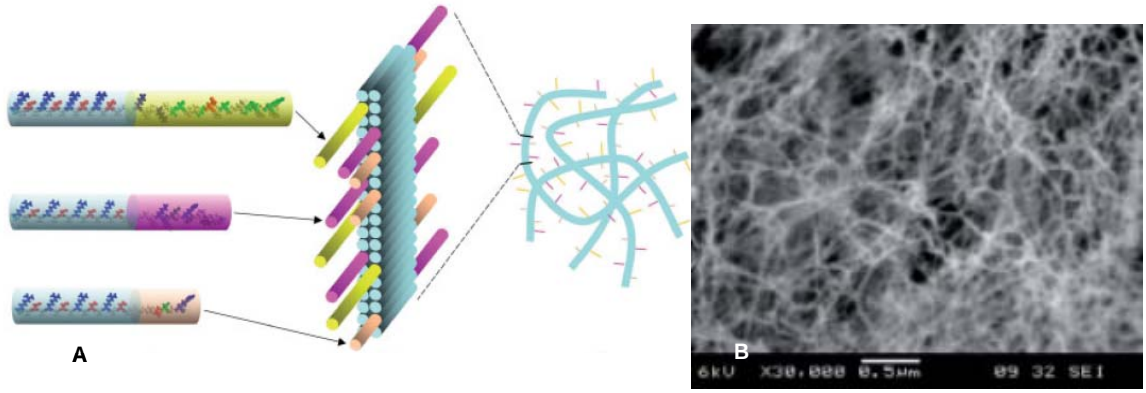

Figure 2: Self assembled nanofibrous scaffold based on ionic complimentarity of peptides. **A**. Cartoon representation of the hierarchy in the self assembly of ionic self-complementary synthetic peptides with functional group modification. The interaction between basic and acidic groups of the backbone drives self assembly into the double β-sheet nanofiber with the functional domains projecting out for cell interaction. Depending on the actual composition, they will then self assemble into a specific functional 3D scaffold. **B**. SEM of a self assembled nanofibrous scaffold. (Gelain et al. Macromolecular Bioscience, 7, 2007. Copyright Wiley-VCH Verlag GmbH & Co. KGaA. Reproduced with permission)

evidence that the cells actively breakdown the nanofibers and internalize the fragments by endocytosis and probably utilize these molecules for metabolism [48].

The application of self assembly scaffolds towards dental tissue regeneration has been gaining popularity. Galler et al. [49] demonstrated biocompatibility and successful remodeling of nanofibrous PA consisting of a MMP-2 cleavable sequence during culture

with two different dental stem cells lines (SHED and DPSC). More interestingly, while SHED cells exhibited much higher evidence of matrix deposition (collagen types I and III) and remodeling (MMP-2), DHSC cells showed a significant increase in mineralization. Kirkham et al. [50] evaluated the ability of self assembled anionic peptides to prevent and /or reverse the effects of enamel demineralization under conditions mimicking the intra-oral environment. Surface anionic peptide treatment not only significantly increased the amount of new mineral deposited but also reduced the tendency of demineralization. The finding is of therapeutic value because this can potentially be used to treat pre-cavitary incipient caries (subsurface demineralization) and cases of enamel hypoplasia.

Collagen is the most abundant structural protein that consists of three left handed helices wound together to form a right handed super-coiled super helix [51]. The ability of collagen to spontaneously form triple helix is dictated largely by its primary amino acid sequence with glycine at every third residue. While this smallest amino acid is buried in the central core of the triple helix, the functional groups of adjacent amino acids project out to the surface and participate in a large number of intra- and inter-molecular non-covalent bonds (including hydrogen bonds) with solvent molecules. Since collagen is synthesized as individual chains that spontaneously orient into a triple helix before further modification and secretion, it provides a perfect paradigm to study self assembly of native ECM proteins.

Gauba et al. [52,53] exploited the ionic interactions between oppositely charged arginine and glutamate to induce self assembly of artificially synthesized peptides into triple helical secondary structures resembling native collagen. They showed in their studies

that while glutamine and arginine are inherently destabilizing to formation of triple helical homotrimers, the same charged groups interacted favorably with each other to form heterotrimers, when incorporated in different peptides. More recently, the same authors [54] developed a successful strategy, based on molecular self assembly, to generate a variety of triple helical structures that mimics normal or mutated collagen. These findings are significant in that we could unearth some clues from nature as to what makes collagen in certain disease states (mutations) more (hyperostosis) or less (fibrous dysplasia) prone to undergo calcification. It would also be very exciting to see if such findings can be exploited into generating matrices for appropriate applications (bone or blood vessel) in tissue engineering.

More recently, Capito et al. [55] reported formation of macroscopic membranes at the interface when solutions of hyaluronic acid and peptide-amphiphile are mixed. These membranes are robust in both dry and hydrated state and are formed almost instantaneously when two solutions with strong zeta potential (oppositely charged) are brought into contact. An amorphous zone at the interface is formed within minutes due to electrostatic complexation of counterions and rapid diffusion of small PAs interactions through the hyaluronic acid layer. This creates a diffusion barrier that prevents random mixing of the liquids. Subsequent reptation of the hyaluronic acid chains through the diffusion barrier into the PA layer results in aggregation and eventual formation of PA nanofibrils perpendicular to the interface. With time this growth of nanofibrous layer increases in density and alignment.

In addition to the exciting research discussed above, self assembly has shown promise in neural tissue [47, 56], bone [57-61], vascular [62] engineering and controlled release applications [63].

2. 3. 2. *Phase Separation*

A phase can be defined as a subset of macroscopic state of matter (solid, liquid or gas) that is homogenous and has identical physical attributes and chemical composition. However, multiple phases can coexist in equilibrium within any given state of matter. Phase separation is a thermodynamic process that involves selective enrichment and purification of the desired phase. The process of phase separation has been extensively used in the fabrication of macroporous foams and membrane films and much of the understanding comes from these sources. These concepts have been only recently been applied in tissue engineering to generate nanofibrous scaffolds.

In order to better understand the concept of phase separation, polymers can be compared to a bowl of spaghetti where individual polymer chains are randomly coiled and entangled with neighboring chains. The shape and structural packing of the polymer chain is dictated by a number of factors including: degree of polymerization, linearity of the polymer chain, bulkiness and orientation of the pendant groups and the degree of crystallinity of the polymer. Familiar forces like hydrogen bonding and van der Waals forces play a very important role in stabilizing the secondary structure (folding and crystallinity) of polymer chains, while mechanical entanglement of individual polymer chains also contribute to the physical properties of the polymer.

When a polymer is dissolved in a solvent, much smaller solvent molecules penetrate the tight network of polymer chains and disrupt the inter-chain forces. Slowly the chains lose their dense packing and start to slide past each other with much more ease due to disruption of stabilizing forces. This presents a network of 'loosened' and extended polymer chains that enclose the solvent in the space separating the chains. Thus it is easy to appreciate the presence of two phases in solution: a polymer rich phase containing the chains and the solvent rich phase around and in between the chains. Controlled phase separation involves selective enrichment of each of the phases throughout the solution that would result in two separate phases or a single bi-continuous phase. Subsequent removal of the solvent will result in generation of a porous structure containing loosely inter-twined polymer chains. Based on the strategy used to induce phase separation and subsequent removal of the solvent there are different variants of phase separation [64,65].

Solid and liquid models have been proposed to explain the concept of phase separation of simple liquids and metals but both theories fall deficient when dealing with colloidal or polymer solutions. Tanaka, in a series of papers [66-68], proposed a unifying viscoelastic model to account for phase separation that occurs in polymer solutions and suggested that solid and liquid models of phase separation as special cases. Unlike phase separation of metals and simple liquids, polymer solutions exhibit two phases that are distinctly different from each other with respect to molecular weight, glass transition temperature, internal degrees of freedom and the ability to resist mechanical stress. Thus these polymer solutions are said to exhibit 'dynamic asymmetry' between the phases and the presence of this inherent asymmetric composition drives the separation of phases under

appropriate conditions. In addition, the attractive forces between the polymer chains overcomes the entropy of the system and leads to the formation of a transition gel network- a hallmark of phase separation in polymer solutions. Eventually the phases separate and phase inversion happens in which the polymer-rich phase forms the continuous phase and solvent becomes the dispersed phase. The strategies employed to induce phase separation for tissue engineering applications include non-solvent induced phase separation and thermally induced phase separation which are discussed in detail below.

Non-solvent induced phase separation:

This process involves addition of a non-solvent to the polymer solution and subsequent selective extraction and replacement of the solvent by non-solvent molecules. This would result in a porous polymer structure that is stabilized in a solution of non-solvent.

Extrusion of collagen fibers: Although not traditionally classified under phase separation, this is definitely a variant of non-solvent induced phase separation also called immersion precipitation [69]. In this technique, collagen dissolved in acetic acid is extruded through silicone tubing into a bath containing a non-solvent [70]. This results in exchange of acetic acid for non-solvent and results in the formation of insoluble collagen fibers. Simultaneous aggregation and self assembly of numerous fibrils result in formation of micron-sized fibers. The rate of extrusion, pH and composition of the non-solvent are important parameters in successful generation of continuous fibers. Even though this review is primarily concerned with nanofibers, micron-sized collagen fiber generated by extrusion is included because these threads are essentially aggregates of nano fibrils, just as they occur

in the body [71]. Other examples of collagen fiber extrusion are listed for interested readers [72-74].

Thermally Induced Phase Separation (TIPS):

Thermally Induced Gelation and Crystallization: Linear polymers in solution undergo a phase transition from relatively low viscosity sol to an elastic gel over a narrow temperature range on cooling. The gelation temperature depends on the polymer concentration and characteristics of solvent itself. Gelatin forms a temperature dependent gel in water as a function of concentration. Chain entanglement and inter chain attractive forces drive the process of gelation. Removal of the solvent while preserving the structure of porous polymer scaffold is a big challenge. In this regard, it was found that crystallization of the polymer following gelation of the solution better preserves the architecture of the polymer scaffold [64].

Thermally Induced Spinodal Decomposition: In contrast to controlled cooling of polymer solutions in phase separation due to gelation/crystallization, thermally induced spinodal decomposition involves rapid quenching of a homogenous polymer solution. This would induce spontaneous phase separation of polymer solution into a polymer rich phase and a solvent rich phase. It is well known that the quality of the solvent (the ability of the solvent to dissolve a solute) decreases with temperature. So any lowering of temperature will result in creation of unfavorable interface and thus phase separation. The driving force for phase separation in TIPS is the decrease in the interfacial free energy between the polymer chains and the solvent.

The boundary of liquid-liquid demixing is called binodal. It is an equilibrium boundary that demarcates stable phase separation and is established at infinitely slow rates of cooling. In contrast, spinodal refers to unstable region bounded by the binodal that captures phase separation of polymer solutions following quenching (instantaneous

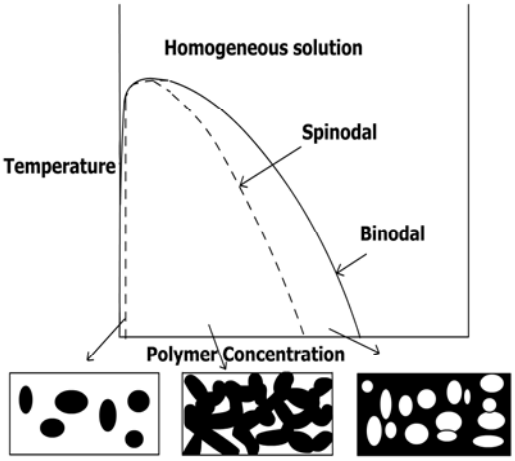

Figure 3: A binary phase diagram showing the boundary conditions of the phases of polymer concentration as a function of temperature. Below a critical temperature, homogenous solution begins to phase separate and forms the binodal boundary under equilibrium conditions. Enclosed within the binodal is the spinodal that demarcates the phases that occur due to rapid quenching. Depending on the initial polymer concentration, different structures evolve (polymer-dark, solvent-light): nucleation and growth of polymer rich phase (left), solvent rich phase (right) or spinodal decomposition resulting in a bicontinuous structure which has interconnected polymer rich and solvent rich phases. (Adapted from P. van de Witte et al. Journal of Membrane Science, 1996)

cooling). The area between the spinodal and binodal is metastable and further demixing occurs by nucleation and growth of either the polymer-rich or polymer-poor phase depending on the initial polymer concentration (**Figure 3**).

Phase separation within the area enclosed by the spinodal occurs as a sinusoidal wave progression throughout the solution instead of nucleation at discrete sites observed in metastable areas of the phase diagram. This results in the formation of a bi-continuous structure that has well interconnected but discretely enriched polymer-rich and polymer-poor phases [69]. Other factors that can play a role in phase separation of polymer solutions include the degree of crystallinity, association of polymer chains at high concentrations and their side groups.

In tissue engineering applications, thermally induced phase separation by spinodal decomposition has been the most promising strategy to generate porous 3D scaffolds. The principles of TIPS in generating porous foams were cleverly exploited by Zhang and Ma to generate fibrous scaffolds of aliphatic polyesters [75]. Their results were the first direct evidence that spinodal decomposition following quenching is the most likely mechanism for the formation of nanofibers because slow annealing caused crystal nucleation and growth into platelet-like matrix. They identified gelation time, temperature and freezing rate to be critical parameters in generation of the fibrous scaffold. The tendency of the polymer to organize into nano-scaled fibers increased with the lower gelation temperature and rapid quenching of the gel to -18°C for 10 minutes was sufficient for fiber formation. Further the average fiber diameter did not change with increase in polymer concentration.

After phase-separation, an important processing step is the removal of the solvent that would eventually result in the generation of porous scaffolds. The space occupied by the solvent becomes the pores of the matrix. The ability to preserve the porous nano-fibrillar structure during this critical processing step is a big challenge as the surface tension of the evaporating solvent can exceed the rigidity of the matrix and cause it to collapse. In addition if the temperature is not low enough, the polymer might re-dissolve and can lead to loss of fibrillar architecture. Both these phenomena can happen with freeze drying and contribute to a dense surface skin. In order to overcome these disadvantages of freeze drying, Ho et al. [76] proposed freeze extraction as a technique to remove the solvent without compromising the structural integrity of the matrix. The strategy employed leaching the solvent for the non-solvent when the fibrillar polymer matrix is still frozen,

thus making freeze drying unnecessary. Since solvent substitution occurs under frozen conditions, there is no danger of polymer re-dissolving and subsequent structural collapse when the temperature is raised. They also exploited the gelation tendency of alginate and chitosan to generate nanofibrous scaffolds using the principles of freeze extraction.

Even though the science driving the process of phase separation is relatively well understood, there has been relatively scanty evidence supporting the viability of this technique in the generation of nano-fibrous scaffolds. Generation of porous foams is very easy with this technique, but the real challenge is to identify the process parameters that would consistently yield fibrous structures. Since this technique is simple and inexpensive, such directed efforts will enable one to exploit this as a fabrication strategy to synthesize fibrous scaffolds for tissue engineering applications.

2. 3. 3. Electrospinning

Electrospinning is a probably the most scalable and versatile strategy to generate nanofibers among the currently available techniques. In this process, either a polymer melt or solution is forced through a nozzle which under the influence of electric field produces a non-woven mat made of sub-micron fibers (**Figure 4A**).

Doshi and Reneker [77], in their classic paper on electrospinning, held that electrostatic charge accumulates on the pendant polymer drop and at a critical voltage becomes sufficient to overcome the surface tension and a charged jet is drawn out from the apex of Taylor cone. As the charged jet accelerates towards the collector plate under the influence of electric field, solvent evaporates, fiber diameter thins and charge

concentration occurs. This increase in charge density was presumed to cause enough repulsion to actually lead to splitting of the primary jet into multiple filaments resulting in a reduction of the fiber diameter with each split.

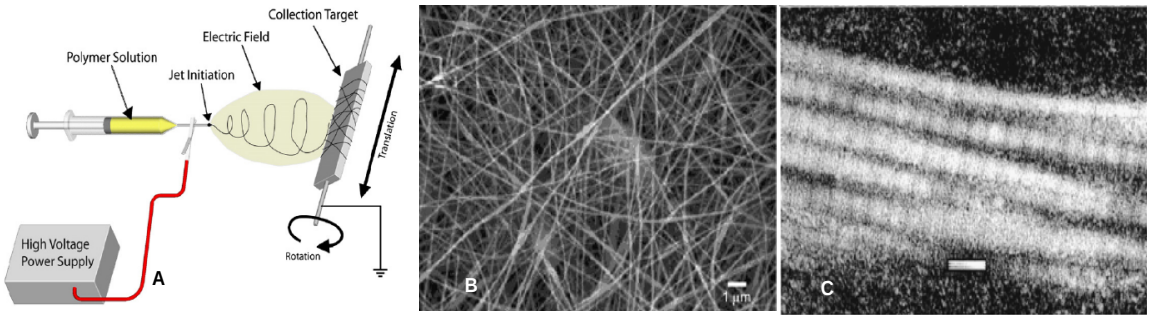

Figure 4: Electrospinning as a fabrication strategy for generating nanofibers. **A**. Schematic of electrospinning setup. The polymer solution is pumped at a constant rate through a needle clamped to a high voltage source. When the electric charge overcomes the surface tension of the liquid, a jet emanates from the tip of Taylor cone and accelerates towards the target and is deposited as dry fibers. **B**. Electrospun type I collagen scaffold showing random orientation of sub-micron fibers. **C**. TEM of the same fibers showing characteristic 67 nm banding. Scale bar is 100 nm. (Reprinted from Barnes et al. in Advanced Drug Delivery Reviews, 59 (14), 1413-33, Copyright (2007), with permission from Elsevier)

Current investigations into theoretical aspects of electrospinning reveal formation of an inverted cone some distance away from the nozzle that represents the whipping instability. Using high speed photography it was identified that the cone is actually a single rapidly whipping jet [78] (**Figure 5**). The whipping frequency is high enough to confound this process with splaying. Modern theories of electrospinning recognize at least three possible types of instabilities that may contribute to the formation of the jet: Rayleigh instability, conducting mode instability and whipping conducting mode instability [79,80]. While the first two modes are axisymmetric, whipping instability is non-axisymmetric. Rayleigh instability is a direct result of surface tension, is dominant at lower electric fields

and is suppressed with increasing field and surface charge density. Conducting mode whipping instability arises due to interaction of higher surface charge with the external

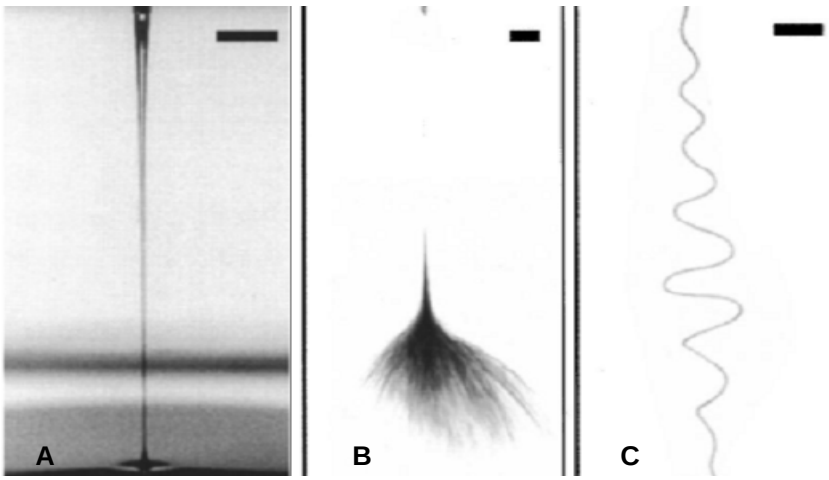

Fig 5: High speed jet images of 2 wt % solution of PEO (MW 2,000,000) in water during electrospinning. **A**. Stable jet at low field, high flow conditions (bar=55 mm). **B**. Unstable jet at high field, low flow conditions (bar=55 mm, 1 ms exposure). **C.** Close-up of the onset of instability (bar=51 mm, 18 ns exposure). Reused with permission from Shin et al. Applied Physics Letters, 78, 1149 (2001). Copyright 2001, American Institute of Physics

electric field and dominates at higher potential. There exists a competition between these different instabilities and the final morphology of collected fibers depends on the net interaction. In fact, Zuo et al. [81] demonstrated that the formation of beads during electrospinning is due to dominance of axisymmetric instabilities while whipping jet instability has been attributed to the formation of smooth fibers. The whipping instability has been proposed to account for the ability of electrospinning to reduce the millimeter sized droplet to sub-micron sized fibers. They reason that this act of whipping greatly enhances the distance that the jet travels before collecting on the mandrel leading to increased stretch and splaying of smaller diameter fibers. The balance between the

competing instabilities defines the narrow operational window within which electrospinning can occur. Electrospinning of polycaprolactone from acetone was shown to form loops, double loops and garland as a result of bending instability of the jet [82].

In addition, the formation of fibers depend on solution parameters (viscosity and conductivity), process parameters (applied electric field and flow rate) and process variables like jet radius, axial velocity, charge distribution, and displacement of the centerline of the jet as a function of the axial distance from the nozzle [78]. Chain entanglements have been implicated as one critical parameter in influencing fiber formation: continuous fibers cannot be generated from solutions that are dilute unentangled or concentrated with tightly entangled polymer solutions [83].

In a recent article, He et al. [84] reviewed novel techniques expanded from conventional electrospinning including siro-electrospinning, vibration electrospinning and magnetic electrospinning to expand the versatility of conventional electrospinning to meet new challenges. Hollow fibers having a core and sheath were generated using co-axial electrospinning of two immiscible solutions by Li et al.[85]. More recently, the same concept was expanded to generate continuous fibers of block copolymers that are otherwise difficult to electrospin. The authors were able to control the diameter of the core by adjusting the flow rates. Micro-phase separation was achieved by subjecting the as-spun fiber to long term annealing. Higher glass transition temperature of the outer shell enabled this process to occur because it provided a confined boundary for long range order of block copolymer in the core [86].

In yet another interesting variation of electrospinning, a co-axial needle was used to incorporate live cells into the biocompatible polymer fiber during electrospinning [87]. A highly concentrated cell suspension in media was pumped through the inner needle while a high viscosity medical grade polydimethylsiloxane (PDMS) was fed through the outer needle. By having a high dielectric medium (PDMS) in the outer needle and adjusting the flow rates of both the solutions independently, the authors demonstrated the encapsulation of more conductive cell aggregates within the PDMS fiber. Cell viability assay after 1 week of culture showed no difference in cell behavior compared to controls. In a more recent study, the same group has developed a novel non-electric field driven technique to fabricate threads for cell encapsulation applications. In this technique pressurized air is directed through the centre of three-needle concentric nozzle while cell suspension and driving polymer medium is ejected out through the outer two needles. A 3 week cell survival assay performed with fluorescent activated cell sorting technique again proved no detrimental effect of the process on cell viability [88].

Electrospinning has been very popular in the field of tissue engineering because it is simple, economical and can generate porous scaffolds made of submicron diameter fibers. In contrast to self assembly and phase separation discussed earlier that generated fibers in true nanometer scale, the diameter of the electrospun fiber is on the upper range of native ECM fibers (>500 μm). But this limitation is offset by the ability of this process to produce a wide variety of scaffolds from both synthetic and natural polymers. In addition, our understanding of the parameters that control the outcomes like fiber diameter and

morphology increase by the day and hopefully we should be able to manipulate these variables intelligently to suit our needs.

The main challenge for electrospinning is to break into the nano-world in true sense (<100 nm). The mechanical and physical properties of nano-world can be fully realized only when fibers are in this range [89]. As an example, natural spider silk that is synthesized as 20 nm fiber is the toughest material on earth today but electrospun silk fibroin is nowhere close. It is the view of the authors that unless the electrospinning technology evolves to generate <100 nm fibers the full potential of this process will not be realized. Gu et al. evaluated the mechanical properties of a single electrospun fiber of polyacrylonitrile by atomic force microscopy and found increased moduli with increasing voltage. They hypothesized that higher voltage during electrospinning causes the jet to accelerate faster resulting in greater elongation force and orientation of the polymer chains in a fiber, contributing to increased modulus [90].

Keeping in pace with theoretical understanding of the process of electrospinning, its application in tissue engineering has resulted in the development of scaffolds intended for a wide variety of tissue-specific scaffolds. Excellent in depth reviews about the use of electrospinning for tissue engineering applications are available [32, 91, 92] and this article does not attempt to recapture the same detail. The most obvious advantage of electrospinning as a fabrication strategy is the wide choice it offers in terms of polymer (synthetic and natural) composition, concentration and in turn the fiber diameter, alignment and density of the scaffolds.

Synthetic materials offer the advantages of low cost, batch to batch consistency, control over mechanical properties and degradation rates. A variety of synthetic polymers including poly(lactic acid) (PLA), poly(glycolic acid) (PGA) [93], poly(lactide-co-glycolide) (PLGA) copolymers [94], polydioxanone (PDO) [95], polycaprolactone (PCL) [82] and different blends of PLA-PCL [96] have been successfully electrospun to yield scaffolds with diverse physical, mechanical and biological properties. The strength of electrospinning lies in generating a plethora of scaffold types which in turn helps in tailoring the scaffolds to suit different needs.

Scaffolds made from natural ECM proteins offer the advantage of increased cytocompatibility and enhanced cell function. In an effort to make bio-mimetic tissue replacements, there has been continued interest in using natural proteins for tissue engineering applications. Various types of collagen and elastin are the primary structural ECM proteins and efforts to electrospin these proteins have been successful. Matthews et al. electrospun type I collagen, isolated and purified from bovine skin and demonstrated preservation of characteristic 67 nm banding with TEM **(Figure 4C).** The fiber diameter varied as a function of starting concentration and these scaffolds had to be cross-linked to render mechanical stability [97]. Recently, however, Zeugolis et al. have shown that the use of fluroalcohols used in electrospinning destroys the secondary structure of native collagen [98] and thus leads to loss of all biologic function. However, our laboratory has evaluated immune responses to electrospun gelatin and collagen following intramuscular implantation in rats and found completely different host responses to these two biomaterials. Collagen scaffolds became integrated to the tissues and showed complete

infiltration but gelatin scaffolds showed chronic inflammatory response. It is the view of the authors that these organic solvents might lead to partial denaturation of proteins or simply place the collagen molecule in a thermodynamically stable conformation [99]. In addition to type I collagen, types II and III, elastin, glycosaminoglycans, globular proteins, fibrinogen have all been electrospun to form non-woven mats [32].

2.4. ELECTROSPUN BONE TISSUE ENGINEERING SCAFFOLDS

Materials that have been used in electrospinning bone scaffolds can be classified into ceramics, synthetic or natural polymers used either alone or as a composite with inorganic fillers.

2.4.1. Bioactive Glasses:

Bioactive glasses are an interesting class of ceramics that can form chemical bond with the host bone at the interface. Such materials have been used in bone replacement therapies predominantly in bulk form. In one study, precursor solution containing calcium and phosphate in the molar ratio of 1.67 was mixed with a high molecular weight polymer and electrospun. Subsequent heat treatment and calcination decomposed the polymer to yield pure HA fibers [101]. Kim et al., electrospun sol-gel precursor solution mixed with poly vinyl butyral to generate nano fibers of HA and fluoridated apatite (fHA). The fibers were heated at the rate of 1^{o}C/min to 700^{o}C and held for 2 hours to remove any polymer components and to induce crystallization of HA and fHA [102]. Subsequently, they developed a novel composite by hybridizing heat treated electrospun bioactive glass nanofiber with reconstituted type I collagen solution. The sol was processed differently and

lyophilized to yield membranes or thick scaffolds. Incubation of these scaffolds on simulated body fluid for 7 days resulted in formation of nanocrystalline carbonated apatites that were chemically bonded to the scaffolds. Osteoblasts cultured on bioactive scaffolds showed enhanced function (alkaline phosphatase assay) compared to those cultured on collagen scaffolds [103].

Alumina and stabilized Zirconia has been used as bioinert ceramic for total hip replacements because of its superior mechanical properties and excellent biocompatibility. A recent study proved the possibility of electrospinning zirconia from an aqueous based suspension of PEO:PEG and it would be interesting to observe if the results could be exploited in tissue engineering [104].

2.4.2. Hydroxyapatite (HA) based scaffold systems:

Bone is a composite of organic collagenous matrix, inorganic hydroxyapatite (HA)/ carbonated apatite (CA) and non-collagenous proteins. Hydroxyapatite, being the normal mineral of calcified tissues including bone, development of HA based scaffolds is being intensely studied. The biological effects of HA including promoting osteoblast adhesion and stem cell differentiation, is limited by its brittleness in bulk form. Polymer:HA composites have been a huge effort designed to couple superior handling and mechanical properties of polymers with biological activity of HA/CA.

2.4.3. ε-Polycaprolactone based systems:

Polycaprolactone has been popular for bone engineering scaffolds because of its biocompatibility, slow degradation and the ease of electrospinning from a variety of solvents. MSCs from rats cultured on electrospun PCL scaffolds supplemented with

osteogenic media for 4 weeks showed complete penetration of the scaffolds with the formation of multilayers, mineralization and collagen I were detected by von Kossa and immunostaining respectively [105]. Incorporation of calcium carbonate and HA powders to the polymer solution resulted in slight increase in the mechanical properties and fiber diameters but did not affect the biocompatibility [106]. Another interesting application of PCL:$CaCO_3$ is guided bone regeneration membranes for periodontal surgery. A bi-layered composite containing a carbonate rich functional layer and a PCL rich mechanical support layer has been developed but has needs further characterization [107].

2.4.4. Chitosan based polymers:

Chitin is the second most abundant carbohydrate next to cellulose and its deacetylated product is chitosan. Its derivatives have been long recognized for its antifungal properties and its ability to induce protease inhibitors in plants [108]. One of the earliest medical applications of chitosan was hemodialysis membranes [109] due to its biocompatibility, high mechanical strength, film forming ability and non toxic degradation products. Recently evidence point to role of chitin in the induction of fibroblasts and angiogenesis [110] suggesting a role in immunity. Electrospinning chitosan:PEO blends from acetic acid solutions has been successful [111, 112] and a preliminary investigation into 90:10 PEO:chitosan blend showed that the scaffold is non-toxic and osteoblast spreading in culture is optimal [113].

2.4.5. Silk fibroin based scaffolds:

Silk, a natural fiber extracted from cocoons of silk worms (Bombyx mori) has long been used as sutures because of its excellent mechanical properties and biocompatibility.

Functional 3D scaffolds generated by solvent casting-particulate leaching showed that these are superior to collagen scaffolds in inducing bone-like tissue *in vitro* [114]. Electrospinning parameters for silk fibroin solutions blended with PEO was first reported by Jin et al., for the generation of submicron sized fibers [115]. In a later study, silk fibroin-PEO based blends were electrospun with or without BMP-2 and nano HA and seeded with h-MSCs and cultured for 4 weeks. Significantly higher levels of calcium deposition, DNA content and elevated levels of mRNA bone marker transcripts were observed in silk-PEO scaffolds functionalized with BMP-2 and HA suggesting electrospun silk-based scaffolds can be used as good delivery systems for cytokines and growth factors [116].

2.4.6. Inorganic polymers: Polyphosphazenes

In contrast to organic polymers that have C-C bonds as the backbone, phosphazenes are inorganic polymers that alternate double bonds between phosphorus and nitrogen backbone. This inorganic backbone gives these compounds desirable properties like optical, thermal and oxidative stability in addition to superior mechanical properties. The versatility of this system is greatly increased by the customizing the organic functional groups to the phosphorus atom of the backbone. Though phosphazenes for tissue engineering applications was first introduced in early nineties [117], electrospinning phosphazenes for bone scaffolds has been reported recently. Laurencin et al., successfully electrospun a solution of polyphosphazene that was loaded 50-90% w/w with nano-crystalline hydroxyapatite and concluded that incorporation of nHA was maximal with a theoretical loading of 50% [118].

2.4.7 Starch based systems

Starch represents an abundant natural biomaterial that degrades into low molecular weight chains of maltose and fructose and has been investigated for biomedical applications including tissue engineering scaffolds. Blending corn starch (S) with organic synthetic polymers-ethylene vinyl glycol (SEVA-C), ε-poly(caprolactone) (SPCL), poly(lactic acid) (SPLA) and inorganic HA has resulted in a wide variety of biomaterials for tissue engineering applications [119, 120]. Fiber bonding and melt based technologies has been used to fabricate starch based matrices yielding micron sized fibers. Recently, electrospinning was used to impregnate nanofibers into porous SPCL in an effort to simulate the native ECM organization. Osteoblast-like cells and bone marrow stem cells showed significant increase in viability and activity on combination scaffolds than on pure fiber-bonded scaffolds [121].

2.5. CONCLUSION

It is now common knowledge that nano-scaled materials have properties that are remarkably different compared to macroscopic systems. High strength, thermal and electric conductivity, surface energy and reactivity are some of the features that make nano-engineering a modern revolution. The field of tissue engineering has been very quick to adopt these principles of nanotechnology and has come a long way in a relatively short span of time. Electrospinning along with self assembly and phase separation are tools that are currently available that allow tissue engineers to explore the avenues of nanoworld. Each of these techniques has something to offer that others fall short of. There is no doubt

in the minds of the authors that continued research will increase the potency of existing techniques and will introduce new ones in the coming decade. The recent explosion in the number of publications and unified global efforts to view the macroscopic world from a nano-scaled lens will act as a catalyst in exploiting these findings for best use in tissue engineering and regenerative medicine.

Advances in preventive medicine (e.g. vaccines) and surgical care have undoubtedly increased the mean life expectancy around the world. With increasing mean patient age, the focus of future therapeutic approaches must now shift from ensuring patient survival to improving the quality of life. Regenerative medicine and tissue engineering are scientific disciplines that specifically arose to meet this challenge but unfortunately advances in patient care are not being paralleled by corresponding contributions from these fields. In spite of intense research for over a decade, the biggest challenge in tissue engineering has been overcoming the barrier between bench work and bedside. This said there is continued expectation from medical professionals and patients alike and translating this promise to patients will be the priority in coming decades.

The techniques discussed in this review are expected to be refined and expand in versatility. Experiments in self assembly of collagen triple helices already point to important clues about the role of extracellular matrix on calcification in normal and pathological states. These lessons from biology will be exploited in designing tissue-specific scaffolds. Phase separation process, though inexpensive, is limited by the number of polymers that could be used. In addition, the specific parameters that would yield fibrous morphology are yet not understood, even though scientific theories explaining the

process exist. In the field of electrospinning, two obvious challenges are to break into the nanoworld (<100 nm) and to address the issue of use of volatile organic solvents. Even though self-assembly, phase separation and electrospinning can yield nanofibrous structures, the operational window is pretty narrow and more importantly, the operator has little or no control over the orientation and organization of these nanofibers into macroscopic structures. Complementary research in nano-engineering, including nano-printing, will provide new routes that offer more precise 3D control over the fabrication process. One major thrust of future research would be to find avenues to make any or all of these processes compatible for large scale-up without losing control over the higher spatial organization of nanofibers. Rapid advances in stem cell biology and the use of *in vivo* mimicking bioreactors for cell and organ culture, for instance, create unforeseen possibilities to make living organ substitutes a reality within the next decade.

2.6. EXECUTIVE SUMMARY

The function of native ECM is intrinsically linked to its form.

- Native ECM is an assembly of nano-scaled fibers that are at least an order of magnitude smaller than the cells themselves.
- Structural organization aside, it has domains that interact very closely with the cells that reside in its vicinity.
- Tissue engineering attempts to create tissue/organ-specific ECM analogues (scaffolds) in terms of structure, dimensions and composition.

Current fabrication strategies to generate nanofibrous scaffolds include

Self Assembly:

- Biomimetic
- Spontaneous organization of individual molecules into progressively higher-order structures.
- Scaffolds generated by this process are completely biocompatible (made from natural biological molecules) and form true nanofibers (<100 nm).
- Limitations include scaling-up and use of small peptide fragments.

Phase Separation:

- Simple technique and does not require expensive equipments.
- Easy to obtain batch to batch consistency.
- Limitations include restricted choice of polymers and scale-up.

Electrospinning:

- Easy, versatile, amenable to scale-up and currently most popular.
- Criticisms include generation of fibers with diameters that are in the upper limit of ECM.
- Offers no precise control over the orientation and organization of fibers during development of macro-scale structures.

Chapter 3: MULTIPLE FACTOR INTERACTIONS IN BIOMIMETIC MINERALIZATION OF ELECTROSPUN SCAFFOLDS

Preface: The following section has been published in Biomaterials, October 2009, Vol.30, Issue 29, 5456-5464.

3.1. ABSTRACT

One of the major limitations in scaffold-based bone tissue engineering has been the inability to increase the loading of biologically active inorganic mineral. The present study introduces a novel two-step strategy to increase overall mineral content of electrospun scaffolds and employs multiple factor interaction as a statistic to identify the combination of factors that yields maximal scaffold mineralization. Different amounts of nHA (0, 10, 25 and 50% by wt. of polymer) were electrospun in combination with polydioxanone (PDO) or poly(glycolide:lactide) to generate composite scaffolds. Successful incorporation of nHA within, on and in between nanofibers was confirmed by transmission and scanning electron microscopy. These scaffolds were immersed in different types (conventional, revised, ionic and modified) of simulated body fluid (SBF), prepared at 1x and 4x concentrations and the incubation was carried out either in static or dynamic setting at biomimetic conditions. At 2 weeks, the total amount of mineral within the scaffold was quantified using a modified alizarin red-based assay. Each of the five independent factors was analyzed independently and tested for interaction using random effects ANOVA. Statistics revealed significant higher order interactions among factors and the combination of PDO containing 50% nHA incubated in 1x revised SBF resulted in maximum mineralization.

3.2. INTRODUCTION

Bone is a composite material composed of organic collagenous matrix and inorganic nanocrystalline hydroxyapatite (nHA). The interaction between these phases begins at the nanoscale when platelet-like HA crystals nucleate the gap regions of collagen fibrils [122, 123] and elongate along the long axis of the fiber to form a mineralized collagen fibril. Such an intimate association of dissimilar material phases is preserved through hierarchical structure and gives bone its unique mechanical properties: high strength, high fracture toughness and low stiffness [124, 125]. The ability of bones to undergo cell mediated resorption and remodeling is critical in load bearing situations and maintaining calcium homeostasis.

Structural bone substitutes made from ceramics, metals and polymers have been popular in load-bearing bone and joint prostheses but problems of wear debris, corrosion, stress-shielding and inadequate integration are still relevant. Efforts to achieve a strong interface between a biomaterial and the host bone resulted in identifying a class of ceramics called bio-glass. These compounds can form a chemical bond to the bone by virtue of forming a calcium-apatite film on the surface [126, 127]. Since this discovery, coating of bone implants with HA (or some form of ceramic) have been successfully exploited to induce osseointegration at the interface [128-130]. However, since ceramic coating (by plasma-spraying, sputtering or electrophoresis) requires the biomaterial to be heat resistant or electrically conductive, success of this approach is restricted to metals having simple shapes [131].

In contrast to conventional methods of incorporating ceramic that involves high temperature treatment, Abe et al. demonstrated new mineral deposition at low temperature by immersion of a biomaterial in an aqueous solution of ions [131]. This method was termed biomimetic because it involved incubation in simulated body fluid (whose ionic concentrations are roughly equal to that of plasma) and mineralization occurred at physiological temperature and pressure. Since such mineralization can occur on any biomaterial, independent of shape, structure or composition and in a temperature range consistent with the glass transition temperature of biocompatible synthetic polymers, we adopted this strategy to increase the mineral content in synthetic polymeric scaffolds. In addition, since low temperature precipitate of calcium phosphate is biologically active *in vivo*, composite bone scaffolds containing this form of apatite would be more amenable for bone tissue engineering.

Scaffold-based bone tissue engineering is a rapidly emerging field that focuses on developing biologically-based substitutes that integrate with and are eventually replaced by host bone [132]. It involves implantation of extracellular matrix (ECM) analogs that can simultaneously support cell function and provide structural support. Incorporation of nHA within the polymer matrix seems to be an attractive strategy in bone tissue engineering because the dispersal of stiff and brittle HA crystals within the tough organic polymer matrix would effectively inhibit crack propagation [133-135]. From a biological perspective, presence of hydroxyapatite enhances protein adsorption, improves osteoblast function [136, 137] and confer osteoconductivity [138] to scaffolds.

In the present study, we sought to increase the loading of HA mineral within electrospun scaffolds in two steps: 1) by directly incorporating nHA during electrospinning and 2) by subjecting these composite scaffolds to incubation with simulated body fluid (SBF). We hypothesized that in addition to directly contributing to overall mineral content, seeded nHA during electrospinning will act as nucleation sites during SBF treatment for further crystal growth. We tested this novel mineralization strategy on two synthetic polymers (polydioxanone and poly (lactide:glycolide)) containing 0, 10, 25 and 50% (by wt. of polymer) nHA. These scaffolds were then incubated in two concentrations (1x and 4x) of four types of simulated body fluids (conventional, revised, modified and ionic) under either static or dynamic conditions. Finally, we took a statistical approach to analyze the interactions effects of each of these variables to identify the best combination of factors that would yield maximum *in vitro* scaffold mineralization.

3.3. MATERIALS AND METHODS

3.3.1. Characterization of Nanocrystalline Hydroxyapatite (nHA)

Commercially available nHA was purchased (Berkeley Advanced Biomaterials, Inc. San Leandro, CA) and crystal structure was confirmed to be hydroxyapatite by electron diffraction. The TEM evaluation shows a favorable elongated platelet-like structure that had crystal size in the range of 30-100 nm, similar to that found in bone. The results are presented in **Figure 6**.

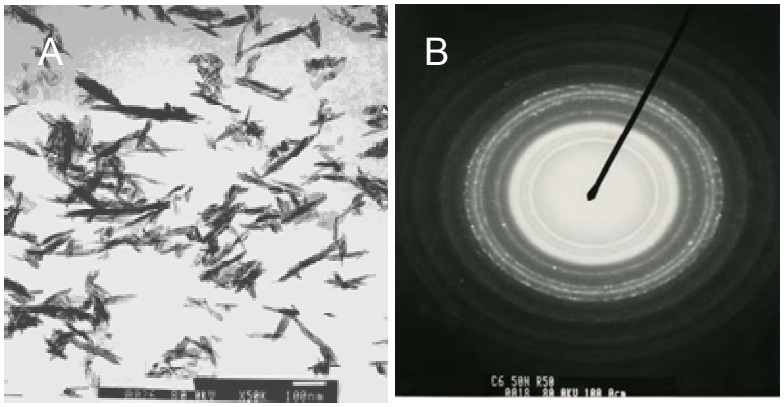

Figure 6: Initial characterization of commercially available nHA used in the study. **(A)** Transmission electron micrograph showing platelet-like crystals having sizes ranging from 30-100 nm. (**B)** Electron diffraction pattern confirming the crystal structure to be hydroxyapatite.

3.3.2. Composite Scaffold Preparation by Electrospinning:

Two different synthetic polymers - polydioxanone (PDO, Ethicon, Inc., NJ) and 85:15 poly(lactide-glycolide) (PLGA, Lakeshore Biomaterials, AL) were used for the study. The final concentration of the polymers was adjusted to 100 mg per ml of electrospinning solvent, 1, 1, 1, 3, 3, 3 hexafluoro-2-propanol (HFP) for all scaffold types. Different amounts of nHA (0, 10, 25 and 50% by wt. to polymer) were dispersed in HFP prior to addition of polymer and electrospinning. Since nHA crystals sedimented in HFP, stable dispersion of nHA was achieved by sonicating the solution in pulse mode (on: 50 sec, off: 10 sec) at 38% maximum amplitude using a tapered tip of a Cole-Palmer Ultrasonic Processor for 10 minutes. The stability of dispersion of nHA was confirmed after 2 hours by visual inspection before adding pre-weighed amounts of PDO or PLGA. Electrospinning conditions were optimized (rate: 7 ml/hour, air-gap distance: 20 cm, voltage: 22kV) to generate continuous non-woven composite nanofibers that were

collected onto a rotating rectangular mandrel (7.5 x 2.5 x 0.5 cm). After electrospinning, scaffolds were removed from the mandrel, dried in the hood for 30 minutes and 10 mm discs punched using a dermal biopsy punch. These discs were used for all mineralization experiments.

3.3.3. Transmission and Scanning Electron Microscopy:

Fibers were collected directly onto copper grids during electrospinning and analyzed using Jeol-JEM-1230 transmission electron microscope. For scanning electron microscopy, air-dried electrospun scaffolds were mounted on aluminum stubs, sputter coated with gold and examined at an accelerating voltage of 10kV using Zeiss EVO 50 XVP scanning electron microscope.

3.3.4. Biomimetic Mineralization with Simulated Body Fluid:

Four different types of simulated body fluids - conventional (c-SBF), revised (r-SBF), ionic (i-SBF) and modified (m-SBF) were prepared following a published protocol [139]. The ionic concentrations in these fluids vary with respect to chloride, bicarbonate and calcium. Each type of SBF was prepared in two concentrations (1x and 4x) to study the effect of increased ion concentration on scaffold mineralization. Electrospun scaffolds were incubated in SBF under two conditions: static and dynamic. In static condition, the discs were placed motionless in a tissue culture grade 24-well plate containing 3 ml of corresponding SBF while dynamic incubation involved using a 55ml slow lateral turning vessel (STLV) bioreactor (Synthecon, Inc., Houston, TX) rotating at 9 rpm. Both static and

dynamic experiments were performed in an incubator at 37°C in 5% CO_2 atmosphere for a total of 14 days with SBF solutions renewed every 5 days.

3.3.5. Quantification of Mineralization using Alizarin Red S (ARS):

The mineralization of scaffolds was quantified using a modification of a published protocol [140]. Alizarin Red S (Sigma, MO) was dissolved in deionized (DI) water to a final concentration of 40 mM and pH was adjusted to 4.1 using 1M NaOH. The solution was then filtered through a 0.8 µm mesh to remove any particulates and stored in the dark. After two week incubation, scaffolds were rinsed thrice for 10 minutes each in DI water, transferred into a new 24-well plate and fixed in 3.7% buffered formaldehyde for 30 minutes. The scaffolds were stained with an excess of Alizarin Red S (ARS) solution for 20 minutes on an orbital shaker, following which the scaffolds were rinsed repeatedly in DI water till all unbound dye was washed off (as evidenced by appearance of a clear wash solution). At this time, the scaffolds were transferred to a new plate and the bound dye solubilized with 50% acetic acid solution. After 30 minutes, the solubilized stain was pipetted out, diluted 1:4 in water, pH adjusted to 4.1 and the absorbance at 550 nm measured in a 96-well plate using SpectraMax Spectrophotometer (Molecular Devices).

3.3.6. Bovine Serum Albumin (BSA) Experiments:

Since plasma is necessary and sufficient to induce mineralization *in vivo*, we evaluated the ability of rSBF (whose ionic composition matches that of plasma) in the presence of albumin – the most abundant serum protein, at 40 g/L concentration [141]. An experiment was designed in which PDO and PLGA scaffolds containing different amounts

of nHA (0, 10, 25 and 50% by wt. of polymer) were incubated with 4x r-SBF with and without 4% BSA under static conditions at 37^{o}C in 5% CO_2 atmosphere. Freshly prepared solution was replenished every 5 days and ARS staining and quantification were done as described above.

3.7. Statistical Analysis:

The five-factor (2 scaffold types x 4 concentrations of nHA x 4 types of SBF x 2 concentrations of SBF x 2 incubation conditions) study (with n=3) yielded a total of 384 scaffolds. The resulting data was analyzed using random effects ANOVA. The outcome of interest was the mineralization after 2-week incubation as measured by alizarin red quantification. The ANOVA model included all the main effects and all possible interaction effects (2, 3, 4, 5 factor interactions). The statistical significance level was set at 5% level. Diagnostics were performed to verify the model assumptions (of normality and homoscadasticity) and to detect outliers. When warranted, transformation of the outcome was considered. The analyses were performed using Minitab 15® (Minitab Inc. PA) and JMP-7® (SAS, NC) software.

One-way ANOVA was performed and results analyzed for significance (α=0.05) to test effects of BSA on mineralization.

3.4. RESULTS

3.4.1. Electron Microscopy:

The transmission electron micrograph provides evidence for the presence of inorganic mineral within the fiber. Pure polymer fiber when examined by TEM is

characterized by a lack of contrast and homogeneous density **(Figure 7A)**, whereas a composite fiber containing both nHA and polymer exhibits a stark contrast between electron-dense inorganic crystals against the pale polymer background. Since the diameter of the representative composite fiber in **Figure 7B** is around 150 nm, yet the longest dimension of the nanocrystals is around 100 nm, we observe a definite trend for elongated crystals to be aligned along the length of the polymer fiber. The SEM shows individual fibers that are not uniform and also discrete clustered aggregates in between fibers. This suggests the presence of hydroxyapatite within, on and in between the surface of fibers **(Figure 7C)**. Hence, the strategy of electrospinning nHA along with the polymer results in oriented incorporation of crystals within the individual fibers as well as random distribution throughout the 3D scaffold.

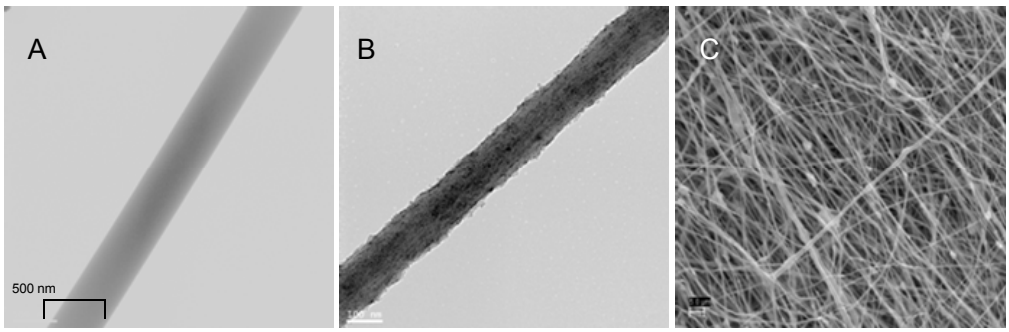

Figure 7: A and B. Transmission electron micrographs confirming successful incorporation of nHA within the electrospun PLGA polymer **(A)** and PLGA-nHA composite scaffolds **(B)**. Note the uniform density of pure polymeric fiber in A. In contrast, fibers containing nHA show a high contrast due to the presence of dense inorganic nHA crystals within the polymeric fiber (scale bar = 100nm). **C** Scanning electron micrograph of the composite scaffold showing irregular particulates on and between individual fibers (scale bar = 5μm).

Scaffolds incubated in different SBFs were analyzed for mineral deposits after 2 weeks by SEM. All scaffolds exhibited mineral deposition to some degree. Whereas some scaffolds showed significant deposits, others had a limited mineralization. **Figure 8** shows

representative PDO and PLGA scaffolds incubated in revised and ionic SBFs that represent the conditions of maximum and minimum mineralization (as confirmed by quantification with alizarin red staining). It can be observed that PLGA scaffolds under both conditions exhibit a surface or layered deposition whereas PDO scaffolds demonstrate mineralization of individual fibers. This observation could partially account for the difference in actual amount of mineral deposited in these two synthetic polymeric scaffolds.

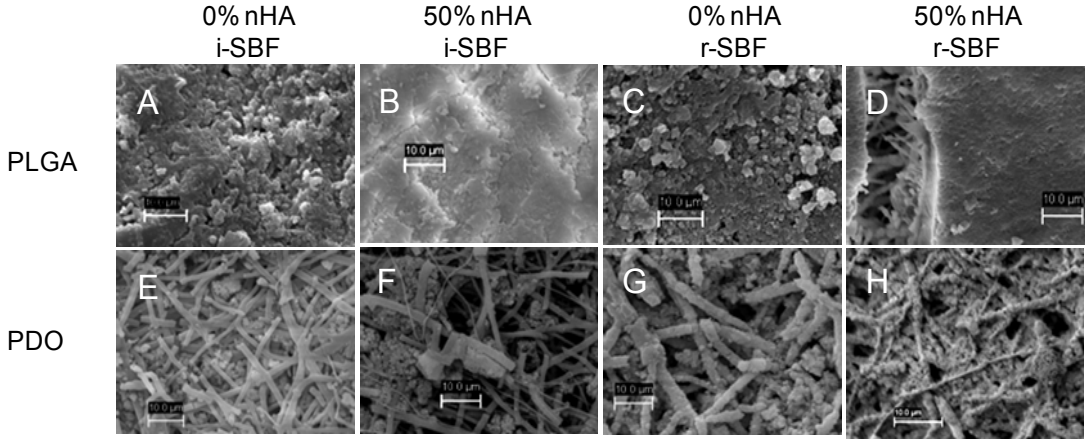

Figure 8: Scanning electron micrographs of electrospun PLGA (top) and PDO (bottom) scaffolds containing 0% and 50% of nHA incubated in i-SBF and r-SBF for 2 weeks. These conditions represent respectively the combination of factors that resulted in minimal **(A)** and maximal **(H)** scaffold mineralization as determined by ARS. PLGA scaffolds show a dense aggregation of mineral restricted to the surface. This is most evident in **D** where even though surface fibers and pores are obliterated by mineral deposition, individual fibers away from the surface do not show signs of mineralization. In contrast, PDO scaffolds exhibit retention of fiber structure and pores on the surface. Yet, mineralization of individual fibers results in greater overall mineral content.

3.4.2. Alizarin Red S (ARS) Staining Quantification- Initial Validation:

Our first efforts were directed to optimize the ARS staining and quantification of hydroxyapatite present in electrospun 3D scaffolds. We electrospun different amounts of nHA (0, 10, 25 and 50 % by wt. of polymer) dispersed in solution of PLGA and PDO to

generate a variety of composite scaffolds. These scaffolds were directly stained with ARS (without subjecting to SBF treatment) to investigate if the staining and quantification protocol is sensitive enough to detect the mineral incorporated during electrospinning. The results shown in **Figure 9** indicate that staining intensity of ARS (measured by absorbance) increased linearly (R^2=0.9477) as a function of amount of nHA added to polymer solution. These data validates the ARS to detect and quantify the amount of mineral present in a 3D scaffold.

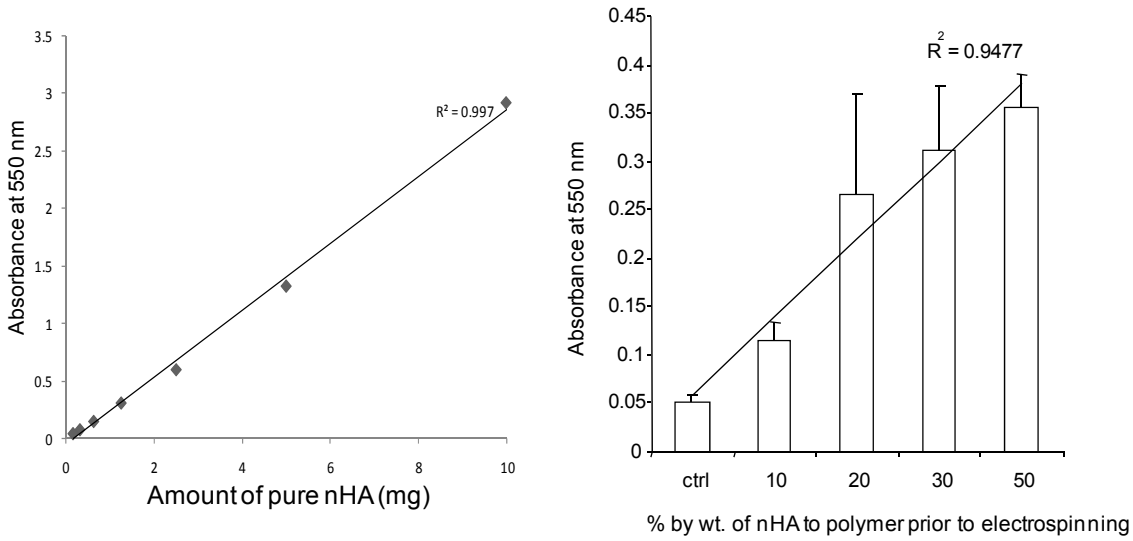

Figure 9: Plot of absorbance (at 550 nm) as a function of amount of pure nHA. **A.** 1:2 serial dilution of nHA dispersed in water was used to quantify the absolute amount of nHA using the alizarin red staining described in the methods section. **B.** PDO was added to a dispersed solution of nHA containing different amounts of nHA and electrospun to generate composite scaffolds. Quantification with Alizarin red shows a good correlation between increasing amounts of nHA and absorbance. This data validates alizarin red staining assay to quantify the amount of mineral even in 3D electrospun scaffolds.

3.4.3. Multiple Factor Interaction:

In the present study, we stained the mineralized scaffolds with Alizarin red S, solubilized the stain in acetic acid and measured the absorbance of this solution at 550 nm (peak absorbance of alizarin red). Hence, absorbance at 550 nm indirectly represents the amount of mineral present within the scaffolds and is the only dependent variable. Since the distribution of residuals revealed non-linearity, logarithmic transformation of actual absorbance values was performed and was used as an indicator of outcome for quantitative purposes. The five independent factors (with corresponding levels in parentheses) represented alphabetically from A-E are: **A**. scaffold type (PDO, PLGA), **B**. concentration of nHA (0, 10, 25 and 50 % by wt), **C.** type of SBF (c-, r-, i-, m- SBF), **D**. concentration of SBF (1x and 4x) and **E**. incubation conditions (static and dynamic).

If the experimental design involves study of more than one independent variable (factor), there is always an interaction within the factors that affects the outcome, whether significant or not. Interaction effect analyzes the effect of one factor on the outcome at various levels of another factor. In contrast, main effects analyze the influence of a factor averaging over the levels of another factor. The presence of significant interaction implies that the main effects are not additive, suggesting potential synergy or antagonism between them. This makes the interpretation (of multiple factor experiment) solely based on main effects at best incomplete or at worst misleading. Hence, the rule of thumb in statistics is to interpret significant highest factor interactions first before examining the lower factor interactions or main effects. As an inference, higher order significant interactions represent the most complete explanation of the observed effects. The interaction effects in the

present study were analyzed with ANOVA to detect, estimate and quantify the strength of interaction among different factors.

The ANOVA results regarding the significance of the 5 main effects, ten 2-way, nine 3-way, five 4-way and one 5-way interaction on the outcome are presented in **Table 1**. Significance was observed on all main effects and 2-way interactions. All 3-way interactions except two and all 4-way interactions with the exception of one were significant. In the present study, the highest factor interactions that were significant involved four factors. Of the four 4-factor interactions possible: ABCD, ABCE, ABDE and BCDE, only ABDE was not significant at α=0.05. All these are presented in a graphical format in the **Figure 10**. Log (abs 550 nm), a direct measure of mineralization, is the outcome plotted along the Y-axis in all the graphs. We explain one such interaction (ABCD) in detail, while reminding the readers that others are interpreted in the same way.

TABLE 1: A table of significance of 5 factor interaction on mineralization (absorbance). All levels of interactions are statistically significant with the exception of three indicated by # ($p<0.05$).

General Linear Model: Log (Abs at 550nm) versus Factors A, B, C, D, E (defined below)

Factor	Levels	Values
A (Scaffold type)	2	PDO, PLGA
B (Concentration of nHA)	4	0, 10, 25, 50
C (Type of SBF)	4	c-SBF, i-SBF, m-SBF, r-SBF
D (Concentration of SBF)	2	1X, 4X
E (Incubation condition)	2	Dynamic, Static

Analysis of Variance for F, using Adjusted SS (sum of squares) for Tests

Source	DF	Sequential Sum of squares (Seq.SS)	Adjusted Sum of squares (Adj. SS)	Adjusted mean squares (Adj. MS)	F	P
A	1	35.06241	23.29145	23.29145	1590.45	0.000
B	3	14.94664	11.56914	3.85638	263.33	0.000
C	3	8.00487	7.48796	2.49599	170.44	0.000
D	1	1.44741	2.09424	2.09424	143.00	0.000
E	1	0.36104	0.80221	0.80221	54.78	0.000
A*B	3	2.76068	2.03271	0.67757	46.27	0.000
A*C	3	2.03314	2.15947	0.71982	49.15	0.000
A*D	1	2.92773	1.37451	1.37451	93.86	0.000
A*E	1	0.00530	0.16470	0.16470	11.25	0.001
B*C	9	0.98436	0.64365	0.07152	4.88	0.000
B*D	3	0.45471	0.45952	0.15317	10.46	0.000
B*E	3	0.61600	0.58263	0.19421	13.26	0.000
C*D	3	5.65736	5.30811	1.76937	120.82	0.000
C*E	3	1.25085	1.11209	0.37070	25.31	0.000
D*E	1	0.45216	0.20719	0.20719	14.15	0.000
A*B*C	9	0.60151	0.45650	0.05072	3.46	0.000
A*B*D	3	2.51492	1.91830	0.63943	43.66	0.000
A*B*E	3	0.40203	0.40133	0.13378	9.13	0.000
A*C*D	3	1.50544	1.37150	0.45717	31.22	0.000
A*C*E	3	0.50891	0.51267	0.17089	11.67	0.000
A*D*E	1	0.08604	0.09686	0.09686	6.61	0.011
B*C*D	9	0.72171	0.71566	0.07952	5.43	0.000
B*C*E	9	1.31584	1.32582	0.14731	10.06	0.000
B*D*E	3	0.04798	0.03862	0.01287	0.88	0.452 #
C*D*E	3	0.07061	0.07061	0.02354	1.61	0.188 #
A*B*C*D	9	0.64875	0.66051	0.07339	5.01	0.000
A*B*C*E	9	0.92130	0.84690	0.09410	6.43	0.000
A*B*D*E	3	0.01364	0.00832	0.00277	0.19	0.904 #
B*C*D*E	9	0.76570	0.76570	0.08508	5.81	0.000
Error	256	3.74902	3.74902	0.01464		
Total	371	90.83806				

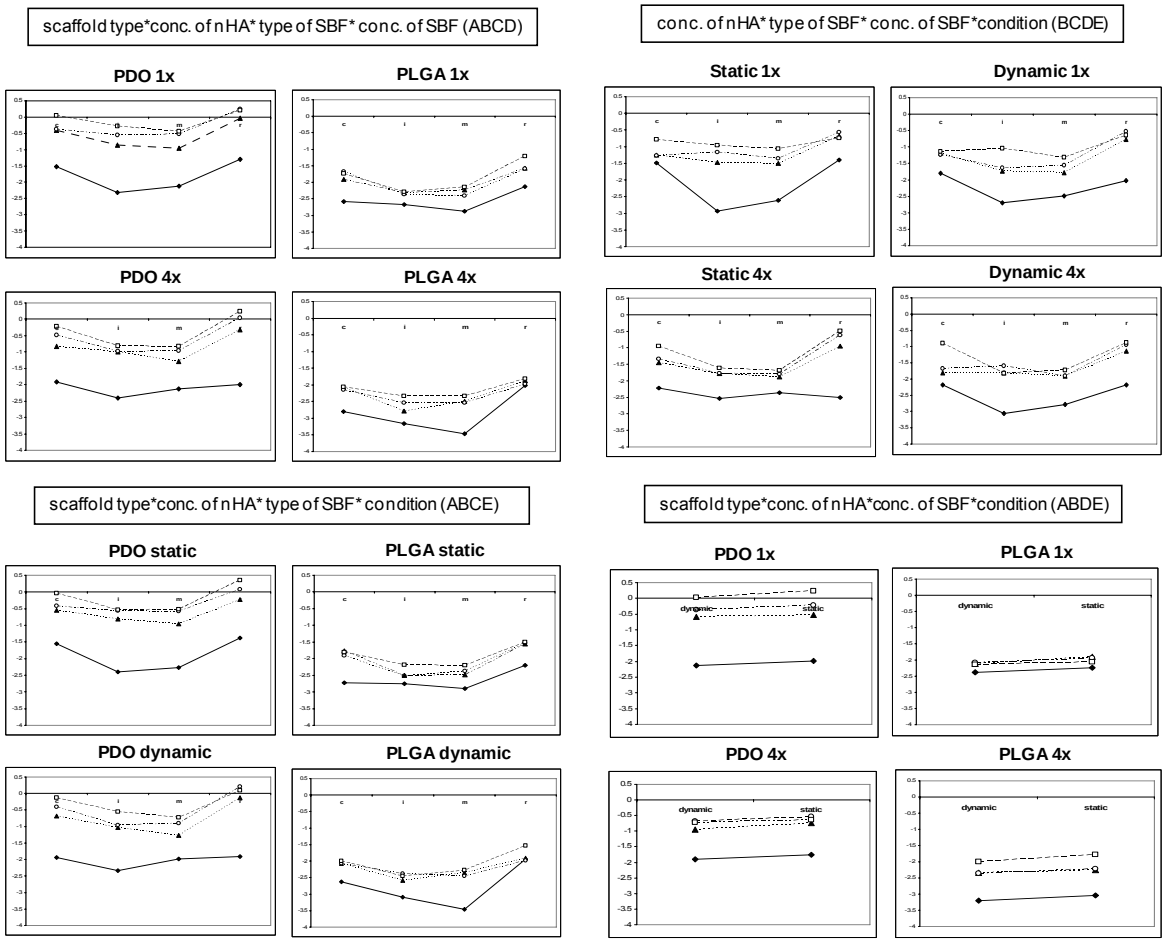

Figure 10: Four factor interaction graphs of biomimetic mineralization of electrospun scaffolds. In multiple factor interaction study, interpretation of highest factor interactions (4 factors here) that are significant accounts for the observed effects. The Y-axis log (absorbance at 550 nm), reflects mineralization. Different concentrations of nHA incorporated are represented as: 0% (filled diamonds), 10% (open circles), 25% (filled triangles) and 50% (open squares). Different types of SBF (c, i, m and r) are labeled along X-axis. The interaction effects observed are quantitative changes in the amount of mineralization. While three interactions are significant, A*B*D*E is non-significant. Note similar trends, superior performance of PDO, greatest mineralization with 50% nHA and r-SBF. While 1x is better than 4x in all kinds of SBF, static or dynamic incubation conditions do not significantly affect the outcome.

The most obvious finding from the graphs of ABCD interaction is that the interaction effects are quantitative, rather than qualitative, in nature. This means the effect of one factor merely increases or decreases the outcome at different levels of another factor

without reversing trends or directions. More specifically, the following inferences emerge from the figure.

First, PDO is always superior to PLGA (in some cases by almost a factor) in its ability to mineralize under biomimetic conditions. This finding is significant, given the popularity of PLGA in bone tissue engineering. Since the tendency to mineralize increases with greater amounts of nHA added during electrospinning, our results indicate that simultaneous electrospinning of PDO and nHA is a successful strategy in bone tissue engineering. Current experiments in the lab are underway to exploit the two-step mineralization process to improve mechanical properties of bone engineering scaffolds.

Second, incorporation of nHA (**B**) during electrospinning significantly increases overall mineralization irrespective of scaffold type (**A**), type of SBF (**C**) or its concentration (**D**). Further, increasing amounts of nHA resulted in progressively greater mineralization, with 50% nHA containing scaffolds yielding the best outcome. This general trend supports our rationale that addition of nHA during electrospinning favors biomimetic mineralization by providing nucleation sites for mineral deposition.

With respect to different types of SBFs for their ability to mineralize electrospun polymeric scaffolds, i- and m-SBF are generally inferior to c- and r-SBF whether at 1x or 4x concentration. The superior performance of r-SBF is also independent of whether PDO or PLGA is used. This would mean that increased ionic density as a strategy to improve mineralization, i.e. use of 4x instead of 1x, is not necessarily advantageous and the use of 1x r-SBF is at least as good as a higher concentration.

To sum up, the combination of PDO containing 50% nHA incubated in 1x r-SBF for 2 weeks gives the maximum scaffold mineralization and with this specific set of parameters, it does not matter whether the incubation is done under static or dynamic conditions.

A full 2-way interaction plot matrix (containing all 10 interactions) is presented in **Figure 11** to give preliminary insight into the process and to verify the findings. The five independent factors are listed along the diagonal. The plot is symmetrical (mirror image) about this diagonal and hence it is typically sufficient to look at either one of the corresponding panels. Graphically, an interaction is identified by comparing the slopes of the lines: if the lines are parallel, there is no interaction; the greater the lines depart from being parallel, greater the degree of interaction. It can be inferred from the graph that there are significant interactions between different factors. One of the powerful attributes of interaction studies is that it enables one to identify the exact combination of factors that would represent the most favorable outcome. The set of parameters that yielded maximum mineralization of electrospun scaffolds are: PDO pre-seeded with 50% (by wt.) of nHA, incubated in 1x r-SBF under static conditions.

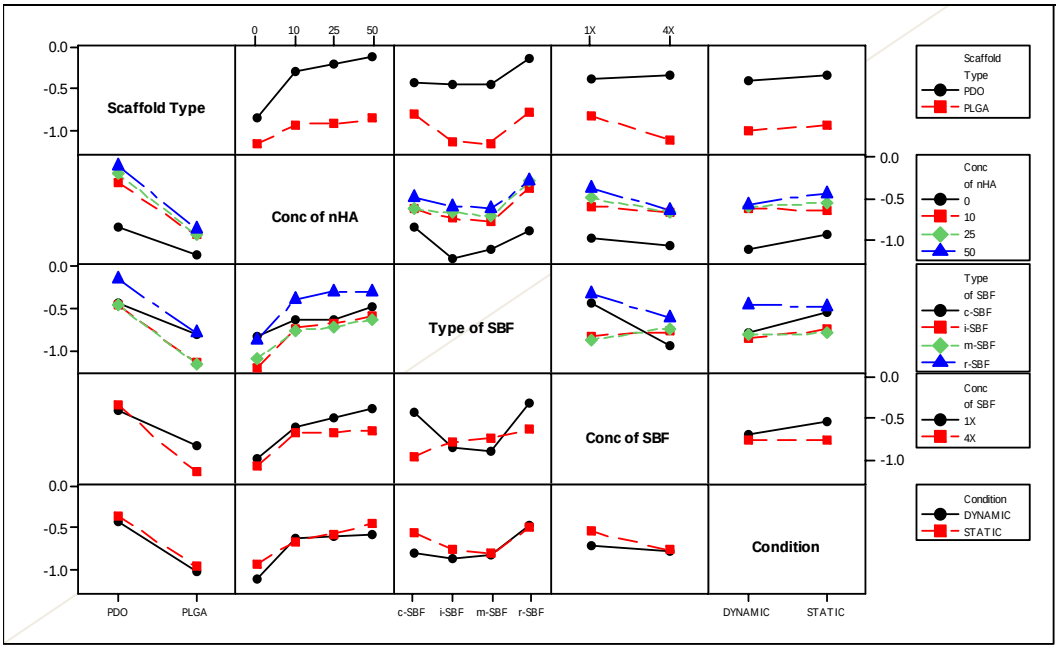

Figure 11: Two-factor interaction plot matrix demonstrating the presence and strength of interactions on mineralization, represented by log (absorbance at 550 nm). The five independent variables are listed along the diagonal and the ten possible two-factor interactions are plotted at the intersection of the corresponding factors. Interaction is present if the slopes of the lines are not parallel and greater this deviation from parallel, greater is the strength of interaction.

3.4.4. BSA Experiments:

The results of mineralization experiments in the presence and absence of BSA is presented in **Figure 12**. First, the previous finding with respect to the superior performance of PDO compared to PLGA was confirmed. Similarly, incorporation of nHA as part of scaffold fabrication during electrospinning is a successful strategy to increase the amount of mineral loaded in the electrospun scaffold. This confirms the rationale for a two step mineralization process. Further, the presence of BSA in the SBF always has a negative impact on the mineralization process. However the inhibitory effect of BSA is more pronounced on PDO scaffolds compared to PLGA scaffolds.

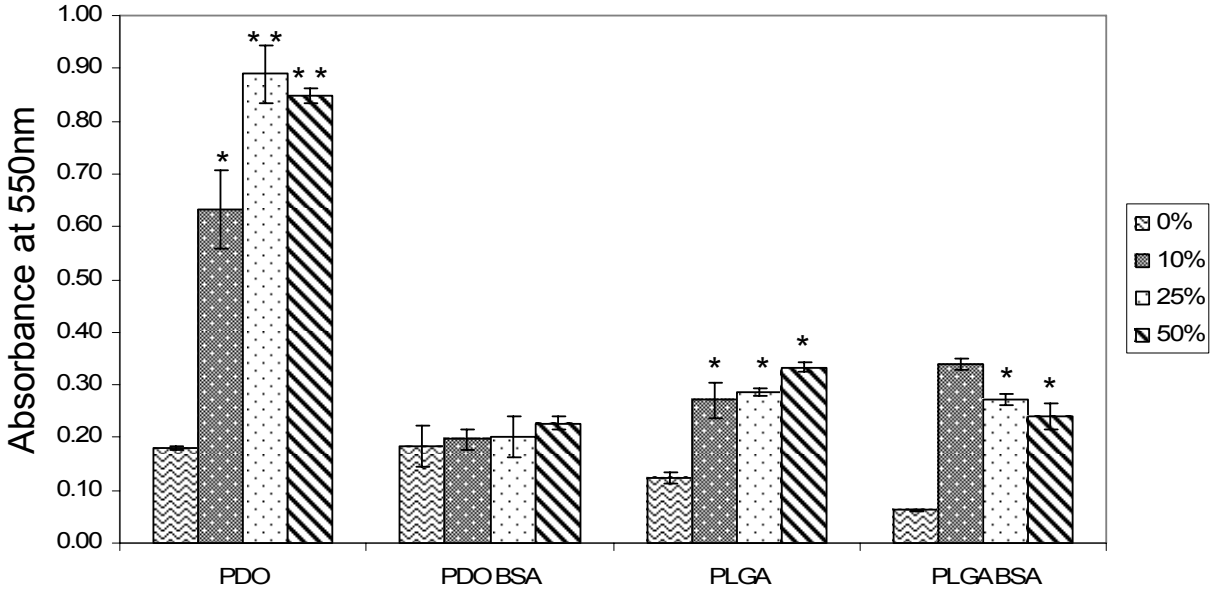

Figure 12: Effect of serum albumin on mineralization of PDO and PLGA scaffolds upon treatment with 4x r-SBF for 2 weeks. The data supports previous observations that mineralization of PDO is superior to PLGA scaffolds and increasing amounts of pre-seeded nHA results in greater mineralization. Interestingly, the inhibitory effect of BSA is more potent in nHA containing PDO scaffolds compared to PLGA scaffolds. This effect might be the result of adsorption of BSA onto nHA and subsequent masking of the critical nucleation sites.

3.5. DISCUSSION:

Calcium phosphates (CaP) have been used as a synthetic bone substitute for almost a century because they are the main constituents of bones and teeth. The family of CaP encompasses multiple compounds including but not restricted to dicalcium phosphate dihydrate, octacalcium phosphate, hydroxyapatite (HA), tricalcium phosphate (TCP), amorphous calcium phosphate (ACP) and carbonated apatite (CAP). These compounds vary mainly in the Ca:P ratio and the form commonly found in bone is carbonated apatite, otherwise referred to as bone apatite. Amorphous calcium phosphates are not normally found in mature hard tissues yet they are an important intermediate in the transition to more stable crystalline forms including hydroxyapatite [142]. Bohner [143] distinguishes

two types of CaP based on the temperature of synthesis: a high temperature sintered form (> 900^{o}C) and a low temperature precipitate (~37^{o}C). The compounds synthesized at low temperature exhibits more solubility, much greater surface area and are inherently more active in biological systems in contrast to biologically inert sintered versions. Solubility of low temperature precipitated HA which is a function of crystal size and foreign ion substitution, is closer to that of fast resorbing tricalcium phosphate. For example, carbonate ion substitution of HA results in the formation of highly soluble carbonated apatite. Sintered HA most commonly used in load-bearing orthopedic implants, on the other hand is not bio-resorbable as they are stable over a lifetime of the individual.

In this regard, it is important to realize that the bone mineral (biological apatite) are non-stoichiometric with different types and foreign ion substitution including sodium, magnesium, potassium, carbonate and fluoride. These substitutions make biological apatites different from stoichiometric hydroxyapatite which has only calcium and phosphate. Ion substitutions affect crystal morphology, decreases crystallinity and increases solubility [144]. This finding is of special relevance because the foundation of tissue engineering rests on the ability of a product to be remodeled and resorbed with time.

Plasma or the extracellular fluid is the source of the ions responsible for physiological and pathological mineralization *in vivo*. Kokubo and others [131, 145] developed a biologically relevant strategy of inducing new mineral formation using simulated body fluid (SBF) whose ion concentrations, pH and temperature are similar to that of human plasma. More importantly, they successfully demonstrated deposition of bone-like apatite on all major classes of biomaterials (ceramics, organic polymers and

metals) when incubated with SBF. Since this mineralization process occurred at biologically relevant pH (7.4) and temperature (37^{o}C), this was called biomimetic mineralization. The final apatite formed, in spite of having variable composition, is predominantly carbonated apatite with low crystallinity and is very similar to the form found in bone, a favorable factor from a tissue engineering perspective [146].

Recently, it has been shown that electrospun poly(l-lactic acid) (PLLA) scaffolds can be used as a substrate for hydroxyapatite mineralization. Chen et al. incubated electrospun PLLA scaffolds in SBF and performed an extensive characterization of the mineral deposited on the nanofiber surface over 4 weeks. They found that while the amount of mineral increased with time, its composition did not change. The predominant mineral deposited by biomimetic mineralization procedure was carbonated apatite [147]. While this work used SBF treatment to mineralize electrospun scaffolds, it differs significantly from the present study: incorporation of a significant amount of nHA during electrospinning (as much as 50% by wt. of polymer) which also primes these electrospun composite scaffolds for better mineralization by providing nucleation sites.

It was identified that the two factors critical to apatite mineralization are the availability of favorable nucleation sites coupled with localized super-saturation of calcium ions [148]. Spontaneous mineralization is seldom observed in meta-stable solutions of plasma or SBF in spite of them being supersaturated with respect to calcium and phosphate ions. This is because of presence of a high energy barrier for the nucleation event to occur. Since apatite mineralization follows the principles of heterogeneous nucleation, the presence, number and potency of nucleation sites are rate-limiting factors [149]. These

specialized areas of the substrate reduce the energy barrier sufficiently to allow nucleation to occur. Once stable nuclei have formed, subsequent crystal growth in solution is thermodynamically driven as long as concentration gradient for the ions exists.

Several approaches have been undertaken to exploit these observations to induce biomimetic mineralization onto substrates. One method is to functionalize the biomaterial surface with reactive groups like Si-OH [150], Ti-OH [151], COO- [152], that would provide nucleation sites for apatite formation. In this regard, some functional groups might be more potent than others in their ability to nucleate apatite crystals. An alternate approach aims at satisfying the second criteria for nucleation to occur: increasing the local concentration of calcium ions. This has been successful by pre-treatment of substrates with $CaCl_2$ or Ca $(OH)_2$ or by increasing the ionic activity product (using higher concentrations of SBF).

Our objective was to integrate both these requirements for mineralization based on the rationale that pre-seeded nHA crystals can act as stable nucleation sites for rapid crystal growth when incubated with SBF in addition to being a local reservoir of calcium ions. Such a strategy would preclude the dependence of mineralization on high energy and dynamic nucleation events by providing stable apatite nuclei. We devised a two-step mineralization process: incorporating nHA crystals within the nanofibrous scaffold during electrospinning (internal mineralization) followed by incubation in SBF (external mineralization) for 2 weeks. The total mineral content at the end of the experiment would be the sum of pre-seeded nHA, crystal growth on pre-seeded nHA as well as *de novo* mineralization of electrospun fiber.

Alizarin Red S is an anthraquinone derivative that forms a water-insoluble salt with calcium. It is a simple, sensitive and inexpensive method and has been routinely used as a qualitative assay for confirming the presence of calcium deposits. Even though the stain binds to calcium mineral in a quantitative manner, the inability to be accurate quantify the bound stain has been its major limitation. Recently, it has been shown that the stain can be solubilized and absorbance measured at 550 nm to quantify the mineral content in 2D culture plates [140]. Our study has successfully adapted this technique to study mineral content in porous 3D tissue engineering electrospun scaffolds. One caveat of using ARS to quantify mineral is that the stain cannot distinguish between different types of calcium phosphate crystals and hence further investigation and confirmation of these individual crystal types by X-ray photoelectron spectroscopy or X-ray diffraction techniques is needed.

Since internal mineralization was designed to incorporate nHA within the polymeric scaffold during electrospinning, initial characterization of commercially available nHA with respect to crystal morphology and size was performed. TEM showed elongated platelet-like morphology of these crystals with size ranging from 30-100 nm, similar to that observed in bone. Since typical electrospun fibers have a diameter in the range of 500-1000 nm, we reasoned that these crystals can be successfully incorporated within the fiber, if electrospinning conditions were optimized.

Efficient dispersal of nHA with the dissolved polymer solution is imperative for successful electrospinning of nHA-polymer composite scaffold. Commercially available nHA formed dense aggregates that sedimented out of solution when added to

electrospinning solvent (HFP). Effective dispersal of nHA in HFP was accomplished by sonication for 10 minutes in pulse mode to prevent overheating and evaporation of solvent. The stability of dispersion was confirmed by visual appearance of a homogeneous milky white appearance of the solution after 2 hours before appropriate amount of polymer was added. Electrospinning parameters were then optimized to generate continuous nanofibers. This sequence of dispersing nHA in the solvent prior to addition of polymer was done to prevent any inadvertent polymer breakdown during sonication.

External mineralization of scaffolds was accomplished by incubation with cell- and protein-free SBF that was designed to mimic plasma with respect to ionic concentrations, pH and temperature. The concentration of chloride and bicarbonate ions in the first prototype of SBF (conventional or c-SBF) differs from that of plasma sufficiently that it can induce apatite formation that is different from that of native bone-apatite. Subsequently, efforts were taken to produce SBFs whose inorganic ions concentration would more closely mimic plasma. These experiments resulted in generation of revised (r-SBF), ionic (i-SBF) and modified (m-SBF) versions of simulated body fluids. The r-SBF was designed to match plasma concentrations of every ion, while i-SBF have concentration of dissociated ions equal to that of plasma and m-SBF is similar to r-SBF except that the concentration of bicarbonate ions is decreased to the level of saturation with respect to calcium carbonate. We included these different compositions of SBFs in our study because each SBF represents one aspect of human plasma and the significance of one or the other in their ability to mineralize electrospun scaffolds has not yet been studied. Even though Oyane et al. [139] concluded that m-SBF was optimal for biomimetic mineralization, we

found that r-SBF gave the maximum mineralization under all conditions, while i- and m-behaved identical and were generally inferior. This apparent contradiction can be accounted for by the difference in our experimental design. The loss of biological activity reported was not observed in any of the SBFs until 2 weeks but became significant only in r- and i-SBFs over a period of 8 weeks. Since we replenished scaffolds with fresh SBF every 5 days, the loss of bioactivity was irrelevant and the changes observed indicate difference in intrinsic mineralization potential of various types of SBF. In addition to varying the types of SBF, the ionic product (IP) of SBFs were studied by repeating experiments with a higher concentration (4x versus. 1x). The results show a predictable increase in mineralization with increasing IP in PDO while PLGA scaffolds showed an opposite effect.

The most striking observation in our experiments has been the behavior of PDO vis-à-vis PLGA with respect to mineralization potential. The superior performance of PDO compared to PLGA can be attributed to the fact that PLGA scaffolds exhibited significant dimensional change (shrunk almost by 60% of its original size) while PDO retained its original form (**Figure 13**). This change is accompanied by a more dense aggregation of fibers and a dramatic decrease in available surface area. Such a structural change in the PLGA scaffold seems to induce overall surface mineralization of the scaffold rather than mineralization of individual fibers as confirmed by electron microscopy. In contrast, individual fibers can still be seen in PDO scaffolds at the end of incubation and mineral deposits are evident on these fibers.

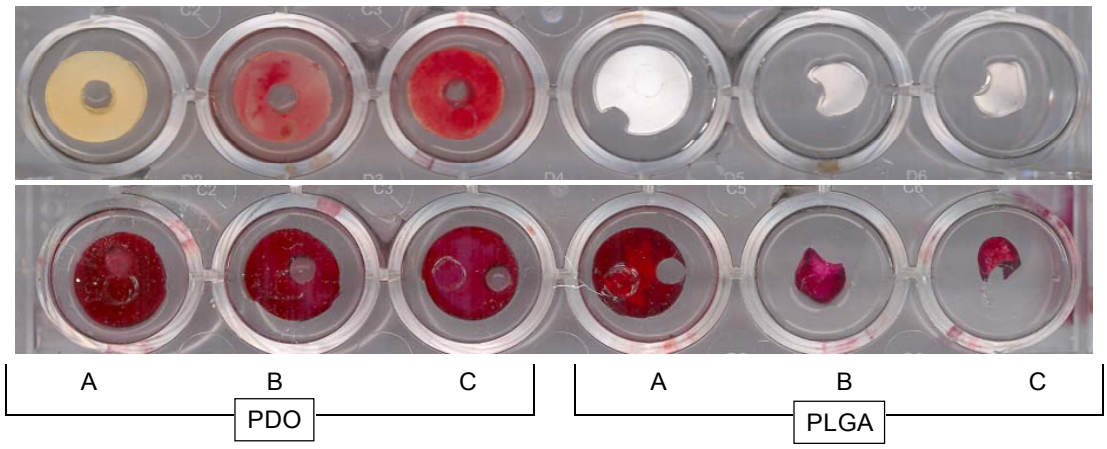

Figure 13: Effect of incubation conditions on mineralization of electrospun scaffolds containing 0% and 50% by wt. of nHA. All the scaffolds shown were incubated in 1x r-SBF for 15 days and stained with alizarin red to visually follow the mineralization. **A** represents incubation at 25°C in a closed environment, **B** incubation at 37°C in a closed environment and **C** incubation at 37°C open to 5% CO_2 atmosphere. It can be readily seen that the PLGA scaffolds exhibit a dramatic dimensional change at 37°C but not at room temperature. PDO scaffolds maintain their form irrespective of the temperature. The intensity of staining seen in nHA containing scaffolds (bottom row) represents both seeded nHA as well as new mineral deposited during SBF treatment. The defects observed in the scaffolds represent areas punched out for SEM evaluation prior to staining.

The cumulative mineral deposition from all the individual fibers seems to account for the significantly superior performance of PDO compared to PLGA scaffolds. Interestingly, the shrinkage in PLGA scaffolds is observed only under incubation at 37°C and not at room temperature. This change occured independently of exposure to CO_2. Another possible reason for inferior mineralization of PLGA scaffolds may lie in the chemistry of the polymer. The PLGA scaffolds used in the present study is ester-capped to delay degradation. The end capping of the polymer with lactic acid ethyl ester prevents formation of free terminal carboxyl groups which might otherwise initiate nucleation of calcium phosphate mineral and increase mineralization.

3.6. CONCLUSION:

A reliable quantitative assay for mineralization that occurs within porous 3D nanofibrous scaffolds has been successfully developed. Our strategy of incorporating mineral in two steps-first during electrospinning and later by incubation in simulated body fluids at physiological relevant temperature, pH and pressure is shown to be capable of inducing new mineral deposits on synthetic biocompatible polymers. Multiple-factor interaction statistics revealed some interesting insights into the mineralization behavior of electrospun polymeric scaffolds that led to identifying the best combination of factors that result in maximum mineralization. The amount of mineral deposited varies directly as a function of concentration of inorganic nHA seeded during electrospinning. This confirms our hypothesis that the nHA seeded act as nucleation sites for further crystal growth upon treatment with SBF. This nHA can act as a reservoir for calcium and phosphate providing localized super-saturation of these ions further facilitating new crystals to be formed. In addition, the two synthetic polymers tested-PDO and PLGA are markedly different in their ability to mineralize with PDO being superior. The r-SBF was the most efficient SBF in inducing mineralization of all types of substrates.

Chapter 4: MULTI-LAYERED ELECTROSPUN SCAFFOLDS - A NEW APPROACH

4.1. INTRODUCTION

Bone tissue engineering faces a twin challenge of satisfying mechanical and biological properties. Since bones play a vital role in bearing load and protecting internal organs, synthetic bone substitutes are subjected to considerable stresses following implantation. In this instance it is important to realize that precise matching of the physical properties of bone with synthetic substitutes is essential. It is becoming increasingly clear that materials that are stiffer than bone itself (metals, ceramics and plastics) contribute to a phenomenon called stress shielding. In this process, there is ineffective transfer of stresses between the high stiffness implant and the healthy bone, resulting in resorption of normal bone around the implant. Ultimately, secondary bone fractures occur and the implant fails. These occurrences further underline the importance of matching bone with the implant in terms of mechanical properties. In addition, such inert implants are not susceptible to physiological bone remodeling that might be induced by changing load patterns, parathyroid hormone and calcium homeostasis. It is the endeavor of tissue engineering to

address these vastly diverse requirements by providing a temporary scaffold that is mechanically strong enough to endure loads during the healing phase before being replaced by healthy host bone formed *de novo*.

One of the reasons metals, ceramics and polymers perform better under loading conditions is because these dense, non-porous materials have excellent bulk material properties. However, being biologically inert and not able to induce a specific cellular interaction is a serious limitation. Electrospun materials are inherently advantageous in this context because they are biocompatible and provide nanofibrillar topography for cells to attach, migrate and proliferate. Even though electrospinning offers great promise in generating biologically optimal scaffold with respect to its geometry, dimensions and to some extent composition, the fact that these scaffolds are more than 90% porous greatly facilitates the above process. However, porous materials have very poor mechanical properties. Efforts to improve the physical properties of electrospun scaffolds without compromising the advantages that the process renders are a pertinent area of research.

Bone is a structural composite with brittle, inorganic hydroxyapatite filler particles closely associated with a tough organic collagenous matrix. A strong bond between these two distinct phases ensures effective transfer of stresses, renders the material bone with excellent mechanical properties and also is critical for biological function. Given the role of hydroxyapatite in determining mechanical and biological properties, we sought to exploit findings of the previous study demonstrating successful incorporation of biological apatite onto electrospun scaffolds. In addition, we introduce pressure-welding as a novel strategy to improve the mechanical properties of electrospun scaffolds.

4.2. MATERIALS AND METHODS

4.2.1. Scaffold Preparation by Electrospinning:

PDO and PDO:nHA composite scaffolds were fabricated by electrospinning following the methods described earlier. Only the 50% nHA (by wt of PDO) was chosen for this study as it was shown to have maximum mineralization potential. Since PLGA was inferior to PDO it was not considered. In addition, control PDO scaffolds with no nHA incorporated were electrospun.

4.2.2. Scanning Electron Microscopy, SBF Treatment and Alizarin Red Staining:

Methods described in the previous section were followed. PDO and 50% PDO:nHA scaffolds were incubated in 1x r-SBF for 2 weeks under biomimetic conditions. Control scaffolds were incubated under similar conditions in DI water.

4.2.3. Pressure Welding:

Electrospun scaffolds were subjected to mineralization and compression in two different sequences: one set of electrospun scaffolds were compressed before mineralizing treatment with SBF (C1M2) while in the other group mineralization was performed first before compressing multiple layers (M1C2). The number of layers stacked during compression was either1, 2 or 4. All scaffolds were cut into flat rectangular sheets carefully avoiding any edges. These scaffolds were placed flush on top of each other on flat stainless steel blocks. These blocks were then placed in a mechanical hydraulic press (Carver Instruments) and subjected to 20,000 psi and the pressure held constant for a

period of one minute. After this the scaffolds were removed and either tested for mechanical properties or stored for SBF treatment. For multi-layered scaffolds that were mineralized first followed by compression (C2M1), a virgin PDO sheet was placed in between two mineralized scaffold to act as a plasticizer i.e. flow under pressure and bond adjacent layers and prevent delamination.

4.2.4. Mechanical Testing:

The scaffolds were punched into dog-bones with a metal punch (2.75 mm wide at their narrowest point, gage length of 7.5mm) and individual specimen thickness was measured on a Mitutoyo IP54 digital micrometer (Mitutoyo American Corp.). These dog-bones were subjected to uniaxial tensile testing using a 50 N load cell MTS Bionix 200 testing system with an extension rate of 10 mm/min. Elastic modulus, strain to failure and energy to break were recorded by the MTS software TestWorks 4.0.

4.2.4. Permeability and Pore Size Measurements:

Both types of scaffolds - C1M2 and M1C2 containing 1, 2 or 4 layers were subjected to permeability and pore size measurements following the protocol developed by Sell et al. [153]. Briefly, a graduated 10-mL pipette was placed horizontally that was connected to a reservoir at a height of 150 cm from the scaffold. The electrospun scaffold was compressed between two silicone gaskets and a large-pore metal screen was placed on the underside of the scaffold to prevent excessive distension of the test scaffold. Fluid flow was recorded every minute for the first 10 min of testing and the permeability was mathematically calculated using Darcy's equation. These permeability values were then

used to determine the average pore sizes of the electrospun scaffold, again using a mathematical equation.

4.3. RESULTS

4.3.1. Scanning Electron Microscopy:

One of the surprising findings from scanning electron micrographs is the preservation of porous structure of nanofibrous scaffolds even after compression. The nanofibrous architecture appear more dense but without obliteration of pores, at least on the surface. This is true even of multilayered scaffolds that were compressed before or after mineralization. There are discrete patches on the scaffolds where the fibers have deformed and flattened after compression and is evidence of fiber welding / bonding that could have occurred (**Figure 14**). Such cold welding of multiple fibers at numerous areas cumulatively resulted in significantly increased stiffness observed in scaffolds subjected to compression. Interestingly, such fiber welding is seen only in PDO:nHA scaffolds and not in PDO scaffolds and is a common finding irrespective of the number of layers.

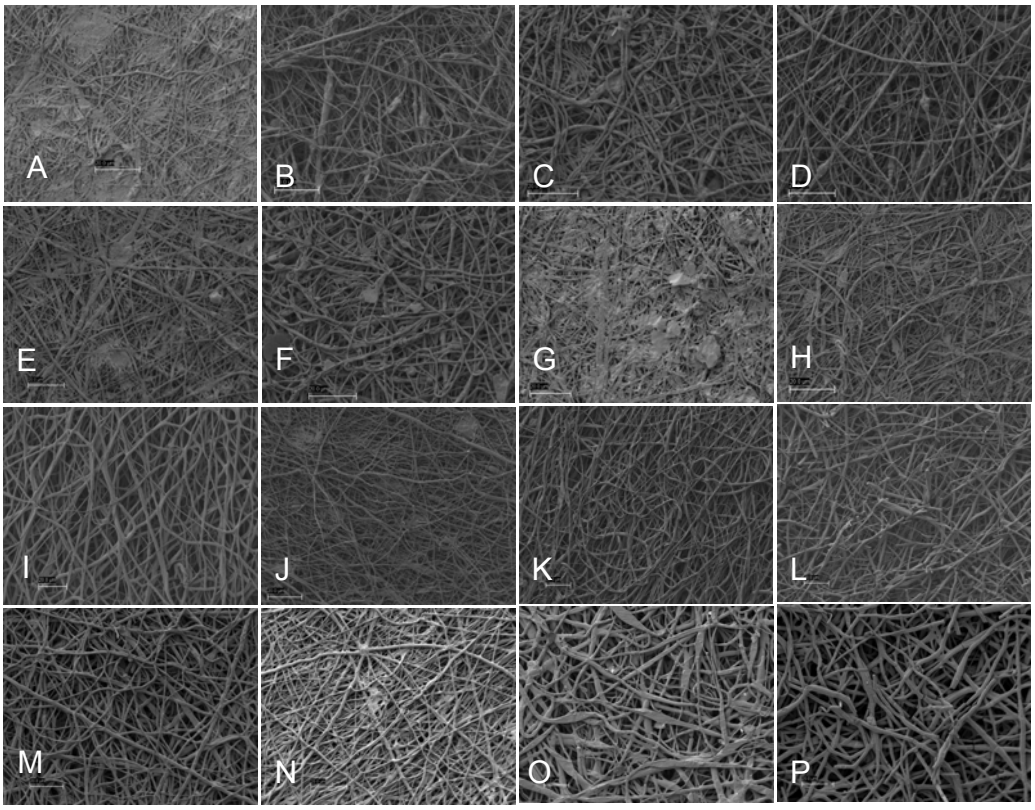

Figure 14: Scanning electron micrographs of electrospun PDO scaffolds containing 50% (by wt. of polymer) after biomimetic mineralization for 2 weeks. **A&B**. Compressed and non compressed control scaffolds in de-ionized water. **C- H**. Compressed and non-compressed scaffolds in SBF: **C& D** - 1 layer, **E&F** - 2 layers, **G&H** - 4 layers. PDO scaffolds are designated in the same format from panel **I-P**. Note the discrete areas of compression resulting in cold welding of individual fibers in all compressed scaffolds. Also note loss of continuity of individual fibers in scaffolds treated with SBF. Cumulative effects of nano-fiber fracture might account for the decreased stiffness observed in SBF treated scaffolds. Greater mineral content can be attributed to individual fiber mineralization rather than mineralization on surface. This pattern also preserves the porosity of the scaffold, important for cell infiltration.

4.3.2. Quantification of Mineralization by ARS:

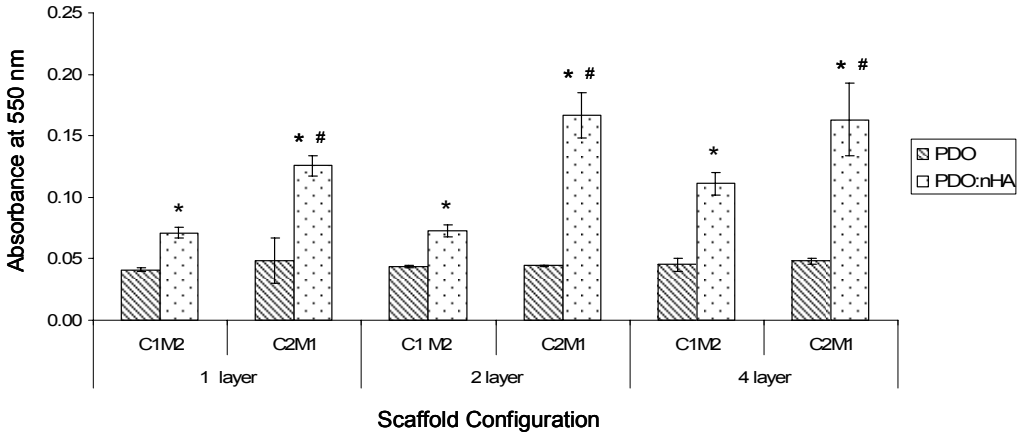

Figure 15: Alizarin red staining of multi-layered scaffolds. Electrospun PDO and PDO:nHA scaffolds were stacked on top of each other to get 2 or 4 layers. One group was compressed first (C1M2) and mineralized as multilayered scaffold while the other group were mineralized as individual sheets and compressed into a single unit (C2M1) after SBF treatment. Following incubation, scaffolds were washed and stained for calcium using Alizarin red staining as described in the methods section. * indicates significant difference within scaffold types (PDO and PDO:nHA) and # indicates significant difference with compression sequence (C1M2 and C2M1).

Statistical analysis shows superior performance of PDO:nHA scaffolds compared to PDO scaffolds in all levels. In addition, there is no statistical difference whether PDO scaffolds were in 1, 2 or 4 layers and if they were compressed before or after SBF treatment. Similarly, mineralization of PDO:nHA scaffolds is independent of multiple layers. Interestingly, PDO:nHA scaffolds mineralize differently depending whether compression was done before or after mineralization. Compression of PDO:nHA scaffolds before SBF treatment, is identical for 1 and 2 layered scaffolds while the 4-layered

scaffolds had superior mineralization. However, the strategy of mineralizing multiple scaffolds separately followed by compression into a single scaffold did not yield increasingly higher mineralization as expected. This might be partly due to difficulty of the stain to access the interior of the multi-layered compressed scaffolds. The presence of a non-mineralized PDO scaffold in between two mineralized layers intended for fusing different layers might also contribute to the observations (**Figure 15**).

4.3.3. Mechanical Testing:

Compression of scaffolds before mineralization generally results in stiffer scaffolds. This finding is true for both PDO and PDO:nHA scaffolds. As expected, testing samples in dry state results in greater stiffness values compared to testing under hydrated conditions. However the effect of hydration is more obvious in PDO:nHA than the PDO scaffolds. Among the single layered scaffolds, non-compressed PDO:nHA was weaker than PDO but compression of PDO:nHA scaffolds resulted in scaffolds stiffer than compressed PDO scaffolds. In 2 and 4 layered scaffolds, compression before mineralization resulted in stiffer compared to scaffolds that were mineralized first. Further, as long as the PDO:nHA scaffolds were compressed before SBF treatment, increase in the number of layers resulted in proportionally greater stiffness values. However, the PDO scaffolds did not have any statistically significant difference whether it has two or four layers and are independent of compression protocol (before or after mineralization).

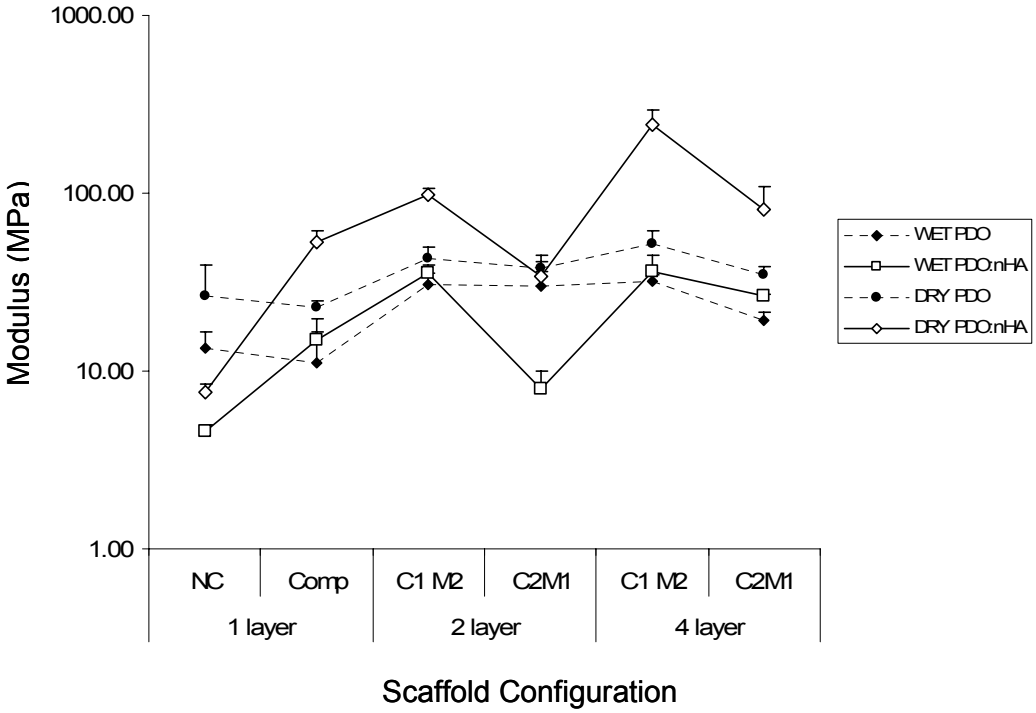

Figure 16: Comparison of stiffness (Young's modulus) in multi-layered mineralized electrospun scaffolds under dry and hydrated testing conditions. The effects of compression welding the scaffolds are also shown. In scaffolds containing more than 1 layer, compression welding of the scaffolds was done before SBF treatment (C1M2) or the scaffolds were mineralized separately and then compressed at the end of 2 weeks (C2M1). NC: non-compressed, Comp: compressed. Ctrl refers to scaffolds that were incubated in DI water while test scaffolds were incubated in 1x r-SBF for 2 weeks.

4.3.4. Permeability and Pore Size Measurements:

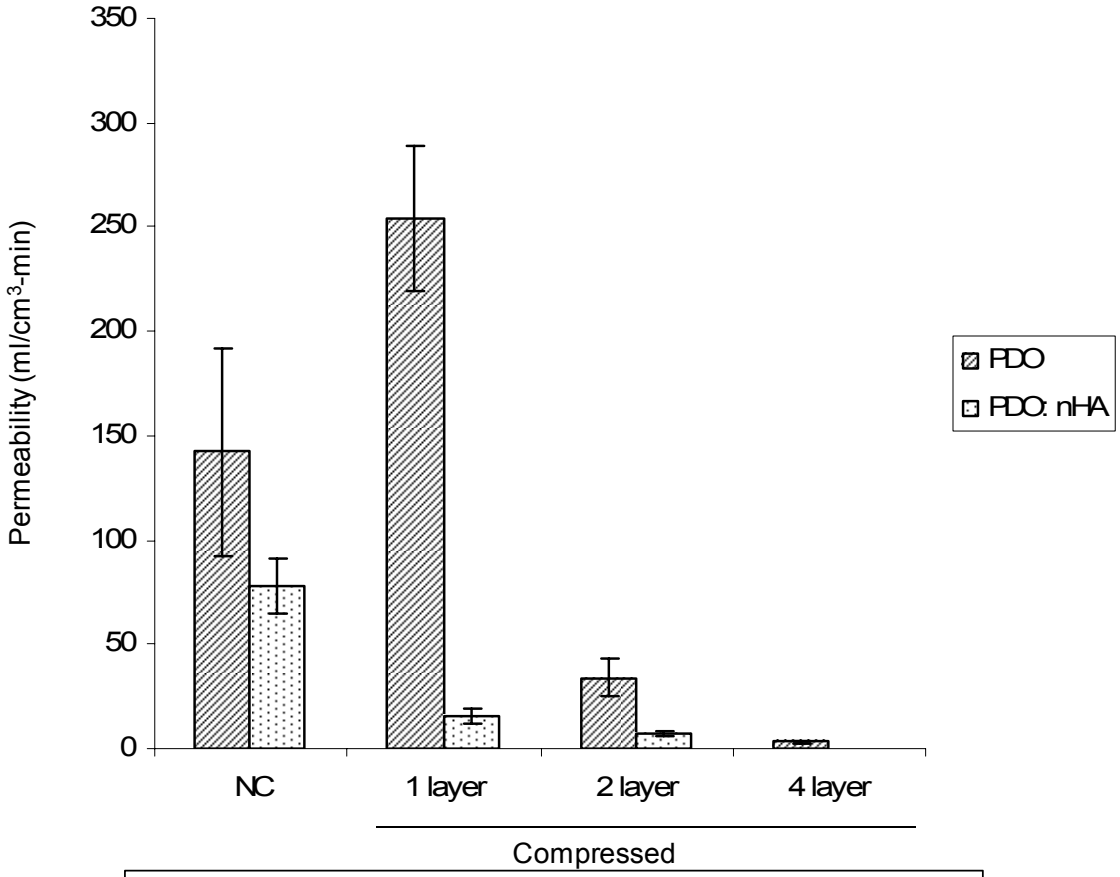

Figure 17: Effect of multi-layered electrospun scaffolds on permeability. PDO scaffolds were significantly more permeable than PDO:nHA scaffolds Irrespective of the number of layers. Compression predictably decreases permeability in all scaffolds with the exception of single layered PDO scaffold.

The effects of compressing single or multi-layered scaffold are presented in **Figure 17**. It can readily be seen that compression of PDO:nHA causes a significant reduction in permeability compared to PDO scaffolds. This finding corroborates with the SEM finding that showed distinct areas of fiber welding seen in all types of PDO:nHA scaffolds. In contrast, PDO scaffolds are more open and seemingly not affected by compression, at least

on the surface. However, the permeability of single layered PDO scaffolds paradoxically increases following compression.

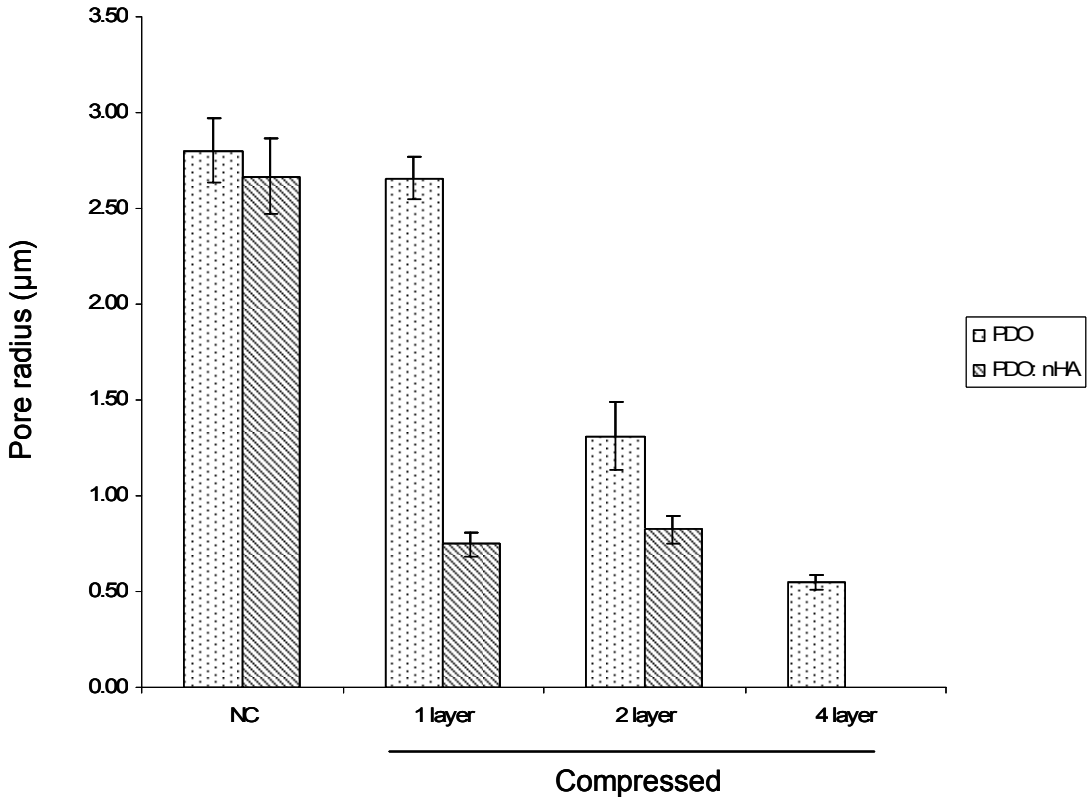

Figure 18: Effect of compression of electrospun scaffolds on pore size. Non-compressed (NC) scaffolds a are much more porous compared to compressed ones. The porosity of single layered PDO scaffolds however seem to be unaffected by compression. In general, pore size decreases with the number of layers the effect being more pronounced in PDO scaffolds. Compressed single and two layered PDO:nHA scaffolds are identical although the 4 layered ones are rendered impermeable.

In general, compression of scaffolds results in decrease in pore size of the scaffolds with the exception of single layered PDO scaffolds that is unaffected by compression. While the compression of single and two layered PDO:nHA scaffolds resulted in similar reduction of pore size, the corresponding 4-layered scaffold was completely impermeable.

4.4. DISCUSSION

Bone tissue scaffolds have to be engineered to have sufficient mechanical and biological properties. Inorganic hydroxyapatite, that forms almost 50% of healthy bone, is present in such high amounts to satisfy both the above mentioned criteria. It provides a brittle, incompressible phase that is effectively dispersed and closely associated with the tough collagenous organic phase. It is this interaction between phases having distinct material properties that contribute to unique mechanical properties of bone.

The SEM has revealed some interesting insights into the scaffold behavior when compressed (at 20,000 psi for a minute) at the nanoscale. There are discrete areas of PDO:nHA scaffolds that have been pressure welded as a result of the compression process. Interestingly, such changes are obviously missing in pure PDO scaffolds. Since the PDO concentration was kept constant during electrospinning (100 mg/ml) for both types of scaffolds, this behavior teases out the important role of nHA (incorporated during electrospinning) in determining bulk material properties of the final scaffold.

The rationale of adding nHA in the present study was to provide sites of nucleation during subsequent treatment with SBF. It was never intended to contribute to the mechanical properties of the scaffold. Infact, the uncompressed PDO:nHA scaffold is considerably weaker than corresponding PDO scaffolds. However, the behavior of PDO:nHA scaffolds changes considerably under compression as shown in Figure 16. The stiffness of compressed PDO:nHA scaffolds shows a 7-fold increase compared to non-compressed scaffolds. This observed increase in stiffness is further enhanced with the

addition of layers, almost proportionally increasing with each layer. These findings provide a novel strategy to improve material properties of electrospun scaffolds. Even though the exact mechanism of improving stiffness is not clear at present, the following observations provide further insights into this interesting behavior.

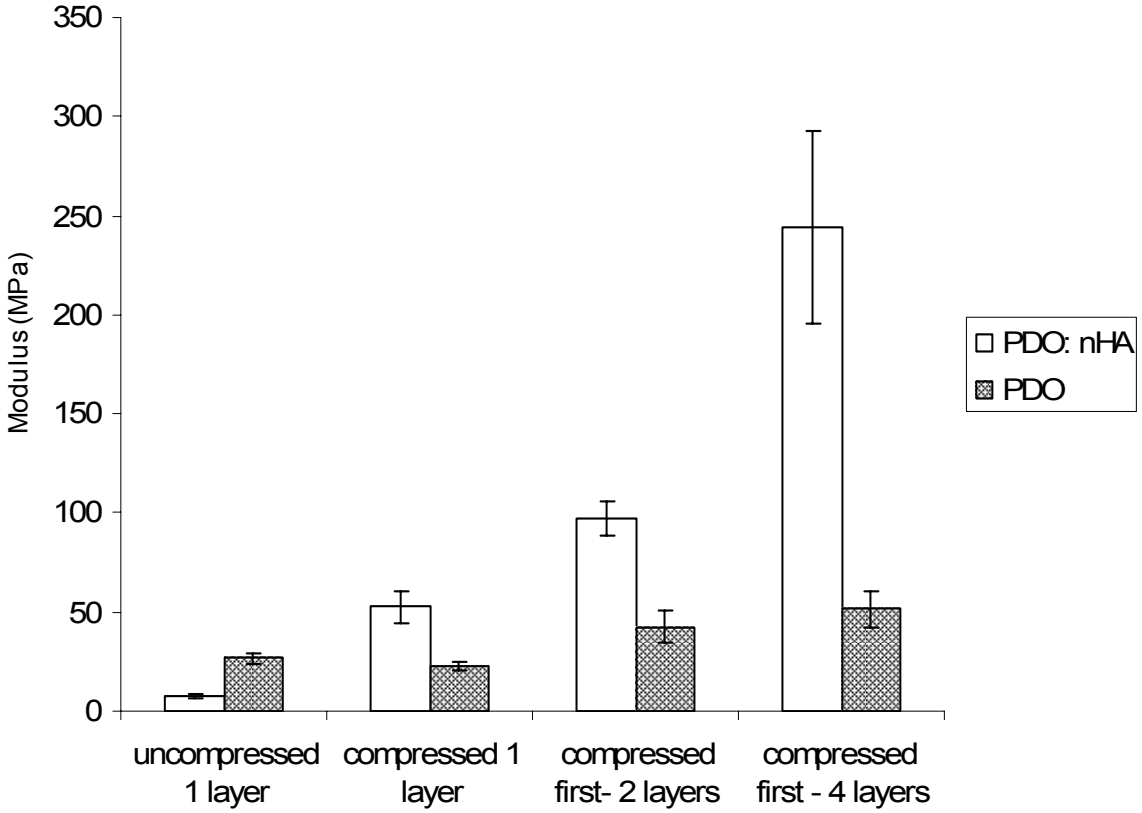

Figure 19: Effects of compression and multiple layers on the stiffness of electrospun PDO and PDO:nHA scaffolds. While compression did not affect the stiffness of PDO scaffolds, it significantly increased the stiffness of PDO:nHA scaffolds. In addition, stacking multiple layers resulted in a proportional increase in stiffness in PDO:nHA scaffolds.

Electrospun PDO:nHA scaffolds are much less dense and has a spongy texture compared to pure dense sheets of PDO scaffold might partially account for the behavior. Being more compressible, PDO:nHA scaffolds deform significantly under pressure that

ultimately would lead to welding of nanofibers. PDO, on the other hand, being dense thin sheets, resist compression, even at the nano-scale. Further, an even compression of porous nanofibrous structure is limited by the occurrence of finite contact points of scaffolds with metal surfaces that are highly irregular at nanoscale.

In addition to determining the mechanical properties, these nHA containing scaffolds are also expected to increase the amount of mineralization when soaked in SBF. The effect of compression and addition of layers to either PDO or PDO:nHA scaffolds on the mineral content is presented in **Figure 19**. Here it is obvious that compression works against mineralization potential. Irrespective of the number of layers present, mineralization is always better if the scaffolds are treated with SBF without compression. Compression of scaffolds decreases the total available surface area (due to fiber welding), makes the scaffolds denser and probably restricts mineralization to the outermost layer. However, mineralization of multiple scaffolds followed by their compression into a single scaffold did not yield greater mineralization outcome, at least in this study. This is most likely due to the limitation of staining process (alizarin red not able to bind to the mineral in the middle layers). Further, to prevent layer delamination, we adopted a strategy of using a PDO scaffold as a sandwich between two mineralized PDO:nHA scaffolds during their compression. It was hypothesized that the PDO will be able to flow under high pressure and act as an adhesive bonding the two mineralized layers together. This might have precluded contact of the stain with the mineral present within the layers.

Overall, the above experiments studied the effects of mineralization with SBF, and compression of multiple layers. Taken together these data represent a significant increase

in the modulus following compression of multi-layered scaffolds. But this process was accompanied with decreased mineralization and decreased permeability. There is essentially a middle ground between optimal mineralization and permeability vis-à-vis improved mechanical properties. Since mechanical properties of bone scaffolds are very critical in its function, further efforts should aim to identify methods to achieve significant mineralization and permeability without compromising mechanical properties.

4.5. CONCLUSION

We have identified main processing parameters that affect two major properties of bone scaffolds-stiffness and mineral content. Use of high pressure to weld nanofibrous scaffolds greatly improves material properties while incubation of electrospun scaffolds in 1x r-SBF provides a convenient and physiological means to improve mineralization of scaffolds *in vitro*. Compression of electrospun scaffolds at very high pressure resulted in significantly higher levels of stiffness of PDO:nHA scaffolds compared to controls. In addition, this technique also permitted stacking of multiple independent electrospun scaffolds on top of each other without fear of delamination. On the other hand, such an approach, limits the amount of mineralization following treatment with SBF due to loss of available surface area. A 4-layered PDO:nHA scaffold compressed first followed by mineralization in r-SBF has maximal stiffness with the mineralization second only to non-compressed scaffolds. Within the limitation of this study, this scaffold configuration represents an optimal midway for desired stiffness and mineral content.

Chapter 5: QUANTIFYING BIOMATERIAL CYTOCOMPATIBILITY VIA IN-CELL ASSAY OF PHOSPHOVINCULIN (pY-822)

Preface: The following chapter has been submitted to Journal of Biomedical Material Research and is under review.

5.1. ABSTRACT

Cell adhesion is a causal event that dictates the eventual global host response to biomaterial implantation including its integration and sequestration. Cell proliferation, function and differentiation are processes that occur secondary to cell adhesion. Cell adhesion to native extracellular matrix (ECM) or any biomaterial is mediated via integrin binding to the adsorbed protein layer occurs at discrete areas on the cell membrane called focal adhesions. These focal adhesions are multi-protein complexes that modulate inside-out and outside-in signaling between the cell and ECM and play a critical role in determining the implantation outcomes. Since focal adhesion formation is the molecular event underlying cell adhesion, we reasoned that quantifying focal adhesions would enable us to predict the cytocompatibility of a biomaterial surface. Vinculin is a cytoplasmic protein that gets phosphorylated upon activation and one form of phosphovinculin, pY-822, has been identified to be enriched at focal adhesions. In this study, we analyzed the expression of vinculin and phosphovinculin (pY-822) by osteoblast-like MG-63 cell lines after seeding them onto different substrates including collagen, gelatin, fibronectin, tissue culture treated plastic and untreated plastic. Western blotting experiments indicated that phosphovinculin is absent in circumstances that are not conducive to focal adhesion formation (cells grown on untreated plastic) while vinculin was detected in all circumstances, even in a non-adherent environment. Confocal microscopy demonstrated co-localization of both vinculin and phosphovinculin at focal adhesions and confirmed the specificity of the antibodies used. Further experiments using In-Cell Western assay

allowed quantification of these molecules irrespective of surfaces or time points studied. Using the above evidence, we propose an improved functional yet quantitative assay of biomaterial cytocompatibility, exploiting the sensitivity of infrared imaging and specific association of phosphovinculin to focal adhesions.

5.2. INTRODUCTION

The focus of biomaterial research is shifting from the structural replacement of diseased or missing tissues in favor of functional organ regeneration. Such a shift in design paradigm has resulted in the development of a new generation of biomaterials. However, the ultimate challenge in biomaterial design and development lies in achieving bio-integration without eliciting any adverse host reactions. Critical to successful integration is the ability of the implant to recruit, retain and facilitate the function of cells native to the tissue or organ it aims to regenerate. A number of important *in vitro* assays (physical, mechanical, chemical, electrical) have been optimized to characterize biomaterials based on their application. Biological performance of materials are being increasingly scrutinized at microscopic, molecular and genetic levels in an effort to appreciate and better understand cell-biomaterial interactions [154-155]. Recent advances in cell signaling and molecular biology have increased our understanding of the events underlying cell-biomaterial response. Unfortunately, this knowledge has not translated into development of more sophisticated *in vitro* assays that would permit biological characterization of biomaterial surfaces [156].

Cell adhesion to the extracellular matrix not only provides vital survival cues but is also necessary for proliferation, differentiation and maintenance of phenotype [157-161]. Cells possess heterodimeric transmembrane receptors called integrins, capable of binding to a wide variety of extracellular ligands. This binding initiates formation of focal adhesions - discrete spots on the cell membrane where components of ECM, integrins and cytoskeleton are in close proximity. Integrin mediated focal adhesions not only establish physical continuity but also mediate inside-out and outside-in signaling pathways that underlie the dynamic reciprocity of the cell-ECM interactions [162, 163]. Since cell adhesion is a primary event that modulates subsequent responses, an assay of cell adhesion will reflect a material's cytocompatibility [164] and quantifying adhesion would be of predictive value in assessing the *in vivo* performance of biomaterials [165, 166].

Experimental methods to quantify cell adhesion have been mostly indirect, based on the ability of cells to resist shearing forces by washing, centrifugation and hydrodynamic shear [167]. Repeated washing, though simple and rapid, is difficult to quantify and lacks reproducibility. While centrifugation assay provides a uniform detachment force, they are relevant only within a narrow window of time (within 60 min) [168]. Hydrodynamic flow assays or micromanipulators are more accurate in determining adhesion but require specialized instrumentation. Assessment of molecules that participate in focal adhesions can provide a direct quantitative measure of cytocompatibility of biomaterials [156]. Since the focal adhesion is a complex of more than 50 different proteins, our objective was to identify a reliable marker and then use it to develop a quantitative assay of cytocompatibility *in vitro*. Vinculin is a well known cytoplasmic

protein that is recruited to focal adhesions upon activation by multiple mechanisms including phosphorylation. Even though vinculin can be phosphorylated at more than one site, phosphovinculin (pY-822) is being shown to represent a specific subset of vinculin that are particularly associated with focal adhesions. In the present study, we introduce a new infrared based detection technique to quantify the expression of phosphovinculin (pY-822) that can be used as a tool to evaluate the cytocompatibility of biomaterials.

5.3. MATERIALS AND METHODS

All chemicals were purchased from Sigma-Aldrich (St. Louis, MO), unless stated otherwise.

5.3.1. Cell Culture:

Human osteoblast-like cells MG-63 were purchased from ATCC (American Type Culture Collection, Manassas, VA) for the study. The cells were cultured in Dulbecco Modified Eagle medium (DMEM) containing 10% fetal bovine serum (FBS) and 1% penicillin–streptomycin (Cat # 15140-122) from GIBCO.

5.3.2 Coating Cell Culture Dishes:

Five different substrates for cell culture were used for the study: a. untreated culture plastic (Cat # 08-772-31, Fisher Scientific, PA), b. cell culture treated polystyrene (Cat # 08-757-168, Fisher Scientific, PA), c. collagen, d. gelatin and e. fibronectin. Circular 60 mm dishes (for western blotting experiments) or 96 well plates (for in-cell western assay)

were used as is or after coating with the extracellular matrix proteins using the protocol described below.

Purified bovine type I collagen was purchased as liquid Purecol at 3 mg/ml (Inamed, Fremont, CA). This solution was diluted with sterile PBS to a final concentration of 0.01% (wt/vol). Powdered bovine gelatin (Cat #: G9391, Sigma, MO) was dissolved in sterile water to a final concentration of 0.05% (wt/vol). Sterile, endotoxin-free, lyophilized human fibronectin (Cat #: 356008, Collaborative Biomedical Products, Bedford, MA) was dissolved in sterile water at 1 mg/ml concentration by gentle swirling until a clear solution was obtained. This solution was filter-sterilized and further diluted with sterile PBS to a final concentration of 50 µg/ml.

For coating, respective solutions were poured into tissue culture dishes till the solutions were 2 mm in depth and left overnight at 4^{o}C. Excess solution was aspirated and dishes left to dry under a laminar flow hood. The dishes were washed thrice with PBS before cell seeding.

5.3.3. Confocal Microscopy:

MG-63 cells were seeded on glass cover slips at a density of 400 cells/mm^2 and cultured in DMEM with 10% FBS. Cells were allowed to attach to the glass surface for 24 hours and fixed with freshly prepared 2.5% paraformaldehyde (pH 7.5). Cells were permeabilized with 0.1% Triton X-100 for 5 minutes on ice and probed with antibodies against total vinculin (1:100 dilution) and phosphovinculin (pY-822) (1:25 dilution). Alexafluor labeled secondary antibodies (Invitrogen) raised against mouse (633 nm) and rabbit (488 nm) were incubated in the dark for half an hour. After washing, cover slips

were mounted on glass slides using ProLong Antifade (Invitrogen) mounting medium containing DAPI. The slides were analyzed using a Zeiss 510 Meta confocal imaging system.

5.3.4. Cell Density Quantification:

The DNA of the cells was first labeled using a cell permeable anthraquinone dye, Draq 5 (Biostatus Ltd, Leicestershire, UK) that fluoresces at 700 nm. Formaldehyde fixed cells were treated with 5 mM Draq 5 solution diluted in PBS and incubated for 10 minutes at 37°C. After washing to remove unincorporated dye, the plates were read directly at 700 nm using Odyssey Imaging System to measure fluorescence emitted by the intercalated labeled DNA. The resulting fluorescence was used as a measure of cell density.

5.3.5. Western Blotting:

All cell culture experiments were done in triplicates for each time point (1, 3, 6, 9, 24 hours). MG-63 cells were grown in T-150 flasks to confluence, detached with 0.25% trypsin and seeded at a density of 10^6 cells/dish. At each time point, cell lysate was collected in cold lysis buffer (20 mM Tris, pH 7.4, 50 mM NaCl, 1 mM EGTA, 5 mM EDTA, 50 mM sodium pyrophosphate, 50 µM sodium fluoride, 100 µM sodium ortho-vanadate, 1 µl/ml protease inhibitor cocktail, 0.5% Triton X-100 and 0.1% phenylmethylsulfonylfluoride). The lysate was vortexed briefly and allowed to stand at 4°C for 15 minutes then centrifuged at 1,000g for 10 minutes. The supernatant was collected and stored at -70^{o}C. An aliquot of the lysate was used for protein quantification to ensure equal loading in the gel. Appropriate amount of the lysate from the samples were diluted in laemmli sample buffer, boiled for 5 minutes, loaded onto a Criterion 10% Tris-

HCl gel (Biorad) and electrophoresis performed at 100 volts under reducing conditions. The proteins were then transferred onto a PVDF membrane (Millipore, Bedford, MA) and reversibly stained with Ponceau S to ensure complete transfer. The membranes were then blocked with Odyssey blocking buffer (Licor Biosciences, Lincoln, NE), probed with primary antibodies for vinculin (mouse anti-human) and phosphovinculin (rabbit anti-human) at 1:1000 dilution for 1 hour at room temperature. The secondary antibodies, conjugated with dyes that fluoresce at 700 and 800 nm, were diluted in the blocking buffer (1:20000 dilution) and incubated with the membrane for 30 minutes in a light proof box. After extensive washing, the membranes were scanned with the Odyssey imaging system (Licor Biosciences, Lincoln, NE) at specified wavelengths and resulting fluorescence recorded.

5.3.6. In-Cell Western (ICW) Assay:

Tissue culture grade microtiter (96 well) plates were used as is or coated with different proteins as described above. MG-63 cells were grown in 150 mm dishes until confluence and collected with 0.25% trypsin. The cells were counted, diluted in fresh media and seeded at 15, 30 or $45x10^3$ cells/well. At every time point specified (1-48 hours), cells were fixed with 10% formalin for 20 minutes at room temperature. The cells were then washed thrice with 25 mM glycine (containing 1% bovine serum albumin) for 5 minutes each, permeabilized with 0.1% Triton X-100 and blocked with Odyssey Blocking buffer for an hour at room temperature. Vinculin and phosphovinculin specific primary antibodies were diluted 1:1000 in the blocking buffer and the cells were incubated for an hour at room temperature. After washing, cells were incubated for 30 minutes with anti-

rabbit (1:1000 dilution) and anti-mouse (1:500 dilution) fluorescent dye coupled secondary antibodies (excitation 800 nm). The plates were optically scanned at 800 nm, the fluorescence intensity recorded and quantified.

5.3.7. Statistical Analysis:

All experiments were performed in triplicates and data analyzed using JMP 7.0 (SAS, Cary, NC). Analysis of Variance (ANOVA) was performed and the means were compared using the multiple comparisons Tukey-Kramer test to detect any statistical difference ($\alpha = 0.05$) in the expression levels of phosphovinculin or total vinculin. The data is presented as means and standard errors.

5.4. RESULTS

5.4.1. Immunohistochemical Staining:

The cells were stained for vinculin, phosphovinculin and DAPI to demonstrate the specificity of the antibodies used and the distribution of the molecules under study. Both the antibodies used bound specifically to their target molecules as can be seen by negligible background fluorescence at corresponding wavelengths. The confocal images clearly illustrate the formation and positively stained focal adhesions on the cell membrane. As expected, both vinculin and phosphovinculin are enriched at focal adhesions and these molecules co-localize **(Figure 20)**.

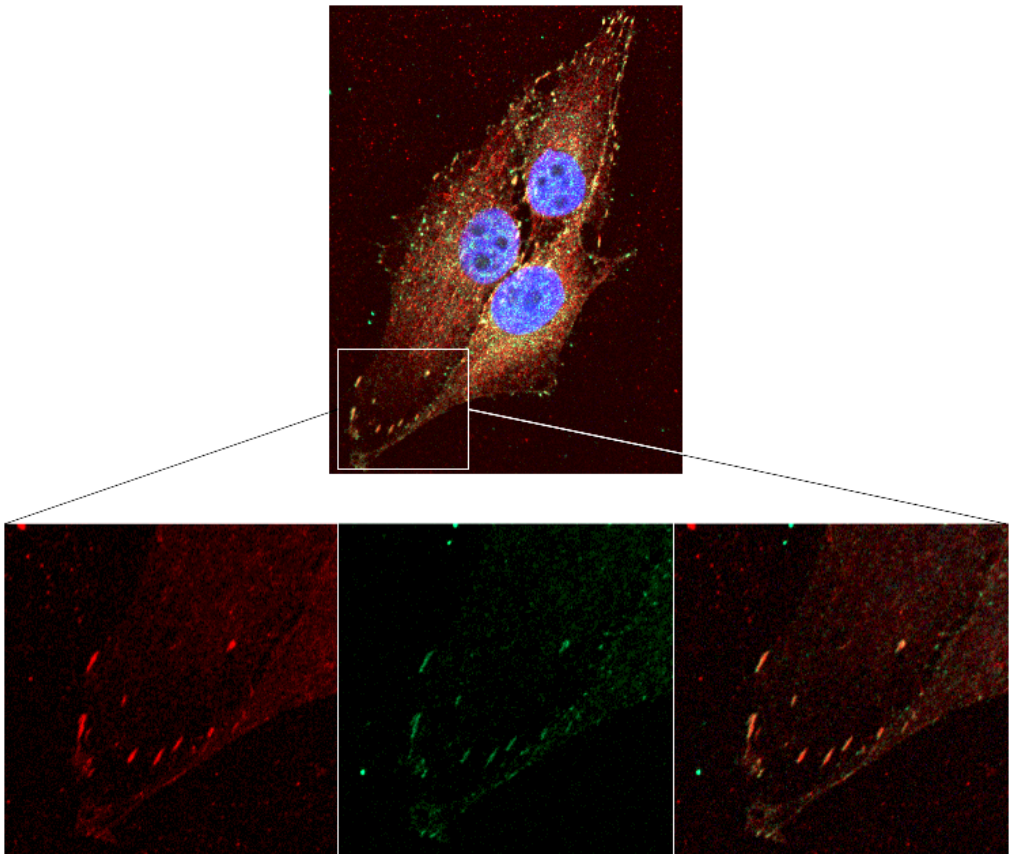

Figure 20: Confocal microscopic images showing co-localization of vinculin and phosphovinculin at focal adhesions. **Top:** A composite confocal image of MG 63 cells grown on tissue culture plastic stained for nuclear DNA (DAPI), vinculin and phosphovinculin. Focal adhesions are readily seen as discrete spots on the periphery of the cell. **Bottom:** A close-up view of the focal adhesions in a selected area of the cell membrane. The images obtained from each laser is separated to demonstrate specificity of the signal and co-localization of vinculin (red) and phosphovinculin (green) at focal adhesions. Left panel shows vinculin at 633 nm, middle phosphovinculin at 488 nm and the right panel is a composite image (yellow).

5.4.2. Cell Density Measurement:

As expected, there is a corresponding increase in the staining intensity with an increase in the cell number. This increase does not appear to be linear and tend to plateau off at $45x10^3$ cells/well **(Figure 21)**. This is probably due to saturation of the signal in this channel. This finding supports the fact that Draq staining of the DNA and measuring the

fluorescence with Odyssey Infrared scanner can be reliably used to quantify cell density. A plot of draq-5 fluorescence versus time reveal no appreciable increase up to 6 hours while the fluorescence intensity shows a significant increase at 9 and 24 hours, corresponding to the presence of mitotic numbers due to asynchronous cell cycle progression in culture. Further, as expected, the substrate on which cells were seeded did not significantly affect the cell replication at least within the short period of time (24 hours). Figure 19 shows a representative data from the sample taken at 9 hours, at which significant increase in DNA was observed.

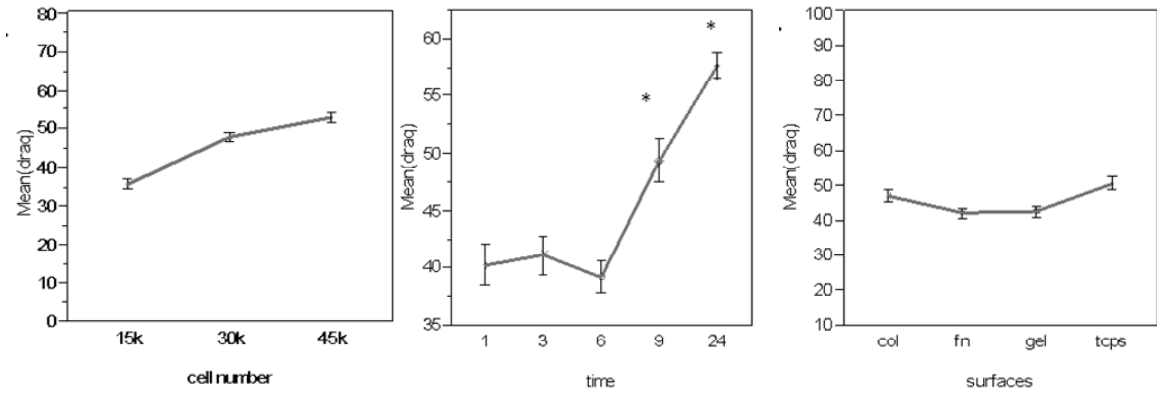

Figure 21: Quantification of DNA using Draq5. **A**. Standard curve showing increasing fluorescence with increasing cell density in a 96 well plate format. Saturation of the signal occurs at $45x10^3$ cells/ well. **B**. shows no significant increase in cell numbers at early time points till at 9 hours due to asynchronous cell cycle. **C**. demonstrates no significant differences in the cell numbers at 9 hours when cells are seeded on different surfaces.

5.4.3. Western Blotting:

Samples from each time point and surface were run in 10% polyacrylamide gels as described. **Figure 22** is a representative western blot of samples that demonstrates the specificity of antibodies and the pattern consistently seen in all the blots. Blots developed

for vinculin **(A)** showed two bands: a faint 150 KDa band and well defined 130 KDa band. The phosphovinculin blot (pY-822) in (**B)** detects one unique band at 130 KDa. Phosphovinculin was absent in cells grown on untreated plastic while it was detected in cells cultured on any other dishes. Vinculin, on the other hand, consistently showed up in all the lanes including cells from untreated plastic, though its intensity was consistently less than in cells grown on adhesion-conducive surfaces. Differences in the intensity of vinculin or phosphovinculin bands across different time points and surfaces were insignificant and could not be quantified with accuracy (hence not shown).

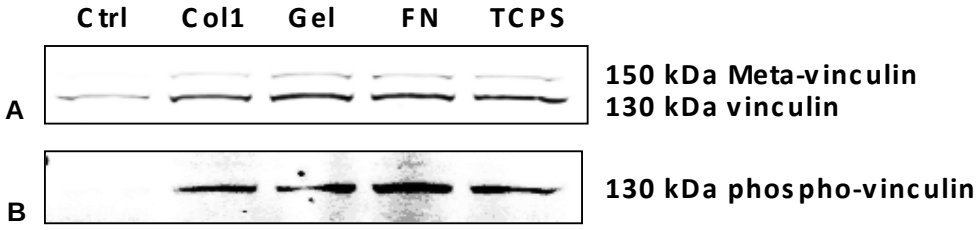

Figure 22: Western Blot of cell lysate from MG 63 cells cultured for 24 hours on ECM protein (collagen, gelatin and fibronectin) coated surfaces, tissue culture polystyrene and non tissue-culture grade plastic surface (control). The blot in **A** was developed for vinculin and phosphovinculin (130 KDa, indicated by arrow) in **B**. While vinculin is expressed in all surfaces including non tissue-culture grade plastic, phosphovinculin is expressed only on surfaces conducive for focal adhesion formation. The 150 KDa fragment detected in A corresponds to meta-vinculin, an alternatively spliced variant of vinculin.

5.4.4. In-Cell Western Assay of Vinculin and Phosphovinculin as a Function of Cell Number:

A plot of vinculin against increasing cell numbers grown in tissue culture plastic shows a saturation effect similar to that observed for Draq 5 at high seeding densities. Phosphovinculin expression on the other hand, shows a highly linear relationship with

increasing cell density. This shows that phosphovinculin can be used as molecular marker for the study of focal adhesions even at high seeding densities, at least when infra red imaging is used as the tool for study **(Figure 23)**.

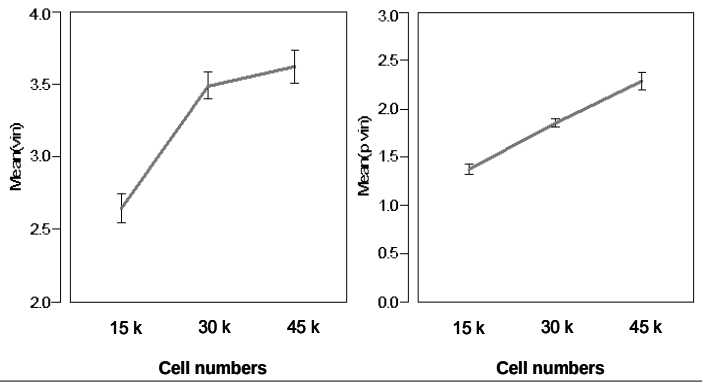

Figure 23: Plots of vinculin (left) and phosphovinculin (right) expression as a function of cell numbers at 9 hours on tissue culture plastic. Expression of vinculin is not only high compared to phosphovinculin (labeled p vin) but also shows saturation at high cell numbers similar to that observed with Draq5. Phosphovinculin, on the other hand, show a perfectly linear expression profile even at high numbers.

Having demonstrated that phosphovinculin expression is linear over the range of cell densities when cells are cultured in TCPS, our next effort was to study its expression on different surfaces. The results show a linear relationship of phosphovinculin expressed as a function of cell number in all types of surfaces studied (R^2>0.99 in all surfaces) **(Figure 24)**.

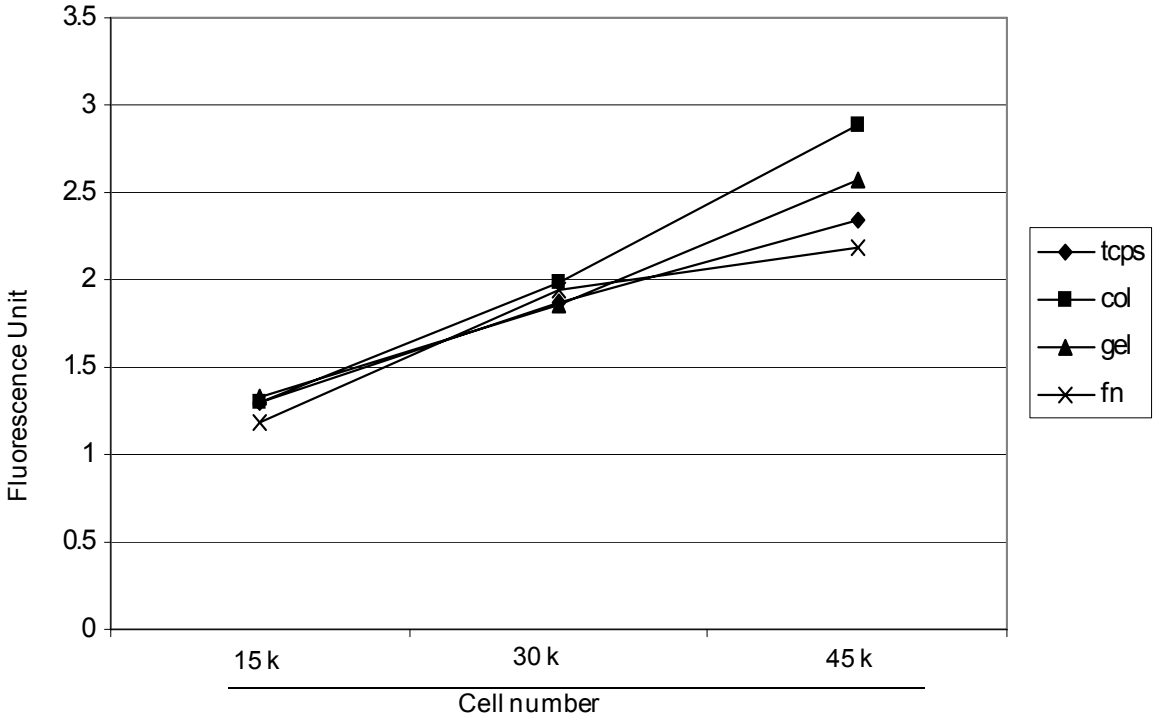

Figure 24: Phosphovinculin expression as a function of cell number cultured On different surfaces for 9 hours. As expected, the number of cells used in ($30x10^3$) falls within the linear detection range of phosphovinculin for all surfaces studied.

5.4.5. In-Cell Western Assay of Vinculin and Phosphovinculin as a Function of Time within Surfaces:

Expression levels of total vinculin in **Figure 25**, shows it reaches a steady state at around 24 hours and does not appreciably change even after 48 hours. Similarly there is no significant difference within early time course (1-4 hours) after cell seeding onto any type of surfaces. Interestingly, these values always drop from 3 hours to 4 hours before showing an increase at 6 hours suggesting a very dynamic turnover of these proteins during initial adhesion and spreading.

Expression levels of phosphovinculin shows an interesting trend: there is single peak intensity at one specific time point for each of the surfaces studied that is statistically significant from other surfaces. Cells grown on TCPS show a maximum expression at 4 hours, those grown on collagen at 6 hours, gelatin at 24 hours and fibronectin at 24-48 hours. This finding suggests that different kinetics for focal adhesion formation exist when cells are seeded onto different matrix proteins and cells modulate their adhesion, spreading and motility differently according to their immediate environment.

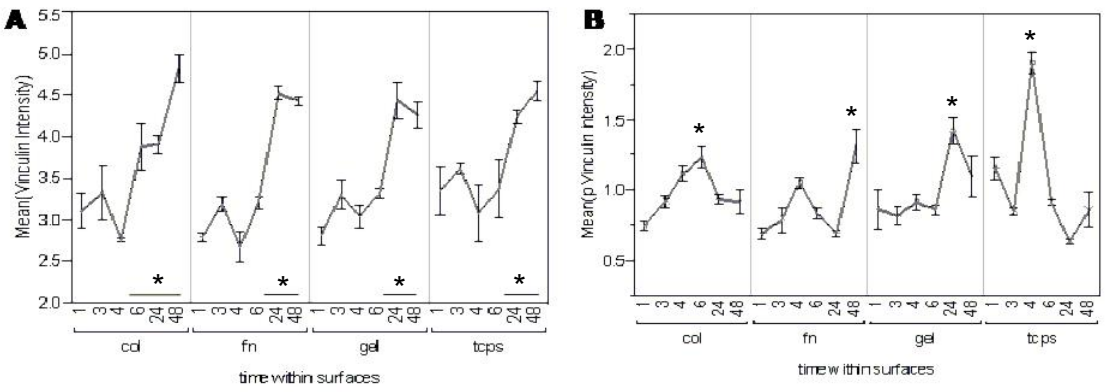

Figure 25: In-cell western assay of changes in expression of total vinculin and phosphovinculin over time on any given surface. **A**. shows the signal from total vinculin (meta-vinculin and vinculin) plateau off around 24 hours and does not change even after 48 hours. Cells grown on collagen, however reached the plateau as early as 6 hours. Groups connected by bars are similar and * denotes significant difference (α =0.05) between the groups. **B**. reveals an interesting pattern of expression of phosphovinculin. Each surface shows a characteristic time point at which the expression is maximal and statistically significant (indicated by *) from other surfaces.

5.5. DISCUSSION

The immediate consequence of implantation of biomaterial *in vivo* is the adsorption of proteins including albumin, fibronectin and fibrinogen. Different biomaterials adsorb proteins differently and ultimate host response depends to a large degree on specific adsorption profile. Cells bind to the adsorbed protein layer through integrins and adhesion occurs at discrete points called focal adhesions. A large complex of structural and signaling proteins assemble at these sites and serve as a functional link between the cell and the ECM [169, 170]. Since host response to a biomaterial is mediated through the formation of focal adhesions, quantification of molecules that directly participate in these structures is logical and presents a relevant measure of cytocompatibility. Even though the list of

proteins that assemble at focal adhesions is growing, integrins, talin, vinculin, paxillin and actinin are perhaps the most studied.

Integrins initiate formation of focal adhesions by binding to the matrix proteins on the extracellular domain and recruiting multiple proteins to form supra-molecular assemblies on the cytoplasmic side. Integrins are composed of an alpha (α) and a beta (β) chain that assemble together to form a heterodimeric complex. They comprise a huge family of proteins assembled from 18 different α chains and 8 distinct β chains that dimerize to form a functional receptor. Integrin binding to ECM ligands can be unique (one integrin type can bind to only one ECM ligand), overlapping (one integrin type can bind to multiple ligands) or redundant (more than one integrin type can bind to one ligand) [162]. Thus even though integrins are the prime component of any focal adhesions and may seem to be the obvious choice, they are also very poor molecular targets to study non-specific focal adhesions as in this study.

When cells come in contact with an implanted biomaterial, they 'see' the biomaterial through the adsorbed protein layer. The patterns of adsorption of various serum and extracellular fluid proteins and their conformation change differ with the type of biomaterial. If the biomaterial is favorable, the adsorbed protein profile and conformations will facilitate binding of integrins and eventual cell adhesion. Adsorption of serum proteins on an unfavorable surface can be accompanied by varying degrees of denaturation and if severe, can render integrin binding impossible. Thus, the adsorbed protein layer is to the cells what a stick is to the blind. Integrin binding to a favorable ligand (protein adsorbed to a friendly biomaterial surface) is followed by clustering of more integrin receptors on the

cell membrane that eventually trigger recruitment of specific cytoplasmic proteins to form focal adhesions. Vinculin is one such cytoplasmic protein that gets activated and recruited to focal adhesions irrespective of the integrin isotype that initiate the process. Such activation and recruitment of cytoplasmic proteins represents a common pathway of focal adhesion formation which is independent of type of integrin binding or the ECM ligand. Thus these cytoplasmic proteins can be reliably and easily used as a marker of focal adhesions and offer a unique opportunity to study them. Since vinculin is a constitutive cytoplasmic protein that gets activated to be recruited to focal adhesions, we reasoned that quantifying activated form of vinculin can serve as a reliable marker of focal adhesions and be used to characterize biomaterial cytocompatibility.

Vinculin is a multi-domain scaffolding protein composed of a globular head (domains D1-D4) and an elongated tail (D5) connected by a flexible proline-rich neck. D1-D3 of the head binds to talin, actinin and catenin, the neck to vinexin, ponsin, VASP and Arp 2/3 complex while the tail binds to F-actin, protein kinase C [171] and acidic phospholipids [172]. Vinculin can exist in at least two conformation states-active and inactive. The multiple binding domains on vinculin are masked by a strong head-tail interaction in the inactive state while these domains are free to interact in the active form. Recent evidence has shown that the resting inactive state is cytosolic while the active form gets recruited to the focal adhesions. The mode of activation of vinculin is still unclear. Evidence exists that the event is combinatorial. Activation occurs (1) when two or more of its binding partners are brought into close apposition [173], (2) secondary to phosphorylation,[174, 175], (3) through PIP-2 binding [176], or (4) a combination of

events [177]. Even though vinculin has more than one phosphorylation site, pY-822 has also been implicated in its activation. Irrespective of the mechanism, once activated, vinculin gets recruited to focal adhesions where it also contributes to adhesion strengthening [178, 179]. A study of F9 vinculin (-/-) cells showed that a single mutation of tyrosine residue (Y-822) markedly reduces the stiffness and elasticity (secondary to defective focal adhesion formation) compared to the F9 wild-type [180]. Since phosphorylation is one of the many events in activating vinculin, we chose to study phosphovinculin (pY-822) as a marker of focal adhesions.

Quantifying focal adhesions in an in-cell format using infrared fluorescence improves accuracy because it permits detection of target molecules an *in situ* context in a spectrum where autofluorescence is greatly reduced. The sensitivity of the technique coupled with the specificity of the antibody, improves accuracy of quantification and reliability of the assay.

Since the basis of quantification in ICW assay is the amount of fluorescence, it becomes imperative that the antibodies used are specific to the molecules of interest. Therefore, the Western blots are necessary to validate the assay. The vinculin antibody was developed against the full length native protein while the phospho-antibody was specific for epitope adjacent to tyrosine residue at position 822 (pY-822). Western blots (Figure 22) from representative lysates of cells grown on different substrates and probed with vinculin and phosphovinculin antibodies demonstrate that pY-822 phosphovinculin antibody was specific to 130 KDa protein while vinculin antibody detected two proteins. The higher molecular weight protein (150 KDa), detected by vinculin antibody is most likely meta-

vinculin, an alternatively spliced variant of vinculin, with which it is immunologically related [181, 182].

Interestingly, phosphovinculin (pY-822) was absent in cells cultured on untreated plastic, surfaces that are not conducive for the formation of focal adhesions. Cells grown on surfaces that favor adhesion and spreading (collagen, gelatin, fibronectin and TCPS) consistently showed phosphovinculin. On the other hand, vinculin was detected irrespective of whether the cells attach to the surface or not. This finding is consistent with the fact that vinculin is a constitutive cytoplasmic protein, only a fraction of which gets activated and recruited to focal adhesions. Thus our rationale for proposing and using phosphovinculin as a specific molecular marker of focal adhesions is validated.

In addition, any assay that use an antibody to full length vinculin is misleading because of the non-specificity of the antibody: it can bind to auto-inhibited native vinculin, activated vinculin and meta-vinculin, representing the total pool of vinculin. This is an important limitation in quantitative assays that involve the use of antibodies.

Data from the ICW assay of cell adhesion using phosphovinculin (pY-822) as a marker allows us to follow the dynamics of focal adhesion formation on different surfaces. Cells adhesion was best on TCPS at 4 hours, while collagen surfaces elicited maximal expression of phosphovinculin at 6 hours. Cells grown on gelatin and fibronectin surfaces showed maximal adhesion during the late time frame (24 - 48 hours).

Differences in matrix composition and protein adsorption profile have been known to control cell adhesion, proliferation and differentiation of mesenchymal stem cells *in vitro*. Chastain et al. provided evidence for the hypothesis that integrin-mediated cell

adhesions to scaffolds controlled the differentiation of mesenchymal stem cells *in vitro* [183]. One possible mechanism could be that different signaling pathways can be activated by binding of different types of integrins to different proteins. It must be remembered that focal adhesion formation is not only a function of biomaterial surface but also depends on the cell type and time. The aim of the present study is to develop a reliable assay that would enable us to follow the kinetics of focal adhesion formation irrespective of the surfaces, time points or the cell types of interest. Future studies could examine signaling pathways involved in cell adhesion to different matrix proteins and possibly account for the difference in kinetics observed.

5.6. CONCLUSION

The present study was successful in identifying phosphovinculin (pY-822) as a reliable and quantifiable molecular marker of focal adhesions irrespective of biomaterial surface studied. Use of total vinculin to quantify focal adhesions is compromised by the presence of multiple isoforms and different conformation states. Phosphovinculin represents a subset of vinculin molecules that undergo activation and are recruited to focal adhesions. These molecules are not expressed when no focal adhesions form, thus iterating their specific association with focal adhesions. ICW assay for phosphovinculin, proposed in this study, provides a simple yet accurate quantitative technique to follow the kinetics of focal adhesion formation when traditional assays have proven difficult. The penetrative ability of infrared rays further expands the scope of the assay to characterize

cytocompatibility of 3D tissue engineering scaffolds by their ability to induce cell adhesion and migration.

Chapter 6: EFFECTS OF EXPOSURE OF BMP-2/7 TO VOLATILE ORGANIC SOLVENTS USED IN ELECTROSPINNING

6.1. INTRODUCTION

Bone is one of unique organs in the adult body that retains a remarkable ability to undergo complete regeneration following injury, as evident in healing following fractures. Bone at the site of fracture, once healed, is virtually indistinguishable from the neighboring normal bone both in terms of histology and mechanical properties. However, there are conditions, where the inherent healing capacity of bone falls inadequate and in these circumstances, external intervention in terms of grafting becomes necessary. Autografts (current gold standard) and allograft have the ability to form new bone following grafting. This is due to couple of independent yet interrelated phenomena: osteoconduction and osteoinduction [184]. While the former refers to the ability of the graft to permit (by acting as a passive template) new bone formation, the latter refers to actively inducing cells to lay down new bone matrix. The process of osteoinduction is exemplified by a group of proteins called bone morphogenetic proteins (BMPs) that reside in extremely small amounts in the organic (non-collagenous) matrix of the bone. These highly potent

molecules are capable of inducing new bone where there are none (subcutaneous and intramuscular sites) or at normal bony sites. It is important to bear in mind that the cellular events following fractures is essentially a recapitulation of the processes associated with embryonic bone development. It should be no surprise that BMPs play a definitive role in fracture repair.

Since its discovery and isolation in 1960s, more than 20 members of BMP family have been identified. The most relevant BMPs in bone research are BMP-2 and BMP-7. Both these are very potent molecules that have been approved for clinical use in specific orthopedic application. BMPs are comprised of two identical chains, each with seven highly conserved cysteine residues. While six of them contribute to an intrachain cysteine knot, the seventh cysteine from each chain participates in the interchain disulfide linkage to form a dimer. BMPs associate to form dimers, bind receptors, activate Smad signaling pathway to regulate a variety of genes including cbfa1 and inhibitor of differentiation (Id1-4) [185, 186]. Mouse Id-1 promoter responds selectively to BMPs and not to TGFβ signaling [187, 188]. Even though homo-dimers of BMP-2 or 7 have been used to induce osteoblastogenesis, recent research indicate that the hetero-dimer of 2/7 is significantly more potent than either of homodimers [189, 190] and hence will be used in this study.

6.2. MATERIALS AND METHODS:

BMP-2, BMP-7 and BMP-2/7, monoclonal antibody to BMP-2/7 heterodimer were purchased from R&D Systems (Minneapolis, MN). The slot-blot apparatus and the nitrocellulose membrane were purchased from Bio-Rad Laboratories (Hercules, CA).

Odyssey Imaging System, blocking buffer and the secondary antibody (goat anti-mouse IR 800 CW) were from LiCor Biosciences (Lincoln, NE). C2C12BRA cells were a kind gift from Dr. Daniel Rifkin, New York University School of Medicine, New York, NY 10016, USA.

6.2.1. Serial Dilutions of BMPs and Detection by Slot-Blotting:

All serial dilutions were performed in 1:2 ratios in solubilization buffer (4 mM HCl and 0.1% BSA), unless otherwise noted. The nitrocellulose membrane was wet in TBS for 10 minutes before the experiment and immobilized in Bio Dot Microfiltration Apparatus under vacuum. Samples were loaded on the template wells and protein solution allowed to drain by gravity through the nitrocellulose membrane. Once filtration was complete, the membrane was removed from the apparatus, washed thrice in 0.1% TBS-Tween for 5 minutes each and blocked for an hour at room temperature. Incubation with the monoclonal primary antibody against the heterodimer (1:1000 dilution) was carried out at 4°C overnight. After extensive washing, the membrane was incubated with infrared-sensitive secondary antibodies (1:10000 dilution) for 30 minutes at room temperature in a light proof container. The membrane was scanned by Odyssey Imaging System at 800 nm wavelength and fluorescence recorded.

6.2.2. Sensitivity and Specificity of the Slot-Blot Assay to BMP-2/7:

Serial dilution of BMP- 2/7 was set up in 1:2 ratios starting from 1 µg (1000 ng) to obtain the range of detection by infrared imaging. Since BMP -2/7 is a heterodimer of

BMP 2 and BMP 7, our next effort was to determine the specificity of binding of the antibody to different BMPs. As described in the earlier section, a 1:2 serial dilution was performed of BMPs 2, 7 and 2/7 (with a starting concentration of 500 ng) in buffer and fluorescence detected.

6.2.3. Exposure of Organic Solvents to BMPs:

Since one of the main critiques of electrospinning tissue engineering scaffolds has been the use of volatile and potentially denaturing organic solvents, an experiment was set up to study the effects of commonly used solvents on BMP-2/7. The solvents used (hexafluroisopropanol-HFP, trifluroethanol-TFE, trifluroacetate-TFA) for serial dilutions were either undiluted or diluted by 50% with buffer to investigate whether increased polarity of the solvent would be beneficial. 100 ng of *BMP-2/7* was dissolved in fresh buffer or in solvents, and serial dilutions performed. The plates were left to dry under the hood overnight. The BMP was then re-solubilized in 100 µl of fresh buffer and dot-blotted onto a nitrocellulose membrane and developed for fluorescence as described.

6.2.4. Electrospinning BMP-2/7 and Characterizing its Release:

For controlled release experiments, 10 µg of BMP-2/7 was dissolved in 100 µl of buffer and added to 3 ml of PDO, PDO: nHA at 100 mg/ml concentration and nHA at 50% by wt of polymer. After mixing, the solutions were electrospun at 3 ml/hr, 26 kV for nHA containing solutions and 28 kV for pure PDO and the scaffolds collected on a mandrel of dimensions 7.5 x 1 x 0.5 cm. Dry scaffolds were cut into 6mm discs using a dermal biopsy

punch. The discs were placed in 100 µl of PBS and incubated at 37°C and 5% CO_2. The PBS was replaced at 1, 3, 6, 12, 24 hours and 2, 3, 4, 5, 7 and 14 days with 100 µl of fresh solution. All solutions were stored at -20°C till analysis. Samples were thawed to room temperature and slot-blotted onto nitrocellulose as described before.

6.2.5. Characterization of Biological Activity of BMPs on C1C12BRA cells:

C1C12BRA are specialized embryonic myoblast cell lines that have been stably transfected with a luciferase reporter plasmid consisting of BMP-responsive elements from the Id-1 promoter that is highly specific to BMP signaling and not any members of TGF-β family. It provides a powerful, highly sensitive and cell based assay for quantification of BMP activity. The peak luciferase activity has been found to occur 10-15 hours following exposure to BMPs [191]. These cells were cultured to 90% confluence in a T-75 flask in DMEM media containing 10% FBS and 1% penicillin and streptomycin. The cells were harvested with 0.25% trypsin, divided into equal aliquots and centrifuged to a pellet. Cells were then resuspended in either serum-free or serum-containing media and seeded in 6 well plates. After allowing adequate time for attachment and once they are at least 80% confluent, BMP-2, BMP-7 and BMP-2/7 in buffer was added in four different concentrations of 0.1, 1, 10 and 100 ng/ml. Control wells received an equal volume of buffer. The plates were returned to the incubator for a period of 10 hours. At this time, cells were washed twice with PBS and the lysate collected in 100 µl of cold reporter lysis buffer (Promega). The lysate was centrifuged at 1200g for 10 minutes and supernatant transferred to a new tube. Protein quantification (Bradford assay) of the lysate was

performed and the volumes normalized to ensure equal protein concentration. 20 µl of this sample was added to 100 µl of luciferase reagent and luminescence measured with a luminometer (Eppendorf, Westbury, NY).

6.2.6. Effect of Organic Solvents on the Biological Activity of BMP-2/7:

The experiment was carried out in a 6-well plate format in triplicate. C2C12 BRA cells were cultured in DMEM with 10% FBS with 1% penicillin-streptomycin until they were at least 90% confluent. 60 µl of BMP-2/7 (containing 60 ng) was mixed in a variety of organic electrospinning solvents- HFP, TFE, TFA, each either at full concentration or diluted in half with buffer to make it more polar. The plates were incubated at 37°C till dry and when the BMP was reconstituted in 60 µl of buffer. Each test well containing cells received 20 µl of reconstituted BMP-2/7 for every ml of media while control wells received an equal amount of BMP-2, BMP-7 or plain buffer. The luciferase activity was recorded as described above.

6.3. RESULTS

6.3.1. Sensitivity of the Assay:

The results from the slot-blot experiments are presented in **Figure 26**. There is an excellent correlation between the concentration of BMP-2/7 and the detected fluorescence. Thus the process parameters have been successfully optimized to enable reliable detection of BMP-2/7 using infrared imaging. The conservative limit of detection of BMP in this method was 15 ng.

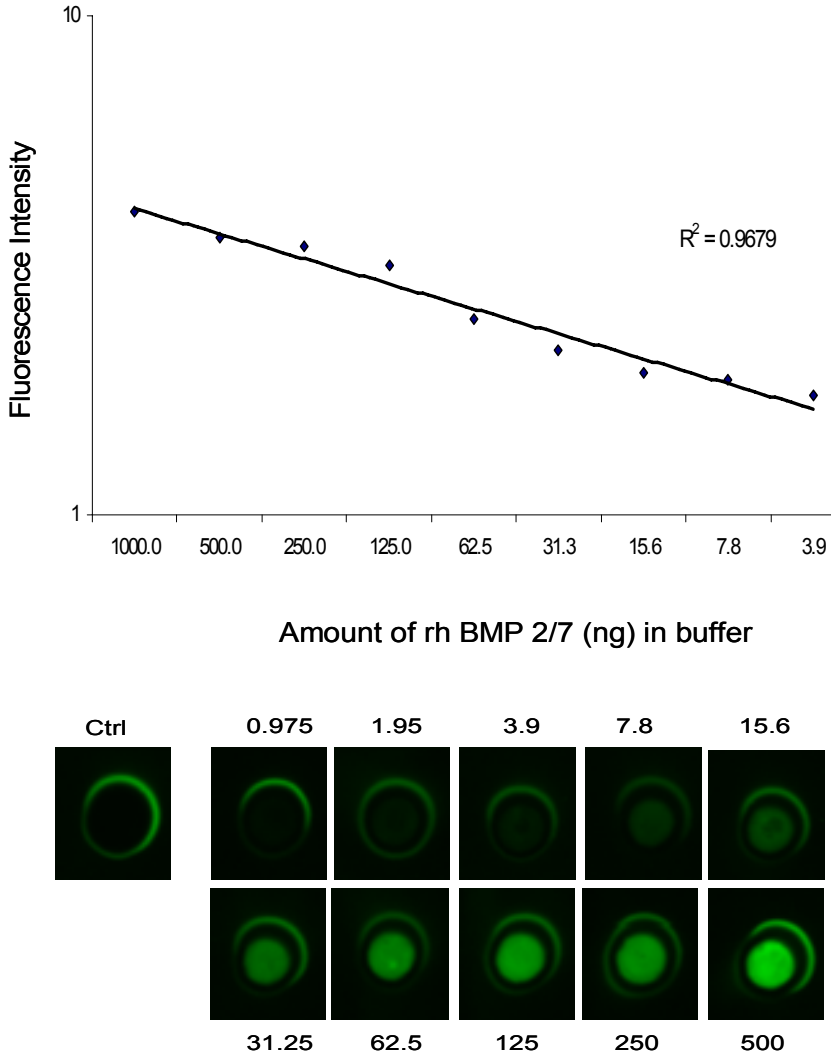

Figure 26: Slot-blot experiment to validate detection and quantification of BMP-2/7. A 1:2 serial dilution was made in buffer and blotted onto a nitro cellulose membrane. The membrane was probed with heterodimer specific antibody followed by incubation with fluorescent dye tagged secondary antibody. The membrane was scanned with infrared rays and fluorescence quantified. Lower panel shows the actual scan image

6.3.2. Specificity of the Assay to BMP-2/7:

The results (**Figure 27**) indicate a very high binding specificity of the antibody to BMP-2/7 heterodimer. The antibody did not bind to BMP-2 or BMP-7 even at very high

concentrations (500 ng). The fluorescence detected for BMP-2, BMP-7 and control lanes having no BMP is identical and remains flat throughout the range of dilutions.

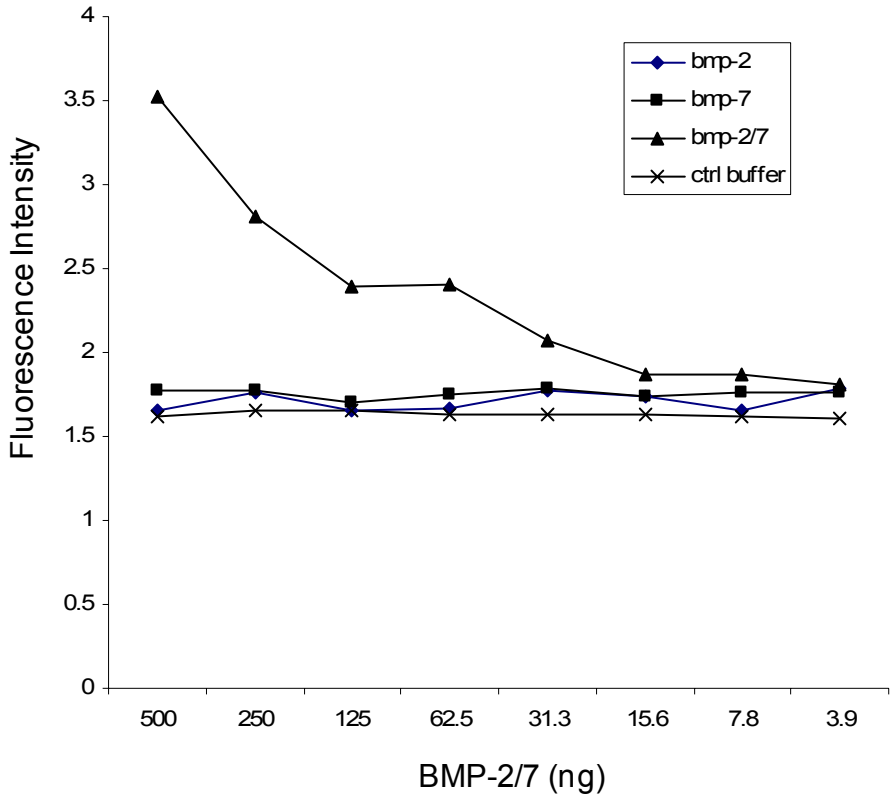

Figure 27: Slot blot experiments demonstrating specificity of the antibody to the dimeric form of BMP. Serial dilutions of BMP-2, BMP-7 and BMP-2/7 were made in buffer and blotted onto a nitrocellulose membrane. While the BMPs 2 and 7 were identical to buffer (control), BMP-2/7 gave a strong and specific signal.

6.3.3. Effect of Organic Solvents on BMPs:

The BMP-2/7 heterodimer consists of BMP-2 and BMP-7 held together by disulfide bonds and the antibody used is highly specific to the dimeric form of the BMP and does not recognize either of the monomeric forms of BMP. The heterodimeric BMP was exposed to an excess of organic solvents, in a period of time similar to that used in

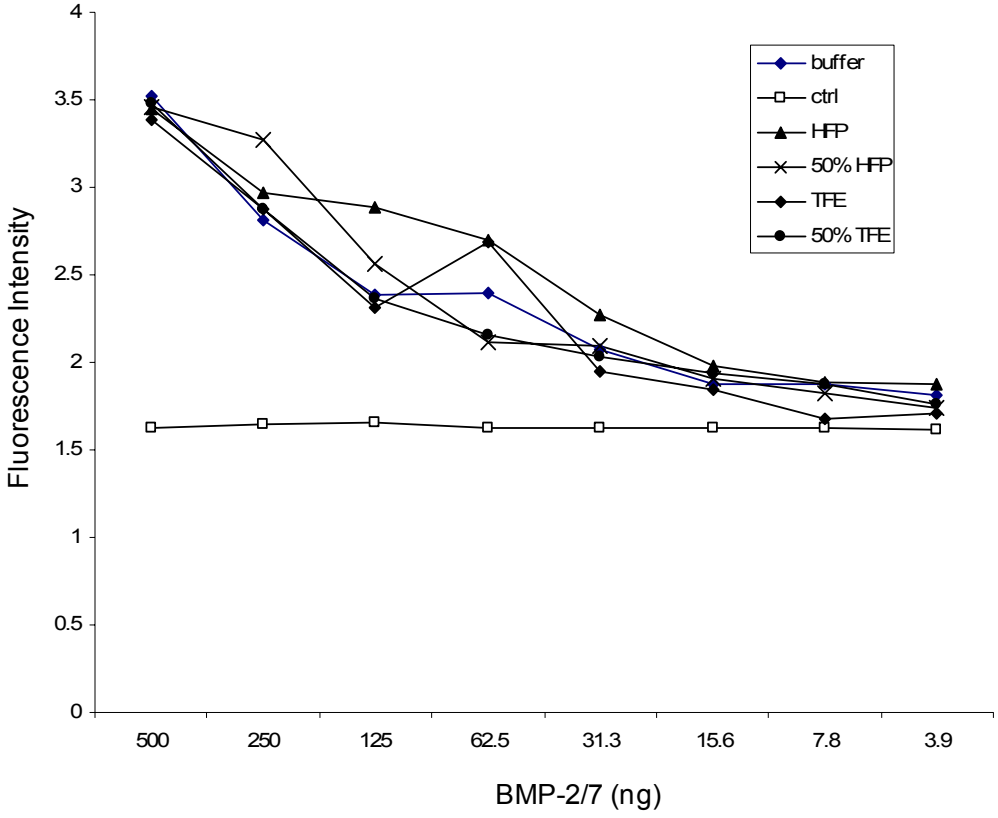

Figure 28: Effect of organic solvents on denaturation of dimeric form of BMP-2/7. Serial dilutions of the BMP was made in a variety of organic solvents and slot blotted onto nitrocellulose membrane. Results show no significant denaturation of the dimer when BMP is exposed to organic solvents. Dilution of solvents with aqueous buffer provided no benefit.

electrospinning. In spite of this exposure to harsh environment, the data shows no difference from BMPs in buffer (**Figure 28**). There is no evidence of dissociation of the heterodimer or protein denaturation sufficient to cause loss of epitope. These data suggest that exposure of BMP-2/7 does not result in denaturation of these biologically active molecules.

6.3.4. BMP-2/7 Release from Electrospun Scaffolds:

The data for release kinetics up to 2 weeks does not reveal anything dramatic (**Figure 29**). There is no difference in the release profile for either the PDO or PDO:nHA

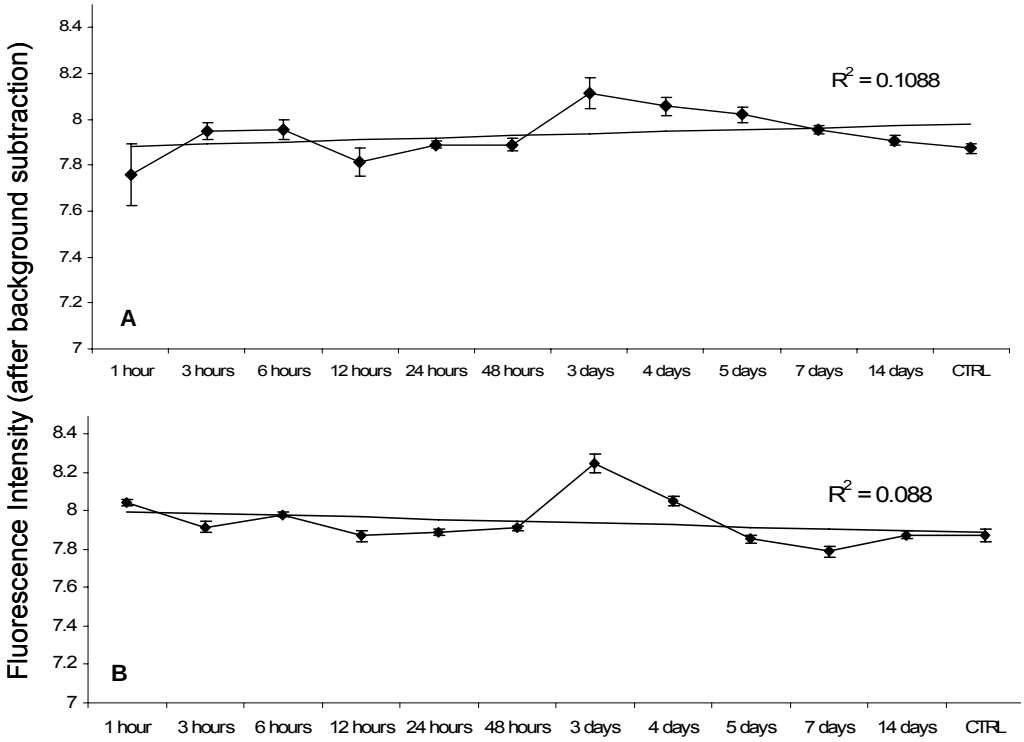

Figure 29: Release kinetics of *BMP-2/7* from electrospun PDO (A) and PDO:nHA (B) scaffolds. Ten micrograms of BMP was co-electrospun from HFP. Representative discs (n=6) were incubated in PBS for a total of 2 weeks and released BMP detected by blotting onto nitrocellulose membrane as described earlier. In spite of lack of an obvious trend, there are no signs of initial burst release from either types of scaffolds

scaffolds. There is no obvious initial burst, with the release peaking at 3 days for both scaffold types and eventually tapering off to control levels.

6.3.5. Efficacy of BMP- 2/7 on C2C12BRA Luciferase Activity:

All types of BMPs, whether homo or hetero dimers, induced luciferase activity. The response however was significantly higher when cells were cultured in the presence of serum. The luciferase induction with BMP-2/7 heterodimer was much more potent than the

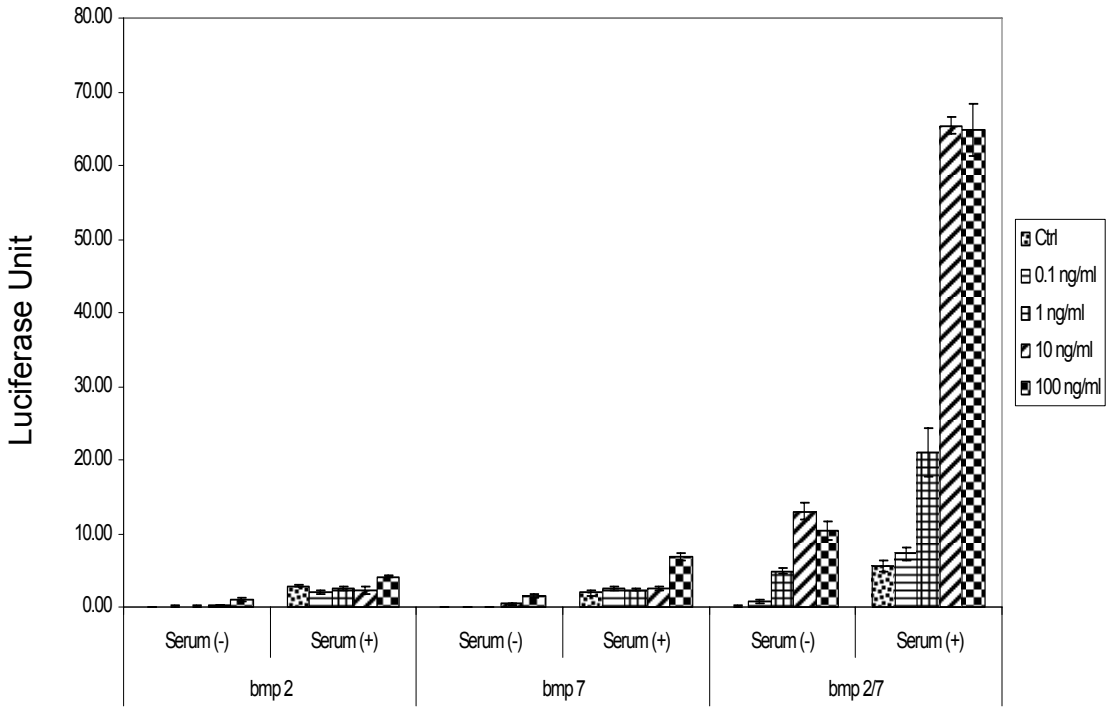

Figure 30: Effects of BMP on C2C12 BRA cells cultured in the presence or absence of serum. Cells were treated with different doses of BMP (0.1, 1, 10, 100 ng/ml) and luciferase activity evaluated after 10 hours of incubation. The heterodimeric BMP-2/7 was the most potent BMP at 10 ng/ ml.

corresponding homodimeric forms. The response observed with 10 ng/ml of BMP-2/7 was the highest and exceeded even 100 ng/ ml dosage. This might probably be due to overstimulation of cells and saturation of system (**Figure 30**). These data confirm that C1C12BRA provide an excellent tool to study the effects of BMPs especially if cultured in the presence of serum. BMP-2/7 showed at least a two fold increase in response at doses that are five times less than BMP-2 or BMP-7. These indicate that the heterodimeric form of BMP is much more potent than either of homodimers

6.3.6. Efficacy of Organic-Solvent Exposed BMP- 2/7 on C2C12BRA Luciferase Activity:

As expected, of the BMPs not exposed to solvents, BMP-2/7 was the most potent. BMP-2 and BMP-7 in buffer was identical in their ability to induce luciferase in C1C12BRA cells. Exposure of either of the homodimers or the heterodimer to HFP or TFE significantly reduced the luciferase activity. Of the two solvents tested, TFE seemed to better restore the activity of BMP-2/7. BMP-2/7 exposed to HFP or TFE has significant loss of biological activity, even though it was much higher than the homodimer controls (**Figure 31**).

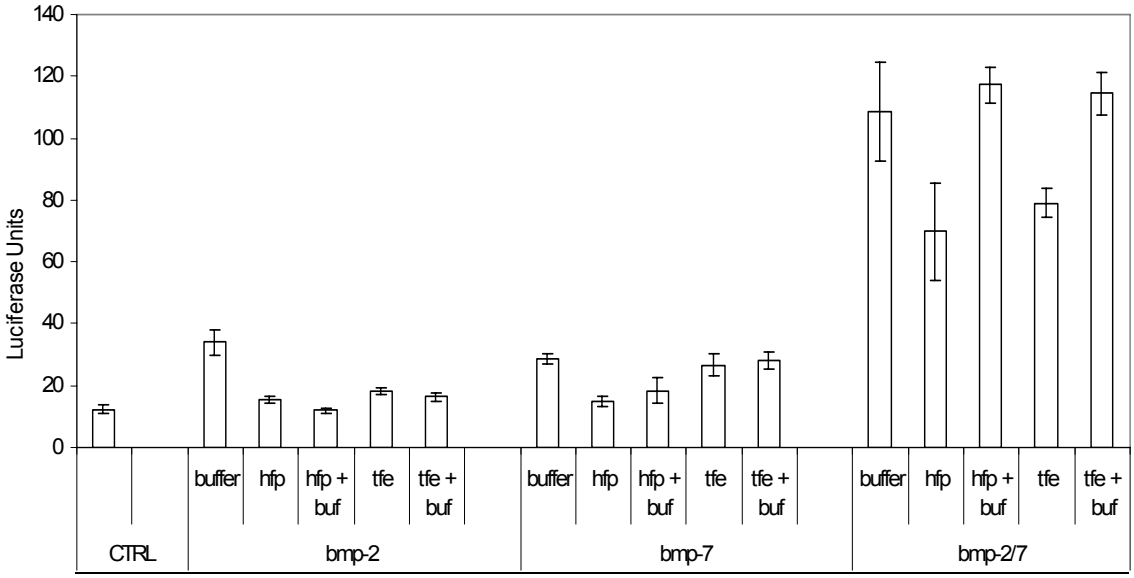

Figure 31: Effect of organic solvents on the biological activity of BMPs. Homodimer (BMP-2 and BMP-7) and heterodimer (BMP-2/7) were exposed to an excess of organic solvents till the solvents completely evaporated. They were then reconstituted in the solubilization buffer and added to the C2C12BRA cells in culture. After 10 hours of incubation, cells were lysed and luciferase activity detected.

More interesting was the effects of HFP and TFE diluted to 50% with aqueous buffer. Not only does this step recover most of the activity of all types of BMP, but achieves this without compromising the ability of the polymers to be electrospun. This is a significant finding given the indispensability of organic solvents in electrospinning.

6.4. DISCUSSION

Growth factors need to be present in a critical concentration for a defined period of time to be effective. BMPs, being water soluble, diffuse from the site of delivery and are inactivated in extracellular fluid when delivered in a buffer [192]. To compensate for losses, BMPs are administered at approximately 200,000 times the estimated physiologic concentration [193].

Our hypothesis was that incorporation of BMP-2/7 during fabrication (electrospinning) of scaffold will ensure their long term retention. In contrast, distribution of BMPs will be restricted to the surface of the fibers if delivered as a buffer to an already electrospun scaffold and will exhibit an initial burst release when placed in bulk media.

Since BMPs are allowed to interact with the polymer (PDO) prior to electrospinning, we rationalize that this would incorporate the growth factor within the scaffold much better. Addition of nHA to PDO is also expected to retain BMPs better mainly due to interaction of BMP to nHA at an atomic scale prior to electrospinning. The high surface energy of HA would also facilitate adsorption of BMPs [194, 195]. Additionally, electrospinning would incorporate BMPs at random within the individual nanofiber and throughout the thickness of the scaffold. These entrapped BMPs will be released into the media only after polymer degradation.

There are several explanations for the observations. First, there is a possibility of favorable interaction between the BMP and polymeric nanofibers resulting in effective incorporation and sequestration within the scaffold. In such a scenario, the BMP would be released only upon fiber degradation which does not happen to PDO scaffolds to any significant extent in 2 weeks. Thus two week duration might be too early for these studies.

On the other hand, amount of BMP-2/7 released from in the discs might be below the detection limit of the slot-blotting technique. This argument does not hold well against theoretical calculations that estimate the BMP content in the discs to be in the range of

150- 300 ng. (The total surface area of the mandrel is 22.5 cm^2). Since about 30% of the polymer solution is typically lost during electrospinning, 7 µg of BMP-2/7 is dispersed within the scaffold. This amount is well within the linear range of detection as described in the standard curve earlier.

The third possibility is that the process of electrospinning can induce sufficient denaturation of the peptide that the antibody can no longer recognize and bind. Even though previous data shows good detection of BMPs following exposure to the solvent, the effect of high voltage field on protein conformation is still not known. Denaturation of proteins under electric field is quite possible and this part of electrospinning can be as much of a problem to deal with as is the solvent. A simple experiment involving exposing the BMPs to high voltage field followed by slot-blot will reveal the nature of interaction.

The slot-blot experiments showed no significant denaturation following exposure to various solvents and near identical results with dilution of the solvent with buffer. While this data was informative, all it means is that the denaturation (if any) was not sufficient enough to prevent binding of the antibody to the epitope on the BMP-2/7 heterodimer. In order to verify the possibility that no denaturation occurred, a biological test of retention of function is necessary. Stably transfected C2C12BRA cells offered a great tool to investigate and explore the retention of biological activity of the BMPs following exposure to electrospinning solvents. If there were indeed no denaturation, all BMP-2/7 should behave identical irrespective of the type of solvent to which it was exposed. Our results from luciferase assay indicate significant loss of biological activity following exposure to

organic solvents – HFP and TFE. Among these solvents, TFE ranked better. However, if these solvents were made more polar by the addition of equal volume of aqueous buffer, there is a complete recovery of the lost activity and the values are no different from the controls.

6.5. CONCLUSION

We have successfully established a reliable slot-blot assay that enables specific detection and quantification of BMP-2/7. Initial validation of BMP function and optimization of dosage was done with C2C12BRA expressing luciferase in response to BMP treatment. BMP-2/7 heterodimer was found to be at least 5 times more potent than either of its homodimer counterparts, BMP-2 or BMP-7. We then coupled the slot-blotting technique and the luciferase expression of C2C12BRA system to investigate the complex questions concerning potential denaturing effects of organic solvents used in electrospinning on BMP-2/7. Our results indicate significant reduction in the biological activity of BMP-2/7 when exposed to an excess of solvent in the time duration relevant to electrospinning. However, much if not all of the lost activity is restored if the organic solvent is made more polar by dilution with aqueous buffer.

Chapter 7: CONCLUSION AND FUTURE STUDIES:

Regenerative medicine and tissue engineering are rapidly growing scientific disciplines that aim to restore structural, mechanical and metabolic functions of tissues and organs that are dysfunctional or absent. In light of growing evidence of the role of extracellular matrix in determining the form and function of the organ, synthesis of a suitable ECM has been the goal of tissue engineering. Electrospinning is one of the most commonly employed techniques in tissue engineering for the generation of nanoscaled fibrous structures that can be exploited to mimic the native ECM with respect to its composition and dimension.

The present study was devoted to developing synthetic bone substitutes intended for cleft palate repair. Cleft palate is a congenital condition of bony deficiency in the critical area of the mouth that significantly affects function and esthetics. Since well documented disadvantages exist with autografts and allografts, a search for synthetic bone analog is of substantial clinical relevance. In the present study, our first goal was to synthesize a 3D porous nanofibrous scaffold as a composite containing inorganic nHA in a

synthetic polymer matrix. This strategy would result in a better interface between the constituent phases of the composite and result in improved material properties. Accordingly, we devised a dual mineralization strategy wherein hydroxyapatite was incorporated into the matrix during electrospinning as a first step. This was followed by biomimetic mineralization of the electrospun scaffolds in SBF to further induce mineral deposition. The amount of mineral deposited varies directly as a function of concentration of inorganic nHA seeded during electrospinning. Using multiple-factor interaction statistics we concluded that PDO scaffolds containing 50% nHA incubated in r-SBF for 2 weeks resulted in maximum mineralization. Future studies can explore natural polymers such as fibrinogen and chitin as scaffold materials. This would be of interest because organized fibrin clot is slowly transformed into woven bone during natural fracture healing. In this sense, fibrinogen may play a direct role in mineralization and osseous healing. Chitin is another material that is not only abundant but also closely associated with inorganic minerals in nature and may prove to be advantageous.

In an effort to further match the material properties of the synthetic bone scaffold to the bone, we sought to exploit its natural plywood architecture. We attempted to mimic bone by stacking multiple electrospun sheets on top of each other and used high pressure to weld layers together. A pressure of 20,000 psi, held for a minute was sufficient in successful welding of the layers without any evidence of de-lamination. In addition the material properties of such multi-layered scaffolds greatly exceeded the values of single layered electrospun scaffolds. On the other hand, the permeability of the multi-layered scaffolds decreased as a function of the number of layers. Thus the strategy of biomimetic

mineralization and cold welding multiple layers of electrospun scaffolds can effectively be used to tailor the properties of the bone analog. Further investigation with respect to the amount and duration of pressure application will reveal interesting insights into the material behavior at the nanoscale.

In order to characterize the biological activity of the electrospun bone scaffolds, we developed an osteoblast adhesion assay by quantifying vinculin that participates directly in the focal adhesion complexes. In addition, a subset of vinculin - phosphovinculin (pY-822) was identified as a reliable and quantifiable molecular marker of focal adhesions irrespective of biomaterial surface studied. This seems to suggest that phosphorylation of vinculin at (Y-822) as one of the potential mechanisms for the formation of focal adhesion complexes. This specific form of vinculin was detected only when cells were grown on surfaces that are conducive for cell adhesion. ICW assay for phosphovinculin, proposed in this study, provides a simple yet accurate quantitative technique to follow the kinetics of focal adhesion formation when traditional assays have proven difficult. The penetrative ability of infrared rays further expands the scope of the assay to characterize cytocompatibility of 3D tissue engineering scaffolds by their ability to induce cell adhesion and migration.

Advances in recombinant technology and bone biology have established the potent role of osteoinductive molecules (BMPs) and adoption of this concept to enhance bone healing in tissue engineering has been quite seamless. However, this has been associated with a lot of challenges in practice: mode of incorporation into the scaffold, preservation of biological activity, ability to control and modulate release from the scaffold. One of the

criticisms in their use in conjunction with electrospinning has been the potentially denaturing interactions with the organic solvents. This study focuses on answering these basic questions. Our data indicated that BMP-2/7 heterodimer was at least 5 times more potent than either of its homodimer counterparts, BMP-2 or BMP-7 and hence was chosen to study solvent interactions. A biologically relevant luciferase assay on C2C12BRA cell lines was used to investigate potential loss of function of BMPs when exposed to organic solvents used in electrospinning. Our results indicate significant reduction in the biological activity of BMP-2/7 when exposed to an excess of solvent but most, if not all of the lost activity can be restored if the organic solvent is made more polar by dilution with aqueous buffer. This is a significant finding given the widespread popularity and use of organic solvents in electrospinning. Reliable detection of distribution of BMP within the electrospun matrix and optimization of its release is another area of tremendous challenge and can form the basis of future studies.

LITERATURE CITED

Literature Cited

1]. Haden NK CF, Alexander CJ, Bailit H et al. Improving the oral health status of all Americans: Roles and responsibilities of academic dental institutions: the report of the ADEA President's Commission. Journal of Dental Education 2003;67(5):563-583.

2]. da Silva Filho OG, Teles SG, Ozawa TO, Filho LC. Secondary bone graft and eruption of the permanent canine in patients with alveolar clefts: literature review and case report. Angle Orthod 2000;70(2):174-8.

3]. Murthy AS, Lehman JA. Evaluation of alveolar bone grafting: a survey of ACPA teams. Cleft Palate Craniofac J 2005;42(1):99-101.

4]. Laurencin C, Khan Y, El-Amin SF. Bone graft substitutes. Expert Rev Med Devices 2006;3(1):49-57.

5]. Silber JS, Anderson DG, Daffner SD, Brislin BT, Leland JM, Hilibrand AS, et al. Donor site morbidity after anterior iliac crest bone harvest for single-level anterior cervical discectomy and fusion. Spine 2003;28(2):134-9.

6]. Arrington ED, Smith WJ, Chambers HG, Bucknell AL, Davino NA. Complications of iliac crest bone graft harvesting. Clin Orthop Relat Res 1996(329):300-9.

7]. Younger EM, Chapman MW. Morbidity at bone graft donor sites. J Orthop Trauma 1989;3(3):192-5.

8]. Jardini MA, De Marco AC, Lima LA. Early healing pattern of autogenous bone grafts with and without e-PTFE membranes: a histomorphometric study in rats. Oral Surg Oral Med Oral Pathol Oral Radiol Endod 2005;100(6):666-73.

9]. Kang JS, Kim NH. The biomechanical properties of deep freezing and freeze drying bones and their biomechanical changes after *in vivo* allograft. Yonsei Med J 1995;36(4):332-5.

10]. Asselmeier MA, Caspari RB, Bottenfield S. A review of allograft processing and sterilization techniques and their role in transmission of the human immunodeficiency virus. Am J Sports Med 1993;21(2):170-5.

11]. Stevenson S. Biology of bone grafts. Orthop Clin North Am 1999;30(4):543-52.

12]. Mastrogiacomo M, Muraglia A, Komlev V, Peyrin F, Rustichelli F, Crovace A, et al. Tissue engineering of bone: search for a better scaffold. Orthod Craniofac Res 2005;8(4):277-84.

13]. Cao Y IC, Vacanti C. Synthetic biodegradable polymer scaffolds. In: Tissue engineering of bone and cartilage: Atala A and Mooney; 1996. p. 199-212.

14]. Karp JM, Shoichet MS, Davies JE. Bone formation on two-dimensional poly(DL-lactide-co-glycolide) (PLGA) films and three-dimensional PLGA tissue engineering scaffolds *in vitro*. J Biomed Mater Res A 2003;64(2):388-96.

15]. Cheresh DA, Stupack DG. Regulation of angiogenesis: apoptotic cues from the ECM. Oncogene 2008;27(48):6285-98.

16]. Stupack DG. Integrins as a distinct subtype of dependence receptors. Cell Death Differ 2005;12(8):1021-30.

17]. Stupack DG, Cheresh DA. Get a ligand, get a life: integrins, signaling and cell survival. J Cell Sci 2002;115(Pt 19):3729-38.

18]. Green JA, Yamada KM. Three-dimensional microenvironments modulate fibroblast signaling responses. Adv Drug Deliv Rev 2007;59(13):1293-8.

19]. Ushiki T. Collagen fibers, reticular fibers and elastic fibers. A comprehensive understanding from a morphological viewpoint. Arch Histol Cytol 2002;65(2):109-26.

20]. Stevens MM, George JH. Exploring and engineering the cell surface interface. Science 2005;310(5751):1135-8.

21]. Pedersen JA, Swartz MA. Mechanobiology in the third dimension. Ann Biomed Eng 2005;33(11):1469-90.

22]. Chen CS, Tan J, Tien J. Mechanotransduction at cell-matrix and cell-cell contacts. Annu Rev Biomed Eng 2004;6:275-302.

23]. Katsumi A, Orr AW, Tzima E, Schwartz MA. Integrins in mechanotransduction. J Biol Chem 2004;279(13):12001-4.

24]. Nelson CM, Bissell MJ. Of extracellular matrix, scaffolds, and signaling: tissue architecture regulates development, homeostasis, and cancer. Annu Rev Cell Dev Biol 2006;22:287-309.

25]. Streuli C. Extracellular matrix remodelling and cellular differentiation. Curr Opin Cell Biol 1999;11(5):634-40.

26]. Lee YJ, Streuli CH. Extracellular matrix selectively modulates the response of mammary epithelial cells to different soluble signaling ligands. J Biol Chem 1999;274(32):22401-8.

27]. Berrier AL, Yamada KM. Cell-matrix adhesion. J Cell Physiol 2007;213(3):565-73.

28]. Kong HJ, Mooney DJ. Microenvironmental regulation of biomacromolecular therapies. Nat Rev Drug Discov 2007;6(6):455-63.

29]. Smith LA, Ma PX. Nano-fibrous scaffolds for tissue engineering. Colloids Surf B Biointerfaces 2004;39(3):125-31.

30]. Vasita R, Katti DS. Nanofibers and their applications in tissue engineering. Int J Nanomedicine 2006;1(1):15-30.

31]. Park H CC, Vunjak-Novakovic G, Langer R, Vacanti CA, Farokhzad OC. Nanofabrication and microfabrication of functional materials for tissue engineering. Tissue Eng 2007;13(8):1867-77.

32]. Barnes CP SS, Boland ED, Simpson DG, Bowlin GL. Nanofiber technology: designing the next generation of tissue engineering scaffolds. Adv Drug Deliv Rev 2007;59(14):1413-33.

33]. Ma Z KM, Inai R, Ramakrishna S. Potential of nanofiber matrix as tissue-engineering scaffolds. Tissue Eng 2005;11(1-2):101-9.

34]. Whitesides GM, Grzybowski B. Self-assembly at all scales. Science 2002;295(5564):2418-21.

35]. Huie J. Guided molecular self-assembly: a review of recent efforts. Smart Mater. Struct 2003;12:264-271.

36]. Ottani V, Martini D, Franchi M, Ruggeri A, Raspanti M. Hierarchical structures in fibrillar collagens. Micron 2002;33(7-8):587-96.

37]. Khoshnoodi J, Cartailler JP, Alvares K, Veis A, Hudson BG. Molecular recognition in the assembly of collagens: terminal noncollagenous domains are key recognition modules in the formation of triple helical protomers. J Biol Chem 2006;281(50):38117-21.

38]. Hulmes DJ. Building collagen molecules, fibrils, and suprafibrillar structures. J Struct Biol 2002;137(1-2):2-10.

39]. van der Rest M, Garrone R. Collagen family of proteins. Faseb J 1991;5(13):2814-23.

40]. Yokoi H KT, Zhang S. Dynamic reassembly of peptide RADA16 nanofiber scaffold. Proc Natl Acad Sci U S A 2005;102(24):8414-9.

41]. Hartgerink JD, Beniash E and Stupp SI. Self assembly and mineralization of peptide-amphiphile nanofibers. Science, 2001; 294 (5547): 1684-88.

42]. Silva GA, Czeisler C, Niece KL, Beniash E, Harrington DA, Kessler JA, et al. Selective differentiation of neural progenitor cells by high-epitope density nanofibers. Science 2004;303(5662):1352-5.

43]. Zhang S. Emerging biological materials through molecular self-assembly. Biotechnol Adv 2002;20(5-6):321-39.

44]. Zhang S. Fabrication of novel biomaterials through molecular self-assembly. Nat Biotechnol 2003;21(10):1171-8.

45]. Zhang S MD, Hwang W, Santoso S. Design of nanostructured biological materials through self-assembly of peptides and proteins. Curr Opin Chem Biol 2002;6(6):865-71.

46]. Gelain F HA, Zhang S. Designer self-assembling peptide scaffolds for 3-d tissue cell
cultures and regenerative medicine. Macromol Biosci 2007;7(5):544-51.

47]. Holmes TC dLS, Su X, Liu G, Rich A, Zhang S. Extensive neurite outgrowth and active synapse formation on self-assembling peptide scaffolds. Proc Natl Acad Sci U S A 2000;97(12):6728-33.

48]. Beniash E HJ, Storrie H, Stendahl JC, Stupp SI. Self-assembling peptide amphiphile nanofiber matrices for cell entrapment. Acta Biomater 2005;1(4):387-97.

49]. Galler KM CA, Yuwono V, Dong H, Shi S, Schmalz G, Hartgerink JD, D'Souza RN. Self-Assembling Peptide Amphiphile Nanofibers as a Scaffold for Dental Stem Cells. Tissue Eng Part A 2008.

50]. Kirkham J FA, Vernals D, Boden N, Robinson C, Shore RC, Brookes SJ, Aggeli A. Self-assembling peptide scaffolds promote enamel remineralization. J Dent Res 2007;86(5):426-30.

51]. Bella J EM, Brodsky B, Berman HM. Crystal and molecular structure of a collagen-like peptide at 1.9 A resolution. Science 1994;266(5182):75-81.
52]. Gauba V HJ. Self-assembled heterotrimeric collagen triple helices directed through electrostatic interactions. J Am Chem Soc 2007;129(9):2683-90.

53]. Gauba V HJ. Synthetic collagen heterotrimers: structural mimics of wild-type and mutant collagen type I. J Am Chem Soc 2008;130(23):7509-15.

54]. Gauba V HJ. Surprisingly high stability of collagen ABC heterotrimer: evaluation of side chain charge pairs. J Am Chem Soc 2007;129(48):15034-41.

55]. Capito RM, Azevedo HS, Velichko YS, Mata A, Stupp SI. Self-assembly of large and small molecules into hierarchically ordered sacs and membranes. Science 2008;319(5871):1812-6.

56]. Gelain F BD, Vescovi A, Zhang S. Designer self-assembling Peptide nanofiber scaffolds for adult mouse neural stem cell 3-dimensional cultures. PLoS ONE 2006;1:e119.

57]. Chen VJ SL, Ma PX. Bone regeneration on computer-designed nano-fibrous scaffolds. Biomaterials 2006;27(21):3973-9.
58]. Firth A AA, Burke JL, Yang X, Kirkham J. Biomimetic self-assembling peptides as injectable scaffolds for hard tissue engineering. Nanomed 2006;1(2):189-99.

59]. Horii A WX, Gelain F, Zhang S. Biological designer self-assembling Peptide nanofiber scaffolds significantly enhance osteoblast proliferation, differentiation and 3-D migration. PLoS ONE 2007;2(2):e190.

60]. Hosseinkhani H HM, Gabrielson NP, Pack DW, Khademhosseini A, Kobayashi H. DNA nanoparticles encapsulated in 3D tissue-engineered scaffolds enhance osteogenic differentiation of mesenchymal stem cells. J Biomed Mater Res A 2008;85(1):47-60.

61]. Hosseinkhani H HM, Tian F, Kobayashi H, Tabata Y. Ectopic bone formation in collagen sponge self-assembled peptide-amphiphile nanofibers hybrid scaffold in a perfusion culture bioreactor. Biomaterials 2006;27(29):5089-98.

62]. Genove E SC, Zhang S, Semino CE. The effect of functionalized self-assembling peptide scaffolds on human aortic endothelial cell function. Biomaterials 2005;26(16):3341-51.

63]. Hosseinkhani H HM, Khademhosseini A, Kobayashi H, Tabata Y. Enhanced angiogenesis through controlled release of basic fibroblast growth factor from peptide amphiphile for tissue regeneration. Biomaterials 2006;27(34):5836-44.

64]. Young A. Microcellular foams via phase separation. J Vac Sci Technol.A 1986;4(3):1128-1133.

65]. Young A. Polymer-Solvent Phase Separation as a Route to Low Density Microcellular Plastic Foams. J Cellular Plastics 1987;23:55-72.

66]. Tanaka H. Universality of viscoelastic phase separation in dynamically asymmetric fluid mixtures. Phys Rev Lett 1996;76(5):787-790.

67]. Tanaka H. Viscoelastic model of phase separation in colloidal suspensions and emulsions. Phys Rev E Stat Phys Plasmas Fluids Relat Interdiscip Topics 1999;59(6):6842-52.

68]. Tanaka H. Viscoelastic phase separation. J.Phys.:Condens. Matter 2000;12:R207-R264.

69]. van de Witte P DP, van den Berg JWA, Feijen J. Phase separation processes in polymer solutions in relation to membrane formation. J Membrane Science 1996;117:1-31.

70]. Pins GD CD, Patel R, and Silver FH. Self-Assembly of Collagen Fibers. Influence of Fibrillar Alignment and Decorin on Mechanical Properties. Biophysical Joumal 1997;73:2164-72.

71]. Cavallaro JF KP, Kraus KH. Collagen fabrics as biomaterials. Biotechnol Bioeng 1994;43(8):781-91.

72]. Zeugolis DI PR, Attenburrow G. Extruded collagen-polyethylene glycol fibers for tissue engineering applications. J Biomed Mater Res B Appl Biomater 2008;85(2):343-52.

73]. Zeugolis DI PR, Attenburrow G. Cross-linking of extruded collagen fibers-A biomimetic three-dimensional scaffold for tissue engineering applications. J Biomed Mater Res A 2008;[Epub ahead of print].

74]. Dunn MG AP, Zawadsky JP. Optimization of extruded collagen fibers for ACL reconstruction. J Biomed Mater Res 1993;27(12):1545-52.

75]. Ma PX ZR. Synthetic nano-scale fibrous extracellular matrix. J Biomed Mater Res 1999;46(1):60-72.

76]. Ho MH KP, Hsieh HJ, Hsien TY, Hou LT, Lai JY, Wang DM. Preparation of porous scaffolds by using freeze-extraction and freeze-gelation methods. Biomaterials 2004;25(1):129-38.

77]. Doshi J RD. Electrospinning process and applications of electrospun fibers. J Electrost 1995;35(2-3):151-160.

78]. Shin YM HM, Brenner MP, Rutledge GC. Electrospinning: A whipping fluid jet generates submicron polymer fibers. Appl. Phys. Lett 2001;78(8):1149-51.

79]. Hohman MM SY, Rutledge G, Brenner MP. Electrospinning and electrically forced jets I:Stability theory. In: Physics of Fluids; 2001. p. 2201-2220.

80]. Hohman MM SY, Rutledge G, Brenner MP. Electrospinning and electrically forced jets II: Applications. In: Physics of Fluids; 2001. p. 2221-2236.

81]. Zuo WW ZM, Yang W, Yu H, Chen YM, Zhang Y. Experimental study on relationship between jet instability and formation of beaded structures during electrospinning. Polym Eng Sci 2005;45(5):704-709.

82]. Reneker DH KW, Theron A, Zussman E, Yarin AL. Nanofiber garlands of polycaprolactone by electrospinning. Polymer 2002;43:6785–6794.

83]. McKee MG LJ, Cashion MP, Long TE. Phospholipid Nonwoven Electrospun Membranes. Science 2006;311:353.

84]. Ji-Huan He LX, Yue Wu, Yong Liu. Mathematical models for continuous electrospun nanofibers and electrospun nanoporous microspheres. Polymer International 2007;56:1323-1329.

85]. Li D XY. Direct fabrication of composite and ceramic hollow nanofibers by electrospinning. Nanoletters 2004; 4(5):933-938.

86]. Ma M KV, Yu JH, Thomas EL, Rutledge GC. Electrospun polymer nanofibers with internal periodic structure obtained by microphase separation of cylindrically confined block copolymers. Nano Lett 2006;6(12):2969-72.

87]. Townsend-Nicholson A, Jayasinghe SN. Cell electrospinning: a unique biotechnique for encapsulating living organisms for generating active biological microthreads/scaffolds. Biomacromolecules 2006;7(12):3364-9.

88]. Arumuganathar S, Irvine S, McEwan JR, Jayasinghe SN. Pressure-assisted cell spinning: a direct protocol for spinning biologically viable cell-bearing fibres and scaffolds. Biomed Mater 2007;2(4):211-9.

89]. He JH WY, Xu L. Nano-effects, quantum-llike properties in electrospun nanofibers. Chaos, Solitons and Fractals 2007;33:26-37.

90]. Gu SY WQ, Ren J, Vancso GJ. Mechanical Properties of a Single Electrospun Fiber and Its Structures. Macromol Rapid Commun 2005;26:716–20.

91]. Teo WE HW, Ramakrishna S. Electrospun scaffold tailored for tissue-specific extracellular matrix. Biotechnol J 2006;1(9):918-29.

92]. Pham QP, Sharma U, Mikos AG. Electrospinning of polymeric nanofibers for tissue engineering applications: a review. Tissue Eng 2006;12(5):1197-211.

93]. Boland ED TT, Simpson DG, Wnek GE, Bowlin GL. Utilizing acid pretreatment and electrospinning to improve biocompatibility of poly(glycolic acid) for tissue engineering. J Biomed Mater Res B Appl Biomater 2004;71(1):144-52.

94]. Kim K YM, Zong X, Chiu J, Fang D, Seo YS, Hsiao BS, Chu B, Hadjiargyrou M. Control of degradation rate and hydrophilicity in electrospun non-woven poly(D,L-lactide) nanofiber scaffolds for biomedical applications. Biomaterials 2003;24(27):4977-85.

95]. Boland ED CB, Barnes CP, Simpson DG, Wnek GE, Bowlin GL. Electrospinning polydioxanone for biomedical applications. Acta Biomater 2005;1(1):115-23.

96]. Kwon IK KS, Matsuda T. Electrospun nano- to microfiber fabrics made of biodegradable copolyesters: structural characteristics, mechanical properties and cell adhesion potential. Biomaterials 2005;26(18):3929-39.

97]. Matthews JA WG, Simpson DG, Bowlin GL. Electrospinning of collagen nanofibers. Biomacromolecules 2002;3(2):232-8.

98]. Zeugolis DI KS, Yew ES, Ekaputra AK, Tong YW, Yung LY, Hutmacher DW, Sheppard C, Raghunath M. Electro-spinning of pure collagen nano-fibres - just an expensive way to make gelatin? Biomaterials 2008;29(15):2293-305.

99]. Telemeco TA AC, Bowlin GL, Wnek GE, Boland ED, Cohen N, Baumgarten CM, Mathews J, Simpson DG. Regulation of cellular infiltration into tissue engineering scaffolds composed of submicron diameter fibrils produced by electrospinning. Acta Biomater 2005;1(4):377-85.

100]. S Weiner HW. THE MATERIAL BONE: Structure-Mechanical Function Relations. Annual Review of Materials Science 1998;28:271-298.

101]. Yiquan Wu LLH, Jing Du, Kwang-Leong Choy andJingkun Guo. Preparation of Hydroxyapatite Fibers by Electrospinning Technique. J. Am. Ceram. Soc., 2004;87(10):1988-1991.

102]. Kim HW KH. Nanofiber generation of hydroxyapatite and fluor-hydroxyapatite bioceramics. J Biomed Mater Res B Appl Biomater. 2005;77(2):323-8.

103]. Kim HW SJ, Kim HE. Bioactive glass nanofiber-collagen nanocomposite as a novel bone regeneration matrix. J Biomed Mater Res A 2006;79(3):698-705.

104]. Edirisinghe HBZaMJ. Electrospinning Zirconia Fiber From a Suspension. J. Am. Ceram. Soc., 2006;89(6):1870-1875.

105]. Yoshimoto H SY, Terai H, Vacanti JP. A biodegradable nanofiber scaffold by electrospinning and its potential for bone tissue engineering. Biomaterials 2003;24(12):2077-2082.

106]. Wutticharoenmongkol P, Sanchavanakit N, Pavasant P, Supaphol P. Novel bone scaffolds of electrospun polycaprolactone fibers filled with nanoparticles. J Nanosci Nanotechnol 2006;6(2):514-22.

107]. Fujihara K, Kotaki M, Ramakrishna S. Guided bone regeneration membrane made of polycaprolactone/calcium carbonate composite nano-fibers. Biomaterials 2005;26(19):4139-47.

108]. Walker-Simmons M RC. Proteinase Inhibitor Synthesis in Tomato Leaves: Induction by Chitosan Oligomers and Chemically Modified Chitosan and Chitin. Plant Physiol. 1984 November;76(3):787-90.

109]. MM. A. Permeability and blood compatibility properties of chitosan-poly(ethylene oxide) blend membranes for haemodialysis. Biomaterials. 1995;16(8):593-9.

110]. Okamoto Y WM, Miyatake K, Morimoto M, Shigemasa Y, Minami S. Effects of chitin/chitosan and their oligomers/monomers on migrations of fibroblasts and vascular endothelium. Biomaterials. 2002;23(9):1975-9.

111]. Geng X KO, Jang J. Electrospinning of chitosan dissolved in concentrated acetic acid solution. biomaTb 2005.

112]. Duan B DC, Yuan X, Yao K. Electrospinning of chitosan solutions in acetic acid with poly(ethylene oxide). J Biomater Sci Polym Ed 2004;15(6):797-811.

113]. Bhattarai N ED, Veiseh O, Matsen FA, Zhang M. Electrospun chitosan-based nanofibers and their cellular compatibility. Biomaterials 2005;26(31):6176-84.

114]. Meinel L KV, Hofmann S, Fajardo R, Snyder B, Li C, Zichner L, Langer R, Vunjak-Novakovic G, Kaplan DL. Engineering bone-like tissue *in vitro* using human bone marrow stem cells and silk scaffolds. J Biomed Mater Res A 2004 Oct 1;71(1):25-34.

115]. Jin HJ FS, Rutledge GC, Kaplan DL. Electrospinning Bombyx mori silk with poly(ethylene oxide). Biomacromolecules 2002;5(3):786-792.

116]. Li C VC, Jin HJ, Kim HJ, Kaplan DL. Electrospun silk-BMP-2 scaffolds for bone tissue engineering. Biomaterials 2006;27(16):3115-24.

117]. Laurencin CT NL. Polyphosphazene nanofibers for biomedical applications: preliminary studies. Nanoengineered nanofibrous materials, NATO-ASI Proceedings. 2004:281-300.

118]. Subhabrata Bhattacharyya LSN, Anurima Singh, Nick R. Krogman, Jared Bender, Yaser E. Greish, Paul W. Brown, Harry R. Allcock, Cato T. Laurencin. Development of Biodegradable Polyphosphazene- Nanohydroxyapatite Composite Nanofibers Via Electrospinning. MRS Symposium Proceedings 2005;845:91-96.

119]. Gomes ME, Reis RL, Cunha AM, Blitterswijk CA, de Bruijn JD. Cytocompatibility and response of osteoblastic-like cells to starch-based polymers: effect of several additives and processing conditions. Biomaterials 2001;22(13):1911-7.

120]. Gomes ME. Alternative tissue engineering scaffolds based on starch: processing methodologies, morphology, degradation and mechanical properties. Materials Science and Engineering: C 2002;20(1-2):19-26.

121]. Tuzlakoglu K, Bolgen N, Salgado AJ, Gomes ME, Piskin E, Reis RL. Nano- and micro-fiber combined scaffolds: a new architecture for bone tissue engineering. J Mater Sci Mater Med 2005;16(12):1099-104.

122]. Glimcher MJ. Mechanism of calcification: role of collagen fibrils and collagen-phosphoprotein complexes *in vitro* and *in vivo*. Anat Rec 1989;224(2):139-53.

123]. Traub W, Arad T, Weiner S. Origin of mineral crystal growth in collagen fibrils. Matrix 1992;12(4):251-5.

124]. Dorozhkin SV, Epple M. Biological and medical significance of calcium phosphates. Angew Chem Int Ed Engl 2002;41(17):3130-46.

125]. Landis WJ. The strength of a calcified tissue depends in part on the molecular structure and organization of its constituent mineral crystals in their organic matrix. Bone 1995;16:533-544.

126]. Ohura K, Nakamura T, Yamamuro T, Kokubo T, Ebisawa Y, Kotoura Y, et al. Bone-bonding ability of P2O5-free CaO.SiO2 glasses. J Biomed Mater Res 1991;25:357-65.

127]. Hench LL. Bioceramics: from concept to clinic. J Am Ceram Soc 1991;74:1487-1510.

128]. Wang IC, Reddy MS, Geurs NC, Jeffcoat MK. Risk factors in dental implant failure. J Long Term Eff Med Implants 1996;6(2):103-17.

129]. Morris HF, Ochi S, Spray JR, Olson JW. Periodontal-type measurements associated with hydroxyapatite-coated and non-HA-coated implants: uncovering to 36 months. Ann Periodontol 2000;5(1):56-67.

130]. Geurs NC, Jeffcoat RL, McGlumphy EA, Reddy MS, Jeffcoat MK. Influence of implant geometry and surface characteristics on progressive osseointegration. Int J Oral Maxillofac Implants 2002;17(6):811-5.

131]. Abe Y, Kokubo T, Yamamuro T. Apatite Coating on ceramics, metals and polymers utilizing a biological process. Journal of Material Science: Materials in Medicine 1990;1:232-38.

132]. Hutmacher DW, Schantz JT, Lam CX, Tan KC, Lim TC. State of the art and future directions of scaffold-based bone engineering from a biomaterials perspective. J Tissue Eng Regen Med 2007;1(4):245-60.

133]. Rho JY, Kuhn-Spearing L, Zioupos P. Mechanical properties and the hierarchical structure of bone. Med Eng Phys 1998;20(2):92-102.

134]. Currey JD. The design of mineralized hard tissues for their mechanical functions. Journal of Experimental Biology 1999;202:3285-3294.

135]. Fratzl P, Gupta HS, Paschalis EP, Roschger P. Structure and mechanical quality of the collagen-mineral nano-composite in bone. Journal of Materials Chemistry 2004;14:2115-2123.

136]. Kilpadi KL, Chang PL, Bellis SL. Hydroxylapatite binds more serum proteins, purified integrins, and osteoblast precursor cells than titanium or steel. J Biomed Mater Res 2001;57(2):258-67.

137]. Woo KM, Seo J, Zhang R, Ma PX. Suppression of apoptosis by enhanced protein adsorption on polymer/hydroxyapatite composite scaffolds. Biomaterials 2007;28(16):2622-30.

138]. Yuan H, Li Y, de Bruijn JD, de Groot K, Zhang X. Tissue responses of calcium phosphate cement: a study in dogs. Biomaterials 2000;21(12):1283-90.

139]. Oyane A, Kim HM, Furuya T, Kokubo T, Miyazaki T, Nakamura T. Preparation and assessment of revised simulated body fluids. J Biomed Mater Res A 2003;65(2):188-95.

140]. Gregory CA, Gunn WG, Peister A, Prockop DJ. An Alizarin red-based assay of mineralization by adherent cells in culture: comparison with cetylpyridinium chloride extraction. Anal Biochem 2004;329(1):77-84.

141]. Dorozhkin SV, Dorozhkina EI. Crystallization from a milk-based revised simulated body fluid. Biomedical Materials 2007;2:87-92.

142]. Konigsberger E, Konigsberger L. Biomineralization: Medical Aspects of Solubility. 2006:80-175.

143]. Bohner M. Physical and chemical aspects of calcium phosphates used in spinal surgery. Eur Spine J 2001;10 Suppl 2:S114-21.

144]. Ben-Nissan., Chai., Evans. Encyclopedic handbook of biomaterials and bioengineering: Marcel Dekker; 1995.

145]. Tanahashi M, Yao T, Kokubo T, Minoda M, Miyamoto T, Nakamura T, et al. Apatite coated on organic polymers by biomimetic process: improvement in its adhesion to substrate by NaOH treatment. J Appl Biomater 1994;5(4):339-47.

146]. Cho SB, Nakanishi K, Kokubo T, Soga N, Ohtsuki C, Nakamura T, et al. Dependence of Apatite Formation on Silica Gel on Its Structure: Effect of Heat Treatment. J Am Ceram Soc 1995;78(7):1769-74.

147]. Chen J, Chu B, Hsiao B. Mineralization of hydroxyapatite in electrospun nanofibrous poly(L-lactic acid) scaffolds. J Biomed Mater Res Part A 2006;79A(2):307-317.

148]. Ohtsuki C, Kamitakahara M, Miyazaki T. Coating bone-like apatite onto organic substrates using solutions mimicking body fluid. J Tissue Eng Regen Med 2007;1(1):33-8.

149]. Takeuchi A, Ohtsuki C, Miyazaki T, Kamitakahara M, Ogata S, Yamazaki M, et al. Heterogeneous nucleation of hydroxyapatite on protein: structural effect of silk sericin. J R Soc Interface 2005;2(4):373-8.

150]. Li P, Ohtsuki C, Kokubo T, Nakanishi K, Soga N, Nakamura T, et al. Effects of ions in aqueous media on hydroxyapatite induction by silica gel and its relevance to bioactivity of bioactive glasses and glass-ceramics. J Appl Biomater 1993;4(3):221-9.

151]. Li P, Ohtsuki C, Kokubo T, Nakanishi K, Soga N, de Groot K. The role of hydrated silica, titania, and alumina in inducing apatite on implants. J Biomed Mater Res 1994;28(1):7-15.

152]. Kawai T, Ohtsuki C, Kamitakahara M, Hosoya K, Tanihara M, Miyazaki T, et al. *In vitro* apatite formation on polyamide containing carboxyl groups modified with silanol groups. J Mater Sci Mater Med 2007;18(6):1037-42.

153]. Sell SA, Barnes CP, Simpson DG and Bowlin GL. Scaffold permeability as a means to determine fiber diameter and pore size of electrospun fibrinogen J Biomed Mater Res 2007;85 A (1):115-126.

154]. Leong DT, Gupta A, Bai HF, Wan G, Yoong LF, Too HP, et al. Absolute quantification of gene expression in biomaterials research using real-time PCR. Biomaterials 2007;28(2):203-10.

155]. Doroski DM, Brink KS, Temenoff JS. Techniques for biological characterization of tissue-engineered tendon and ligament. Biomaterials 2007;28(2):187-202.

156]. Owen G, Meredith D, ap Gwynn I, Richards R. Focal adhesion quantification - A new assay of material biocompatibility? Review. European Cells and Materials Journal 2005;9:85-96.

157]. Folkman J MA. Role of cell shape in growth control. Nature 1978;273:345.

158]. Ruoslahti E RJ. Anchorage dependence, integrins, and apoptosis. Cell 1994;77:477-478.

159]. McBeath R, Pirone DM, Nelson CM, Bhadriraju K, Chen CS. Cell shape, cytoskeletal tension, and RhoA regulate stem cell lineage commitment. Dev Cell 2004;6(4):483-95.

160]. Badami AS, Kreke MR, Thompson MS, Riffle JS, Goldstein AS. Effect of fiber diameter on spreading, proliferation, and differentiation of osteoblastic cells on electrospun poly(lactic acid) substrates. Biomaterials 2006;27(4):596-606.

161]. Woo KM, Jun JH, Chen VJ, Seo J, Baek JH, Ryoo HM, et al. Nano-fibrous scaffolding promotes osteoblast differentiation and biomineralization. Biomaterials 2007;28(2):335-43.

162]. Simpson DG. Integrins. In: Encyclopedia of Biomaterials and Biomedical Engineering: Taylor and Francis; 2006.

163]. Garcia AJ, Boettiger D. Integrin-fibronectin interactions at the cell-material interface: initial integrin binding and signaling. Biomaterials 1999;20(23-24):2427-33.

164]. Wilson CJ, Clegg RE, Leavesley DI, Pearcy MJ. Mediation of biomaterial-cell interactions by adsorbed proteins: a review. Tissue Eng 2005;11(1-2):1-18.

165]. Garcia AJ. Get a grip: integrins in cell-biomaterial interactions. Biomaterials 2005;26(36):7525-9.

166]. Keselowsky BG, Garcia AJ. Quantitative methods for analysis of integrin binding and focal adhesion formation on biomaterial surfaces. Biomaterials 2005;26(4):413-8.

167]. Garcia AJ, Gallant ND. Stick and grip: measurement systems and quantitative analyses of integrin-mediated cell adhesion strength. Cell Biochem Biophys 2003;39(1):61-73.

168]. Reyes CD, Garcia AJ. A centrifugation cell adhesion assay for high-throughput screening of biomaterial surfaces. J Biomed Mater Res A 2003;67(1):328-33.

169]. Petit V, Thiery JP. Focal adhesions: structure and dynamics. Biol Cell 2000;92(7):477-94.

170]. Gilmore AP, Burridge K. Molecular mechanisms for focal adhesion assembly through regulation of protein-protein interactions. Structure 1996;4(6):647-51.

171]. Woods A, Couchman J. Protein Kinase C involvement in focal adhesion formation. Journal of Cell Science 1992;101:277-290.

172]. Ziegler WH, Liddington RC, Critchley DR. The structure and regulation of vinculin. Trends Cell Biol 2006;16(9):453-60.

173]. Demali KA. Vinculin--a dynamic regulator of cell adhesion. Trends Biochem Sci 2004;29(11):565-7.

174]. Sefton BM HT, Ball EH, Singer SJ. Vinculin: a cytoskeletal target of the transforming protein of Rous sarcoma virus. Cell 1981;24:165-174.

175]. Schwienbacher C, Jockusch BM, Rudiger M. Intramolecular interactions regulate serine/threonine phosphorylation of vinculin. FEBS Lett 1996;384(1):71-4.

176]. Johnson RP CS. The carboxy-terminal tail domain of vinculin contains a cryptic binding site for acidic phospholipids. Biochem Biophys Res Commun 1995;210:159-164.

177]. Jockusch BM, Rudiger M. Crosstalk between cell adhesion molecules: vinculin as a paradigm for regulation by conformation. Trends Cell Biol 1996;6(8):311-5.

178]. Gallant ND, Michael KE, Garcia AJ. Cell adhesion strengthening: contributions of adhesive area, integrin binding, and focal adhesion assembly. Mol Biol Cell 2005;16(9):4329-40.

179]. Gallant ND, Garcia AJ. Quantitative analyses of cell adhesion strength. Methods Mol Biol 2007;370:83-96.

180]. Wolfgang H Goldmann RG, Markus Ludwig, Weiming Xu, Eileen D Adamson, Ning Wang, Robert M Ezzell. Differences in Elastcity of Vinculin- Deficient F9 Cells Measured by Magnetometry and Atomic Force Microscopy. Experimental Cell Research 1998;239:235-242.

181]. Siliciano JD, Craig SW. Meta-vinculin--a vinculin-related protein with solubility properties of a membrane protein. Nature 1982;300(5892):533-5.

182]. Belkin AM, Ornatsky OI, Glukhova MA, Koteliansky VE. Immunolocalization of meta-vinculin in human smooth and cardiac muscles. J Cell Biol 1988;107(2):545-53.

183]. Chastain SR, Kundu AK, Dhar S, Calvert JW, Putnam AJ. Adhesion of mesenchymal stem cells to polymer scaffolds occurs via distinct ECM ligands and controls their osteogenic differentiation. J Biomed Mater Res A 2006;78(1):73-85.

184]. Seeherman, H, Wozney, J. M. Delivery of bone morphogenetic proteins for orthopedic tissue regeneration. Cytokine Growth Factor Rev ; 2005, 16 (3): 329-45,

185]. Rengachary SS. Bone morphogenetic proteins: basic concepts. Neurosurg Focus 13 (6), 2002

186]. Xiao YT, Xiang LX, Shao JZ, Biochemical and Biophysical Research Communications 362 2007, 550–553.

187]. ten Dijke P, Korchynskyi O, Valdimarsdottir G, Goumans MJ. Controlling cell fate by bone morphogenetic protein receptors. Mol Cell Endocrinol. 2003 Dec 15;211(1-2):105-13.

188]. Korchynskyi O, ten Dijke P. Identification and functional characterization of distinct critically important bone morphogenetic protein-specific response elements in the Id1 promoter. J Biol Chem. 2002 Feb 15;277(7):4883-91.

189]. Israel DI, Nove J, Kerns KM, Kaufman RJ, Rosen V, Cox KA, Wozney JM. Heterodimeric bone morphogenetic proteins show enhanced activity *in vitro* and *in vivo*. Growth Factors. 1996;13(3-4):291-300.

190]. Zhu W, Kim J, Cheng C, Rawlins BA, Boachie-Adjei O, Crystal RG, Hidaka C. Noggin regulation of bone morphogenetic protein (BMP) 2/7 heterodimer activity *in vitro*. Bone. 2006 Jul;39(1):61-71. Epub 2006 Feb 20.

191]. Zilberberg L, ten Dijke P, Sakai LY, Rifkin DB. A rapid and sensitive bioassay to measure bone morphogenetic protein activity BMC Cell Biol, 2007; 8:41.

192]. Seeherman H, Wozney J and Li R. Bone Morphogenetic Protein Delivery Systems.Spine, Volume 27, Number 16S, pp S16–S23

193]. Chin M, Ng T, Tom WK, Carstens M. Repair of alveolar clefts with recombinant human bone morphogenetic protein (rhBMP-2) in patients with clefts. J Craniofac Surg 2005;16(5):778-89.

194]. Xiuli Dong, Qi Wang, Tao Wu and Haihua Pan. Understanding Adsorption-Desorption Dynamics of BMP-2 on Hydroxyapatite (001) Surface *Biophysical Journal* 93:750-759 (2007).

195]. Hailong Zhou, Tao Wu, Xiuli Dong, Qi Wang and Jiawei Shen. Adsorption mechanism of BMP-7 on hydroxyapatite (001) surfaces Biochemical and Biophysical Research Communications, Volume 361, Issue 1, 14 September 2007, Pages 91-96.

VITA

Parthasarathy Annapillai Madurantakam was born in Chennai, India, on June 30, 1976. He started his career in dentistry with a degree from Tamilnadu Government Dental College and Hospital, Chennai, India in 1998 and went on to specialize in Orthodontics from the same institution in 2003. He was inducted as the Member of Royal College of Surgeons, Edinburgh, (Orthodontics) in 2004, shortly before his journey to the US to pursue doctoral program in Biomedical Engineering at Virginia Commonwealth University. His passion in clinically relevant research motivated him to initiate a project in bone tissue engineering under Dr. Gary Bowlin. He was a finalist in the National Inventors Competition in 2008, Kansas City, MO, for his work on hemostatic bandages. He is a member of Phi Kappa Phi and Alpha Eta Mu Beta honor societies and loves being a clinician, scientist and teacher. He hopes to carry forward the legacy of independent research and ignite the spark of innovation among youth to advance science and positively impact patient care. He is married to Lathika Mohanraj and they have been blessed with an eleven month old child, Shravan.